January 2019

Development Of More Light Sensitive And Red-Shifted Channelrhodopsin Variants For Optogenetic Vision Restoration

Tushar Harishkumar Ganjawala
Wayne State University, tganjawa@gmail.com

DEVELOPMENT OF MORE LIGHT SENSITIVE AND RED-SHIFTED CHANNELRHODOPSIN VARIANTS FOR OPTOGENETIC VISION RESTORATION

by

TUSHAR H. GANJAWALA

DISSERTATION

Submitted to the Graduate School

of Wayne State University,

Detroit, Michigan

in partial fulfillment of the requirements

for the degree of

DOCTOR OF PHILOSOPHY

2019

MAJOR: ANATOMY AND CELL BIOLOGY

Approved by:

_____

Advisor Date

_____

_____

_____

_____

DEDICATION

To my parents, Harishkumar and Hemaben Ganjawala

To my parents-in-law, Chetankumar and Pannaben Jariwala

To my dear brother, Mayank

To my loving wife, Ronak

To my son, Darshish

To all of my teachers and professors

I could not have achieved this without your unconditional love and support. Your contribution was way beyond just a thank you.

ACKNOWLEDGMENTS

First, and foremost, I would like to express my deepest gratitude to my mentor Dr. Zhuo-Hua Pan. I was fortunate to join his lab as a research assistant in 2010. His guidance, support and advice have led to my success. His confidence and belief in my abilities created enthusiastic environment for me to explore science, and has allowed me to develop into scientist I am today. His passion for research and pure scientist personality has and will always inspire me.

I would like to thank my committee members, Dr. Tomomi Ichinose, Dr. Shunbin Xu and Dr. Markus Friedrich for their constant support and guidance throughout this project. Their feedback has greatly improved my scientific thinking. I would like to thank two of my graduate program directors Dr. Paul Walker and Dr. Susmit Suvas for their advising. I would also like to thank Salina Letimore-Hall for managing all the paperwork timely.

I would like to thank my colleague Dr. Qi Lu for helping me with Apotome microscopy, ImageJ analysis and patch-clamping. I would also like to thank Shengjie Cui, Mitchell Fenner, Andrea Krstevski and Chase Hellmer for all your help. I am also thankful to the sponsors of the Rumble fellowship and GRA for supporting me.

Finally, I would like to thank the department of Ophthalmology, Visual and Anatomical Sciences (OVAS, formally Anatomy and Cell Biology) for its core research facilities.

TABLE OF CONTENTS

LIST OF TABLES

LIST OF FIGURES

CHAPTER 1: BACKGROUND AND SIGNIFICANCE

Degenerative photoreceptor diseases and vision loss

The retina is a specialized neuronal tissue of the vertebrate eye consisting of multiple different cell types with distinct morphology and synaptic connections orchestrated in layers (Figure 1). Photoreceptors (PRs) are the main retinal cells involved in initiating visual signal processing, especially for image forming vision. There are two types of PRs found in a mammalian retina, i.e. rods and cones. PRs carry a special type of protein called opsin, i.e. rod-opsin and cone-opsin. Rod and cone opsins combine with chromophore 11-cis retinal form photosensitive rhodopsins in rod and photopsins in cones (together also called photopigments) respectively, which enables them to sense the light (photon). Rod and cone photopigments belong to the family of G-protein coupled receptors (GPCRS) (Spudich et al., 2000; Placzewski, 2006). The rod and cone PRs facilitate scotopic (in dark or dim light) and photopic (day light) vision, respectively. Additionally, there are three types of cone photopigments with their peak spectral sensitivity at blue (λ_{max} ~425 nm), green (λ_{max} ~530 nm), and red (λ_{max} ~560 nm), enabling color vision (Nathans et al., 1986; Oprian et al., 1991; Ernst et al., 2013).

The visual signal pathways are complex and tightly regulated by different retinal cell types. In responding to light PRs reduce the release of neurotransmitter glutamate and relay the information to horizontal and bipolar cells. Horizontal cells provide an inhibitory feedback signal to PRs and thereby emphasize differences in signaling strength among neighboring PRs. Bipolar cells segregate PR's signals to multiple parallel pathways. Bipolar cells sort the signal and passes to amacrine and ganglion cells. Both bipolar cells and ganglion cells broadly classified into ON and OFF types

according to their light response polarity. In light, both of the ON type of bipolar and ganglion cells depolarize whereas, the OFF types hyperpolarize to generate ON and OFF responses, respectively. Reversibly, in dark both the OFF type of bipolar and ganglion cells depolarize while the ON types hyperpolarize. Based on such prime responses, visual processing pathways are divided into ON-pathway and OFF-pathway modes (Wassle, 2004; Zhang et al., 2009).

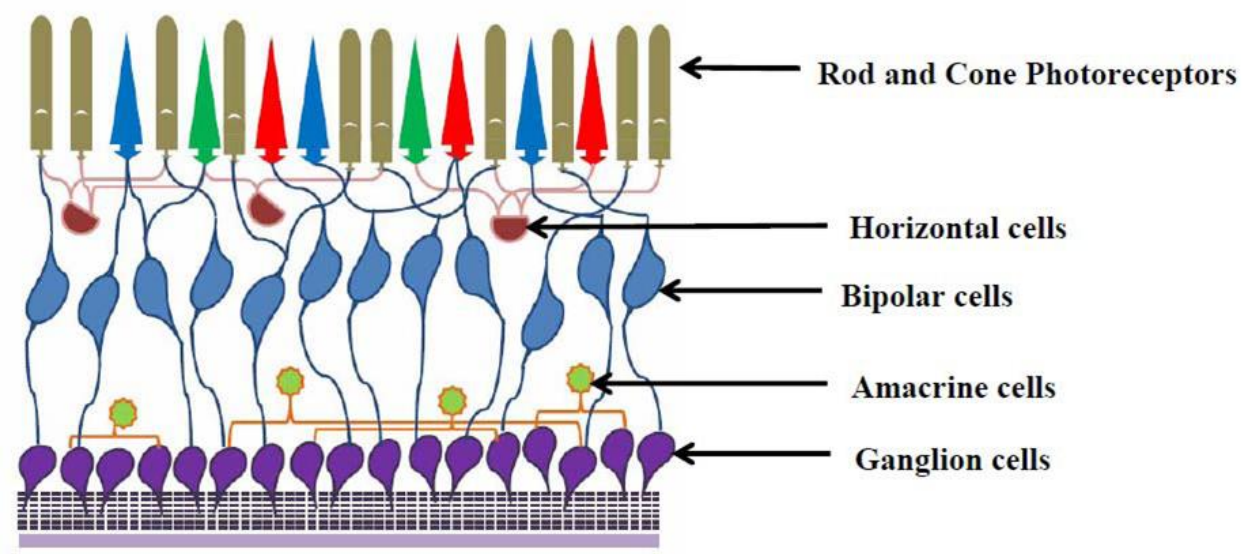

Figure 1: Schematic of the major retinal cell types of the human retina.

In general, retinal ganglion cells integrate signals from the bipolar cells and convey them via the optic nerve to the higher visual processing centers in the brain. These integrated signals include information about many parameters, such as i) Spatial information, e.g. object location, ii) Temporal information, i.e. variations with time or movement of an object, iii) Light intensity, and iv) Color. The summation of all these creates an image and scene. Thus, PRs are essential for initiating visual signal perception.

Many blinding diseases occur because of loss of function and/or degeneration of PRs (Figure 2). Examples include retinitis pigmentosa (RP) and age-related macular

degeneration (AMD). The worldwide prevalence of RP is estimated as 1 in ~4000 people (https://nei.nih.gov/health/pigmentosa/pigmentosa_facts, last updated December 2015), i.e. ~1.84 millions of people worldwide (calculated based on world population in 2015). The RP is heterogeneous disease caused by either genetic defects in the PRs leading to dysfunction or genetically damaged retinal pigment epithelium (RPE) cells failing to recycle the retinal chromophore (Hartong et al., 2006). To date, over 110 genes (RetNet, http://www.sph.uth.tmc.edu/RetNet/; last updated January 4, 2019), and over 3000 mutations have been identified to be associated with the RP (Daiger et al., 2013). AMD is more prevalent in older people. AMD patient population is projected to grow up to 196 million by 2020 (Wong et al., 2014). The visual impairment in AMD occurs specifically in the macular region, a center point of the retina, which involves high acuity visual functions (de Jong, 2006). Both of these diseases are still lacking efficient treatments.

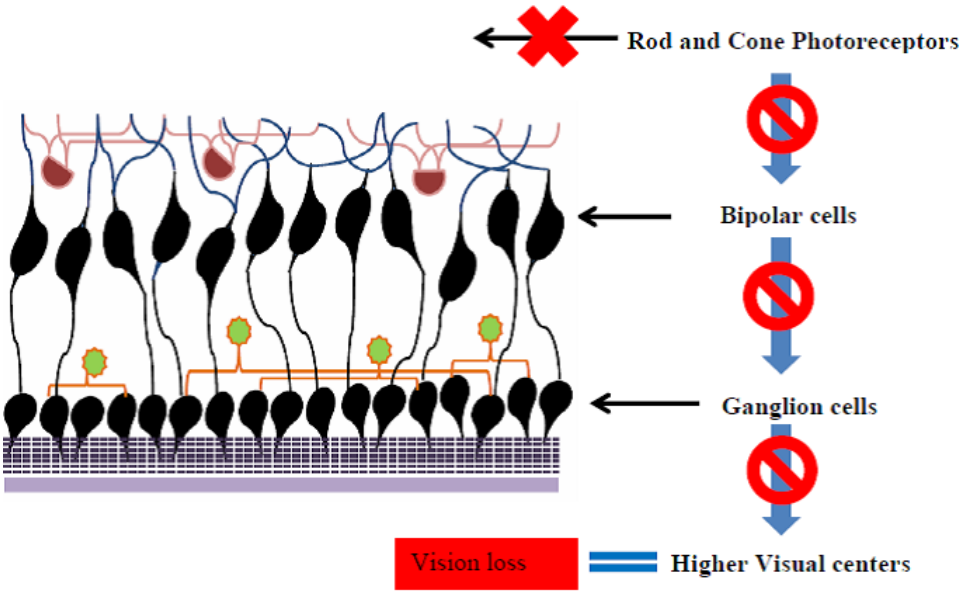

Figure 2: Schematic of the photoreceptor degeneration mediated vision loss. Loss of photoreceptors leaves bipolar cells and ganglion cells unresponsive to the light, especially for the image forming vision, and blocks the flow of visual information that ultimately causes vision loss.

Previous studies of postmortem human retinal tissues have revealed that second and third order retinal neurons remain partially preserved after the death of PRs (Stone et al., 1992; Santos et al., 1997; Milam et al., 1998). Similar observations in animal models of retinal degeneration were also reported (Chang et al., 2002; Olshevkaya et al., 2004; Lin et al., 2013). At the same time, following PRs degeneration the retinal remodeling was also observed (Fariss et al., 2000; Marc et al., 2003). The preserved retinal neurons have set the bases for the development of treatment strategies, discussed below, whereas the retina remodeling may limit the expected level of vision restoration.

Strategies for treating RP and AMD

Many attempts to stop, slow down, or reverse the PR degeneration have been made (Cai et al., 2000; Cideciyan, 2010; Berson et al., 2012; Wen et al., 2012; Cuenca et al., 2014). Unfortunately, no success has been achieved for these attempts so far, and PR degeneration is still inevitable and irreversible. However, there are some other promising approaches include gene replacement therapy, retinal prosthesis, optogenetics, stem cell implantation, and endogenous regeneration which are currently under investigation to treat blindness caused by PR degeneration (Scholl et al., 2016; The Lasker Foundation report, 2014).

Gene replacement therapy is about genetically inserting a wild type copy of the gene mutated in a specific cell type. The gene therapy for RPE65 gene mutation associated Leber congenital amaurosis (LCA), commercially known as Luxturna (voretigene neparvovec-rzyl), is a first gene therapy drug approved by FDA for clinical use (FDA News release, December 19, 2017). However, this is only applicable to the patient carrying the mutation in RPE65 gene. More recently, proof-of-concept study on

mutation-independent rhodopsin gene replacement therapy has been reported (Cideciyan et al., 2018). It has proposed to knockdown mutant rhodopsin gene expression and introducing the wild type one, by single adeno-associated viral (AAV) vector carrying sequences that encode both the knockdown shRNA (short RNA) element and the replacement rhodopsin protein. Indeed, this seems to have great potential, but it is essential to have intact PRs.

The retinal prosthesis approach employs an implant of an electronic chip with multiple micro-electrodes that can electrically stimulate second or third order retinal neurons, i.e. bipolar cells or ganglion cells. Based on placement of these implants, they can be typically classified as epiretinal, subretinal and suprachoroidal implants. Both, epiretinal and suprachoroidal implants have light sensors connected extra-occularly, while subretinal implants have light sensors coupled with stimulating electrodes. Primarily, subretinal and suprachoroidal implants stimulate bipolar cells while epiretinal implants stimulate ganglion cells. Examples include Argus II and Alpha-IMS systems that are now commercialized. However, the best-restored visual acuity is reported to be 20/546 (Stingl et al., 2013), which is still worse than 20/200 which is defined as legally blind in US. Therefore, the development of effective retinal prostheses is facing huge technical challenges (The Lasker Foundation report, 2014).

Implanting stem cells that are programmed to differentiate into PR cells is another strategy under research (Lund et al., 2001; Lamba et al., 2009; West et al., 2009). Stimulating endogenous retinal regeneration, specifically PRs regeneration, has also been considered. Recent report has shown successful regeneration of PRs by

stimulating endogenous retinal Muller glia cells in a mouse model, yet it only proved the feasibility of the approach and needs further development (Yao et al., 2018).

Optogenetic strategy is based on imparting photo-sensitivity in the RP degenerative retina via expressing genetically encoded light sensors in inner retinal neurons. Details of this approach are discussed further in next section. Another approach involves the use of chemical or optopharmacological photoswitches which are conjugated with native ion-channels or ectopic expressed receptors to render light sensitivity to the degenerative retina. The photoswitches upon light activation alters the state of ion-channels or ligand-gated receptors and causes them to generate electrical signals. Two examples are DENAQ (diethylamine-azobenzene-quaternary ammonium; Tochitsky et al. 2014) and MPC088 (Yue et al., 2012). Both, DENAQ and MPC088 are chemically azobenzene derivatives, and undergo cis/trans isomerization upon light stimulation. The DENAQ was designed to regulate hyperpolarization-activated cyclic nucleotide-gated (HCN), and has spectral sensitivity between 450-500 nm. The MPC088 was designed to regulate ligand-gated receptors such as glutamate and GABA receptors. A potential drawback of the chemical photoswitches is their short life span requiring its continuous supply (Pan et al., 2015).

Rhodopsin based optogenetic approaches

In 2003, a novel optogenetic approach was launched (Bi et al., 2006; Pan et al., 2015). This strategy is based on converting surviving inner retinal neurons into photosensitive cells, thus imparting light sensitivity to a retina affected by PR degeneration. Technically, this could be achieved by introducing light sensing proteins in the plasma membrane of bipolar cells or ganglion cells (Figure 3A). Critical to the feasibility of this approach is to have suitable genetically encoded light sensors.

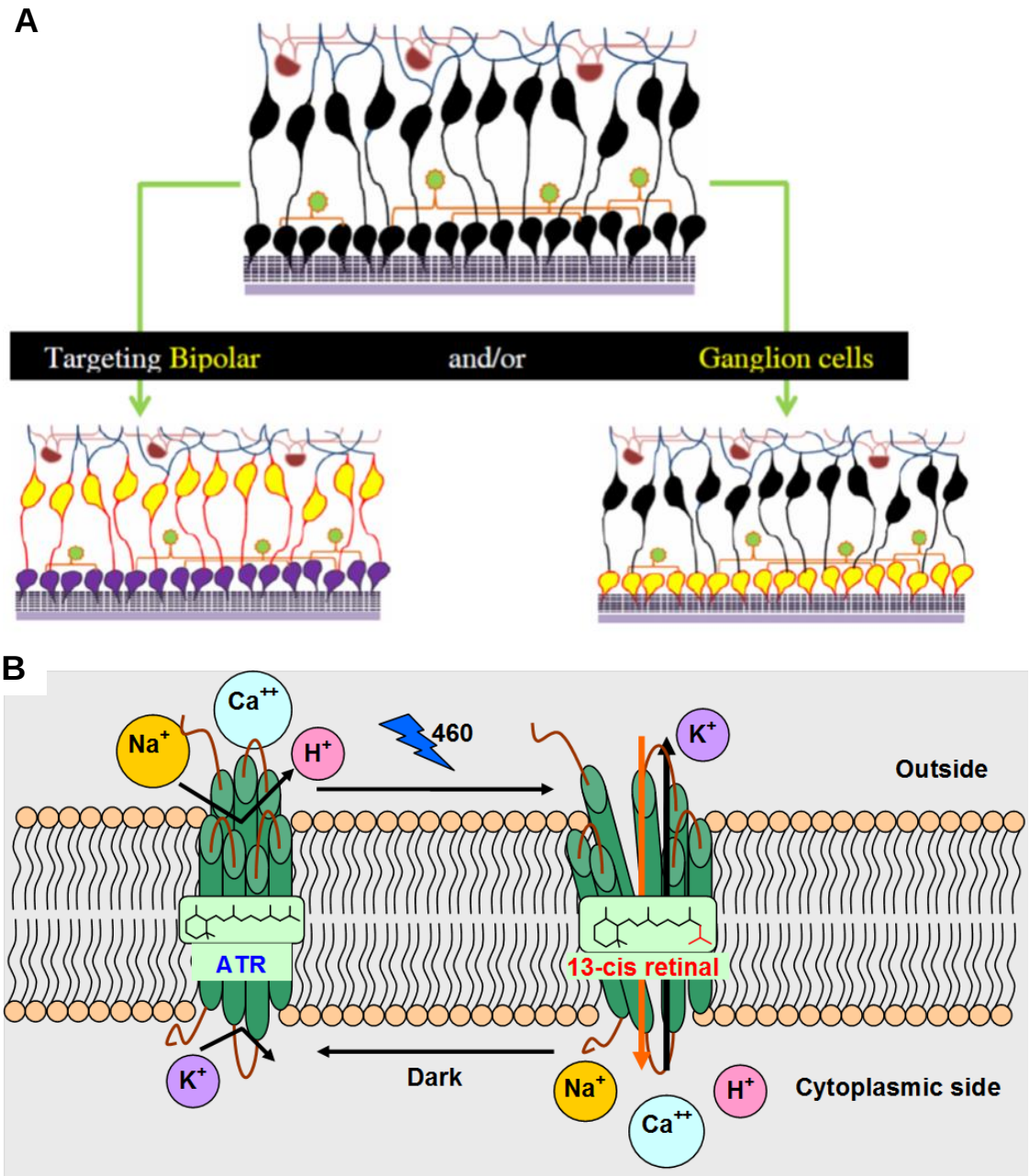

Figure 3: Optogenetic strategy and optogenetic light sensor. A) Schematic of optogenetic vision restoration via targeted expression of ChR; the yellow colored cells with red outlines indicate expression of channelrhodopsin (ChR). **B)** Schematic of ChR structure and light activation.

The discovery of channelrhodopsin-1 (ChR1) and channelrhodopsin-2 (ChR2) (Nagel et al., 2002 and 2003) led to the development of technology known as "Optogenetics" (Deisseroth, 2006), which is to excite a neuronal cell with light and study its effect on connected networks, specifically in brain tissue which was previously

inaccessible (Yizhar et al., 2011). In addition, it prompted the beginning of exploring the optogenetic approach to restore vision (Bi et al., 2006). ChR1 and ChR2 are blue light sensitive, non-selective cation channels from the green alga species *Chlamydomonas reinhardtii*. They are microbial type (type1) rhodopsin (Spudich et al., 2000). In general, ChR1 and ChR2 are cell membrane proteins composed of extracellular amino terminal (N') with seven trans-membrane (TM) helixes (TMH), intracellular carboxyl terminal (C') and a chromophore, i.e. all-trans retinal (ATR), covalently attached. The seven TMHs are linked via either extracellular loop (ECL) or intracellular loop (ICL) domains (Figure 3B). Throughout this document, TMHs are described with respective number, for instance TMH one as TM1 or TM1.

The attached chromophore ATR enables ChRs to sense the light of particular wavelengths, which is mostly in the range of 400-600 nm. Upon light stimulation, ATR isomerizes to 13-cis retinal conformation. Subsequently, many conformational changes in TMHs take place and initiate channel opening that ultimately leads to cation flux into the cell (Figure 3B). Such cation influx increases the intracellular cation concentration and, as a result, the cell's membrane potential depolarizes. ChR functions as sensory PRs and guide the algae for phototaxis based on light intensity and availability. Wild type ChRs (ChRs-Wt) proteins are more than 600 amino acids long, encompassing a very long C-terminus. In the green algae, such long C-terminus assists ChRs in trafficking to eyespot (Awasthi et al., 2016). However, it is not required for their ion-channel activity, instead only the first 300-350 amino acid residues are sufficient (Nagel et al. 2005).

Proof of concept studies

The first proof of concept for optogenetic approach to restore vision demonstrated that ectopic expression of ChR2 in the retinal ganglion cells could restore visual response in rd1 mouse, a mouse model of PRs degeneration (Bi et al., 2006). In this study, adeno-associated virus serotype 2 (AAV2) carrying ChR2-GFP transgene was injected intravitreally into the eye and the ChR2 was shown to express stably in the retinal ganglion cells. The transfected retinal ganglion cells (expressing ChR2) were shown to fire action potential in response to the blue light (460nm) specifically, indicating ChR2 mediated light responses. Using similar strategy, Tomita et al., (2007, 2010) also showed successful restoration of optomotor response in Royal College of Surgeons (RCS) rat model of RP. Both of these groups demonstrated use of ChR2 to regenerate ON response in different animal models. Furthermore, long-term stable expression of ChR2 in vivo with restored photosensitivity lasting for nearly an entire life span (64 weeks) of murine models had also been validated (Ivanova et al., 2009 and 2010).

On the other hand, Busskamp et al., (2010) used halorhodopsin (eNpHR) which functions as a hyperpolarizing optogenetic tool, and expected to generate OFF response from transfected remaining cones. Progressively, many successful attempts to generate both ON and OFF responses in the diseased retina (mouse or rabbit models) by dual transduction of ChR and halorhodopsin (NpHR/eNpHR) were also made (Zhang et al., 2009; Greenberg et al., 2011; Wu et al., 2013). Additionally, the retinal cell specific expression of ChRs in ON bipolar cells were made possible using either an optimized promoter, e.g. mGluR6, or its combination with a capsid mutant variant of

AAV, e.g. AAV2/8 (Lagali et al., 2008; Doroudchi et al., 2011; Cronin et al., 2014; Lu et al., 2016).

Thus, ChR based optogenetic strategies are promising for vision restoration in PR degenerative diseases. Furthermore, the vertebrate opsin based optogenetic approach, i.e. using melanopsin or human rod-opsin instead of ChRs, had also been tested (Lin et al., 2008; Cehajic-Kapetanovic et al., 2015). There are advantages and limitations of ChRs as an optogenetic tool as described below.

Channelrhodopsins (ChRs) as an optogenetic tool

There are several advantages of using ChRs as an optogenetic tool. First, unlike an animal rhodopsin, ChRs provide both light sensitivity and ion-conducting property without any secondary signal cascade event. Second, their chromophore ATR does not detach from opsin during light activation, and is capable of re-isomerizing, i.e. from 13-cis to all-trans conformation, by itself in dark. Hence, ChRs can work in the inner retinal neurons which are away from the RPE and cause no photo-bleaching. Third, the ATR isoform is abundantly present in all cell types in mammals, and thus, no exogenous supply of chromophore needs (Bi et al., 2006). Forth, ChRs have fast on-off kinetics compared to melanopsin (Pan et al., 2015). Finally, there are ChR variants with different peak spectral sensitivity, which may provide the potential to restore color vision in the future.

On the other hand, although the ChR based optogenetics could restored light sensitivity in the diseased retina, a major limitation of using wt-ChRs as an optogenetic tool is their low-light sensitivity. In the optogenetically treated retina, the ganglion cells fire action potentials evoked by ChR2-meditaed membrane depolarization in response to light. Therefore, the light sensitivity of the transfected retinal ganglion cells is

dependent on the light sensitivity of an individual ChR, which is referred to as operational light sensitivity of the ChR (Mattis et al., 2012; Pan et al., 2014). The minimal required light intensity to activate ChR2-Wt expressing retinal ganglion cells is close to 10^{15} photons/cm^{2}s (Pan et al., 2014). In contrast, the light activation thresholds for rods and cones are ~10^{10} photons/cm^{2}s and ~10^6 photons/cm^{2}s, respectively (Lagali et al., 2008). Thus, the light sensitivity of ChR2-Wt expressing retinal ganglion cells is at least 4-5 log units lower than that of cones. Recently, via molecular engineering, the operational light sensitivity of ChR2 was improved up to ~2 log unit, e.g. ChR2-L132C/T159S mutant variant (Figure 4; Pan et al., 2014). However, the improved light sensitivity of ChR2 is still ~3 log unit lower than cone threshold and needs further enhancement.

Additionally, ChR variants with improved light sensitivity are blue light sensitive. An extra-ocular imaging device has been proposed for use in combination with available optogenetic tools in order to overcome the low light sensitivity of ChRs (Barrett et al., 2014). Such device enhances the visual signal (in terms of light intensity) to better fit into ChR's sensitivity range. However, the blue light at high light intensities can potentially damage retinal tissue by phototoxicity since photons of shorter wavelength light have higher energy than that of longer wavelength light (red light). Therefore, shifting the peak spectrum sensitivity (λ_{max}) towards the red is also desired (Pan et al., 2015).

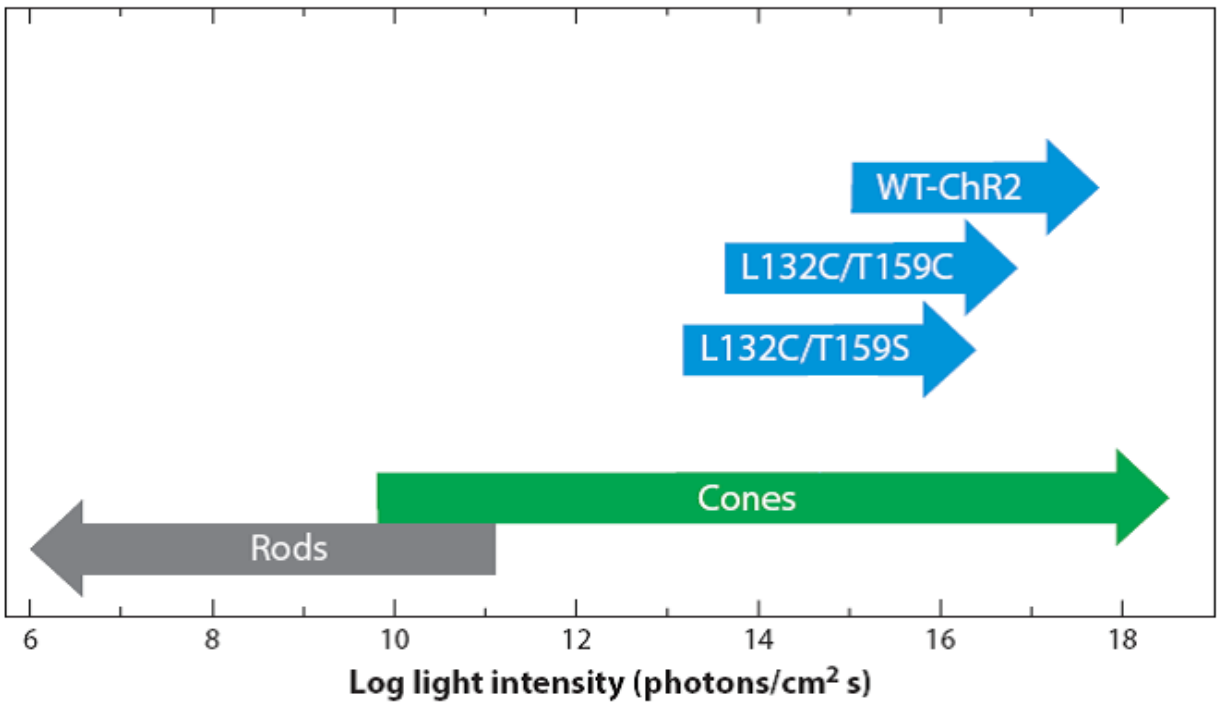

Figure 4: Comparison of light sensitivity range of different opsins. Note that threshold is higher for different ChRs, which were estimated from their expressing retinal ganglion cells. (Adapted from Pan et al., 2015).

In conclusion, ChRs are the superior choice as optogenetic tools because of their fast kinetics, simple signal transduction pathway, and potential of improving their light sensitivity by molecular engineering.

Optimizing light sensitivity of ChRs

As mentioned earlier, the light sensitivity of the ChR treated retina largely depends on the operational light sensitivity of the ChR used. Thus, optimizing ChR's light sensitivity is to create a ChR variant that can generate large photocurrent, especially at lower light intensity (Pan et al., 2014). Understanding the ChR mechanism of action is a key to improving its light response properties.

In the dark, when channel is closed complex bonding between definite amino acids block its cation permeation pathway. Essentially, upon light stimulation reorientation of the chromophore ATR and changes in hydrogen bond networking opens

the channel. The channel opening and closing is termed as “On-gating” and “Off-gating” respectively (Hegemann et al., 2005; Nikolic et al., 2009; Lorenz-Fonfria et al., 2014). For the ChR2, several amino acid residues have been identified to play critical role in regulating its gating. Some of the polar amino acid residues form cation accumulation site and two gates, i.e. ‘central gate’ and ‘inner gate’ that are key structural elements for ion conduction pathway. In ChR2, the central gate is formed by S63, E90 and N258, and the inner gate is formed by E82, E83, H134 and H265 (Kato et al., 2012; Schneider et al., 2015). Complex hydrogen bonding network at both of these gates keeps the channels close internally and prevent the cation and water flow from the cell. Mutating central gate residues have resulted in reduced photocurrent, e.g. ChR2-E90Q/A, N258D (Kato et al., 2012).

Apart from all these, residues C128 and D156 of the ChR2 are fundamentally relevant to its gating and were found linked via hydrogen bond, better referred as either “DC-pair” or “DC-gate” (Kato et al., 2012; Schneider et al., 2015). Both, weakening and recovery of the DC-gate hydrogen bond during channel opening and closing state, respectively, have been reported (Nack et al., 2010). Moreover, individual or combined mutations at these sites evidently showed retarded “Off-gating” seizing channel open state (Berndt et al., 2009). Because of their stable extended channel open state, these DC-gate mutants, especially the mutant variants ChR2-C128T/S/A and ChR2-C128S/D156A, could responded to the light at 300-fold lower intensity level than ChR2-Wt (Berndt et al., 2009; Yizhar et al., 2011). Thus, these DC-gate mutant variants of ChR2 showed improved light sensitivity, however, they are too slow to be useful for vision restoration purposes. Nevertheless, an important outcome of these mutant

studies is that slowing off-kinetics of ChRs can improve its light sensitivity. It is hypothesized that extended channel open state of DC-gate mutant variants allows more cation influx that in turn makes them more operationally light sensitive. Discussed below are some of the engineered variants with marked altered properties

Molecular engineering based ChR variants with altered light sensitivity

Hereafter, the term “ChR variants” refers to the ChRs from different algae species, ChRs with any modification including a single base pair mutation to multiple mutations, and chimeras. Since the discovery of ChR1 and ChR2, many attempted to explore the molecular determinants of their respective properties like photocurrent kinetics and spectral sensitivity. Additionally, several consecutive efforts made to improve ChR2 functional properties. The primary approach used was site directed mutagenesis to create mutant variants and determine its role in channel function.

Although both ChR1 and ChR2 are from the same algal specie Chlamydomonas reinhardtii, and shares ~65% sequence similarity, they have major differences in their peak spectral sensitivity (λ_{max}), ion selectivity, as well as activation, desensitization, and deactivation kinetics (Nagel, G. et al., 2002, 2003). Specifically, these differences are: (i) ChR1 has its λ_{max} around 500 nm which is red shifted compared to 460 nm λ_{max} of ChR2, (ii) ChR1 is more of proton (H+) selective, while ChR2 prefer other cations, e.g. Na+, K+, Ca++, and hence can function at physiological pH, (iii) ChR1 exhibits less desensitization than ChR2 in response to continuous light stimulation (Nagel et al., 2002, 2003; Lin et al., 2009). Such differences also exist among other ChRs (Mattis et al., 2012; Weiteck et al., 2016). In 2009, Lin Y.J. et al. reported a chimera variant “ChIEF” in which TM5 (E) to TM6 (F) of ChR1 were replaced with that of ChR2 and a point mutation I170V (ChEF-number) was introduced. This ChIEF was shown to exhibit

reduced desensitization like ChR1, and large current amplitude like ChR2. This was the first successful attempt reported to improve ChR properties, and importantly, it involved molecular engineering techniques like chimera design, and site-directed mutagenesis. Similar efforts were continued following this report. In 2010, Gunaydin et al. reported another interesting variant “ChETA” (ChR2-E123T accelerated) with fastest channel kinetics. Berndt, A. et al. (2011) targeted several mutations in ATR binding pocket region of ChR2 and found the variant “ChR2-T159C”, which exhibited large photocurrent than wild type ChR2. Kleinlogel et al. (2011) reported an ultra-light sensitive ChR2 variant “CatCh” (ChR2-L132C) that was named after its calcium ion (Ca^{++}) permeability. They proposed a new principle that shifting the ion-channel’s permeability from monovalent to divalent cations will increase sensitivity without altering kinetics. Additionally, double mutant ChR2-L132C/T159C showed further improvement in photocurrent generated (Prigge et al., 2012).

Several other improved mutant variants of ChR2 namely ChR2-L132A/T159C, and ChR2-L132C/T159S were recently reported (Pan et al., 2014). In particular, the operational light sensitivity of ChR2-L132C/T159S variant was shown to be improved up to 2 log units compared to the ChR2-Wt (Figure 4), which was a significant improvement considering its applicability in restoring vision via optogenetic approach. The study concluded that the prolonged off rate, indicating extended channel open state, allowed greater cation influx and hence increased operational light sensitivity of mutant ChR2 variants (Pan et al., 2014). Nevertheless, channel’s kinetics put a limit to an extent ChRs light sensitivity could be improved. Specifically, Pan et al. (2014) projected limiting slower off rate to 1 second based on their results of temporal coding ability of

the retinal ganglion cells expressing ChR2 mutants (with an off rate up to ~1 s). Since this limit has already been reached for ChR2, targeting new ChR variants with naturally superior photocurrent properties is one of the possible ways to develop better optogenetic tool to restore vision. Discussed below are some of the potential candidates.

Newly discovered ChRs with potential to be better light sensitive optogenetic tools

Recently, around sixty different algal ChRs were discovered (Klapoetke et al., 2014). Two of these many new ChRs, CoChR and Chrimson (CnChR1), were considered for this study. The CoChR is from the species *Chloromonas oogama* (Co), and was shown to generate large photocurrent than ChR2 at its peak spectral sensitivity (λ_{max}) around 470 nm. The CnChR1, from the species *Chlamydomonas noctigama* (Cn), was named as Chrimson because of its sensitivity to far-red spectrum of 660 nm and λ_{max} at 590 nm. The reported channel properties are summarized in the Table1. From the Table-1, it is clear that the CoChR was one of the highest photocurrents producing ChR reported. Especially at the 470 nm CoChR was shown to generate roughly seven-fold higher current than that of the ChR2. The light response kinetics, particularly channel on-rate, of the CoChR appeared faster than ChR2 as indicated by their respective time to reach the peak current. In contrast, the channel off rate (Toff) is slower for CoChR compared to that of ChR2. Thus, CoChR appears to be more efficient than ChR2 in conducting cation.

Moreover, although the variant Chrimson could not generate as large current as others could, it can provide the basis for developing ChR with red spectral sensitivity and improved lower light sensitivity (operational light sensitivity).

Table 1: Comparison of the light response properties of ChR2, CoChR, and Chrimson (CnChR1) (Klapoetke et al., 2014).

ChR Variants	Peak Current			T_{off}	Time to 90% I_p	λ_{max}
	470 nm	530 nm	660 nm			
ChR2	479 pA	38 pA	0	14.59 ms	~6.0 ms	470 nm
CoChR	3253 pA	1196 pA	0	86.03 ms	~4.5 ms	470 nm
Chrimson (CnChR1)	282 pA	432 pA	674 pA	22.40 ms	~7.0 ms	625 nm

Shifting spectral sensitivity toward red

Key structural determinants of ChR's spectral properties

In general, the spectral sensitivity of the chromophore ATR depends on: i) electrostatic interactions between protonated retinal Schiff base ($RSBH^+$) and counter-ions (Cis) that helps in stabilizing excited or ground state of the chromophore, ii) polarity around β-ionone ring and polyene chain of retinal, and iii) retinal distortion (Babitzki et al., 2009, Katayama et al., 2015).

Earlier studies with ChR1 and ChR2 concluded that TM5 and TM6 are key regions for the wavelength sensitivity (Wang et al., 2009; Wen et al., 2010; Prigge et al., 2012). In 2008, Zhang et al. identified genetically distinct ChR, from the algae *Volvox carteri*, with naturally red-shifted λ_{max} at 535 nm and named it VChR1, as it was more related to ChR1. The four amino acid residues of VChR1, i.e. S176, L177, S178 and A251 (corresponding residues of ChR2; G181, L182, C183 and S256) were predicted to be critical for the red-shifted spectrum of VChR1. The first three are probably located near β-ionone ring of ATR, whereas A251 (of VChR1) is possibly near the nitrogen of the ATR polyene chain (Zhang et al., 2008). Noticeably, among the proposed amino acids, only serine (S) is the polar amino acid. Corresponding amino acid residues of ChR2 appeared to have polarity differences, e.g. S256 of ChR2 analogous to A251 of

VChR1. This indicated that polar and non-polar residues near ATR are important for spectral selectivity of ChRs.

According to a recent report, the spectral difference of 30 nm between primate green and red sensitive pigments is solely due to presence of polar amino acids near the β-ionone ring (in case of red sensitive pigment) as there was no difference found in hydrogen bond networking among two pigments (Katayama et al., 2015). As described in following section, several attempts were made to change the spectral sensitivity of ChR2.

Molecular engineering based ChR variants with altered Spectral sensitivity

By systemic replacement of TMH regions between ChR1 and ChR2, Wang et al. (2009) concluded that TM5 and TM6 are important molecular determinants of ChR's wavelength sensitivity, desensitization, and kinetics. In particular, they found that the N187Y mutation in TM5 region was one of the key determinants. In 2010, Wen et al. designed new variant ChRGR (ChR Green Receiver) by replacing TM1 and partial TM7 (C terminus side) of ChR1 with those of ChR2. This ChRGR was shown to generate large current at long wavelength light (~520 nm), i.e. green light. By combining mutagenesis with chimera engineering approach, Lin et al., in 2013 successfully optimized a ChR variant with red-shifted λ_{max} and named it ReaChR (Red activable ChR). This variant was founded on VChR1 and VChR2. Recently, the ReaChR has been shown to restore visual response in mouse models of retina degeneration (rd1), non-human primate (macaque) retina, and human's post mortem retinas (of RP patients) (Sengupta et al., 2016). However, its poor sensitivity to dimmer light has remained unresolved.

In summary, molecular engineering approach is applicable to modify spectral properties of ChRs. Upon amino acid sequence alignment, it was noticed that some polar and non-polar residues are conserved in both ReaChR and Chrimson (two red light sensitive ChRs), while corresponding residues in both ChR2 and CoChRs (blue light sensitive) are of opposite polarities. These includes S86, M87, G161, I163 and S236 of the CoChR (Figure 5, red boxes), and it was hypothesized that polarity difference at these particular sites may influence the λ_{max} of the CoChR.

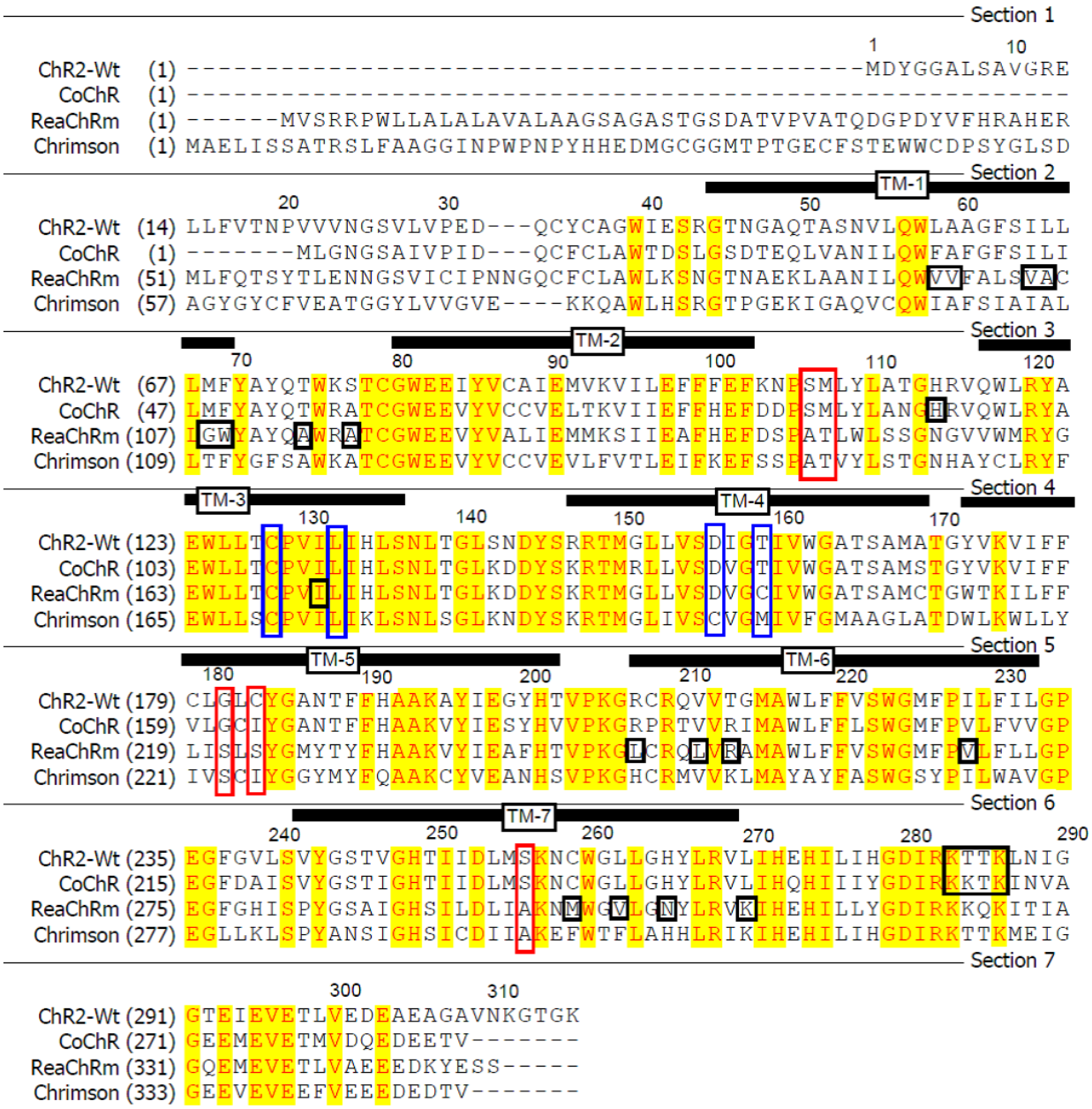

Figure 5: Sequence alignment for ChR2-Wt, CoChR, ReaChR and Chrimson. Numbers above the sequence represents ChR2 amino acids numbering. To find analogous residues, relative amino acids numbering for other ChRs are mentioned in the respective parentheses on the left in each section. Based on ChR2, trans-membrane domains (TM 'number') are marked as black bars (with respective numbers) above the sequence. Amino acid residues before the TM1 belong to the amino (N) terminal, whereas those after the TM7 belong to the carboxyl (C) terminal end (Kato et al., 2012). Highlighted in blue boxes are ChR2 residues C128, L132C, D156 and T159C, and amino acids analogous to these were mutated for the CoChR and the ReaChR. Residues targeted for red spectral shift are highlighted in red boxes. Other residues targeted are highlighted in black box.

Significance

ChR based optogenetic approach to restore vision in photoreceptor degenerative disease seems promising, and it is currently under phase I/II human clinical trial (ClinicalTrials.gov ID # NCT02556736) for evaluating optimal virus dosage and its safety concerns. Although the light sensitivity of ChR2 has been improved by molecular engineering, the ChR2-expressing RGCs are still at least three log units less light sensitive than cone photoreceptors (Figure 4). For retaining useful temporal resolution for the restored vision, the light sensitivity of the ChR2 could not be improved by further slowing its kinetics (Pan et al., 2014). Hence, ChRs with better conductance were needed. The newly discovered ChR variant CoChR has been shown to generate light response (photocurrent) larger than the ChR2-Wt, and its off-kinetics is fast compared to the most light- sensitive ChR2-L132C/T159S (Klapoetke et al., 2014). Therefore, there was a possibility of slowing CoChR's off-kinetics (off rate), up to and within an optimal range of 200-1000 ms, to enhance its light sensitivity further.

ReaChR has been shown to restore visual response in different RP models (Sengupta et al., 2016). Its red shifted λ_{max} at ~530 nm (i.e. ~60 nm shift compared to ChR2) was emphasized as an advantage over ChR2. However, its sensitivity to low intensity light is poor. Thus, improving light sensitivity of ReaChR by molecular engineering was desired. Furthermore, ReaChR and Chrimson could provide the basis for developing highly light sensitive ChR variants with red-shifted spectrum. This study was aimed to develop more light sensitive CoChR and ReaChR variants by molecular engineering.

CHAPTER 2: IMPROVING LIGHT SENSITIVITY OF CoChR

Introduction:

CoChR is a ChR variant from the algal species *Chloromonas oogama* (Co). It was shown to exhibit lager photocurrent than ChR2, suggesting that it has a higher single channel conductance (Klapoetke et al., 2014). The channel conductance determines the flux rate of ions across the channel upon its opening. Hence, a ChR with higher conductance can generate a lager photocurrent upon stimulation, which indicates its higher light sensitivity. However, increasing channel conduction for a ChR would be more challenging. Alternatively, the photocurrent of a ChR could also be increased by increasing its mean single channel open time. That is because the longer the time a channel remains open more the cations move into the cell. At the macroscopic level, this appears as a slower current kinetics or off-rate. The change in ChR's kinetics by molecular engineering is more feasible by site-directed mutagenesis. In particular, despite its larger photocurrent, CoChR's off rate (~112 ms) is faster than the previously optimized and most light sensitive ChR2 variant, ChR2-L132C/T159S (>1 s; Table 2). Therefore, CoChR's operational light sensitivity could be further enhanced by slowing its kinetics via molecular engineering.

Table 2: Comparison of light response properties of the wild type CoChR (CoChR-Wt) with that of the ChR2-Wt and its optimized variants. Data for ChR2 and its variants were taken from Pan et al., 2014. Data presented as mean ± SEM.

ChR Variants	N	Off-rate (ms)	Peak Current (pA)	
		ND 0	ND 0	ND 2.5
CoChR-Wt	10	112 ± 11	1468 ± 254	368.5 ± 44
ChR2-Wt	7	18 ± 1	782 ± 84	26 ± 2.5
ChR2-L132C/T159C	6	199 ± 17	1062 ± 11	212 ± 19
ChR2-L132C/T159S	9	1090 ± 64	1037 ± 69	470 ± 34

Aim 1: Improving light sensitivity of CoChR via molecular engineering

Rationale:

Many mutations in ChR2, C128T, D156A, L132C, L132A, T159C, T159S, and double mutants L132C/T159C, L132C/T159S, have been reported to slow down its off rate (Berndt et al., 2009; Pan et al., 2014). Performing mutations at these corresponding sites in CoChR would be a logical starting point. For CoChR, the sites of L112, T139, C108 and D136 are analogues to the L132, T159, C128 and D156 of ChR2 (see Figure 5). The L112 was mutated to A, C, D and S, the T139 to A, C and S, the C108 to A and T, and the D136 to A, C and T via site directed mutagenesis. These specific mutations at respective sites were chosen because similar mutations, at corresponding sites, have been shown to slower ChR2's off-rate. Similarly, for CoChR too, these mutants were expected to slow down the off rate and consequently, for some of them, their current at lower light intensity might enhance.

Next, upon amino acid sequence alignment, a possible endoplasmic reticulum (ER) retrieval signal sequence "KKXX" signal sequence, specifically "KKTK", was observed in CoChR but not in the ChR2 (Figure 5 and 6A). Such signal sequence can be recognized as two lysine (K) residues followed by any two amino acids (XX; hence KKXX). It can affect the protein trafficking and expression depending upon its position, which in turn may affect the functional properties it provides to the cell (Vincent et al., 1998). Moreover, in the in-vitro cell culture of HEK cells, the membrane expression level of the CoChR was found to be significantly lower than that of ChR2 (Figure 6B). It was suspected to be an effect of "KKTK" signal sequence, hence, tested a hypothesis that interrupting such signal sequence via point mutation K264T (according to that of ChR2)

may improve CoChR's membrane expression and consequently its light response properties.

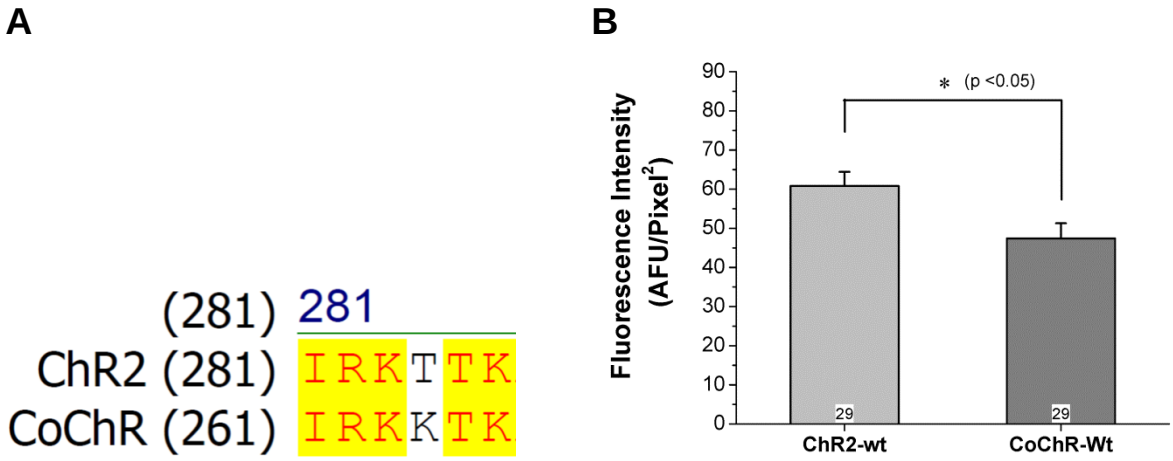

Figure 6: A likely ER-retrieval signal peptide in CoChR affecting its expression. A) Amino acids sequence alignment between ChR2 and CoChR (only respective portion of the report) showing presence of "KKTK" (KKXX) ER-retrieval signal peptide in CoChR, **B)** Expression level comparison between ChR2-Wt and CoChR-Wt based on quantitative GFP fluorescence analysis.

Recently, a positively charged amino acid arginine (R), specifically R88, has been shown to inhibit anion flux of the GtACR1, an anion ChR (ACR) from the algae *Guillardia theta* (Gt), emphasizing on the opposite charge inhibiting ion flux. Interestingly, CoChR also possess a positively charge amino acid histidine (H) at the corresponding site, i.e. CoChR-H94. The H94E (HE) mutation was created to test whether or not a negatively charged amino acid glutamic acid (E) inhibits cation influx of the CoChR. Additionally, it was tested in combination with L112C and K264T variants of the CoChR by creating H94E/L112C (HE/LC), H94E/K264T (HE/KT) and H94E/L112C/K264T (HE/LC/KT or 3Mt) mutants. To identify promising mutant variants, all variants were first screened for their off rate and current amplitude at low light intensity (ND2.5). Details of the methods and materials are described below.

Methods and Materials

A) Molecular engineering to generate variants:

The wild type CoChR gene sequence (Gene bank id # AHH02107.1) was synthesized (GeneScript, Piscataway, NJ, USA) and sub-cloned in the mammalian expression vector with CMV promoter to drive its expression (Figure 7). A single or multiple point mutations were created by site-directed mutagenesis (Quick Change Lightening, Agilent Technologies, Santa Clara, CA, USA). All the variants including wild type were fused with GFP at C' which aided to track their expression and membrane trafficking.

Figure 7: Schematic of the mammalian expression vector cassette showing cytomegalovirus promoter (CMV) driving expression of ChR fused with green fluorescence protein (GFP).

B) HEK293f cell culture and transfection:

The human embryonic kidney cells (HEK293f or HEK cells) were grown in Advance Dulbaco's Minimum Essential Medium (DMEM; Life Technologies, Grand Island, NY, USA) supplemented with 1x MEM-non-essential amino acid solution and 5% Fetal Bovine Serum (FBS; Sigma Aldrich, St. Louis, MO, USA), and kept at 37°C with 5% CO_2 humidified incubator. For transfection experiments, cells were seeded in 35 mm dish at the density of 5 x 10^5 cells/ml (3 ml per dish) and ATR was also added at final concentration of 1 µM. At about 48 hrs post-seeding, cells were transfected with 1µg of plasmid DNA carrying either wild type or mutant variant using lipofectamine reagent (Lipo2000; Life Technologies, Grand Island, NY, USA).

C) Expression levels quantification and patch clamp recordings:

Expression level analysis and whole cell patch clamp recordings were performed at about 48 hrs post-transfection. The expression levels were quantified based on the GFP fluorescence in plasma membrane regions of the HEK cells. To measure GFP fluorescence, transfected HEK cells were fixed with 4% paraformaldehyde solution made in 0.1 M phosphate buffer (pH 7.2) for 10 minutes, followed by three washes with 0.1 M phosphate buffer (pH7.2) for 10 min each, as previously described (Pan et al., 2014). After washes, a drop of vectashield was applied and area was covered with cover slip. All the images were taken under similar settings (i.e. 400 ms light exposure time, 20x lens magnification) using Zeiss Axioplan2 microscope (Carl Zeiss) aided with the Apotome oscillating gratings to reduce out of–focus stray light. Single optical section images were used to calculate fluorescence intensity. The fluorescence intensity per pixel area of cell plasma membrane region was determined by ImageJ software as previously described (Pan et al., 2014).

D) Whole cell patch-clamp recordings:

Light response properties were obtained via whole cell patch clamp recording under voltage clamp (holding at -60 mV) conditions, as previously described (Pan et al., 2014). The patch-clamp recordings were performed two days after plasmid DNA transfection. The chromophore ATR (1µM) was added to HEK cell growth medium at the time of seeding. All the recordings were done at room temperature, with EPC9 amplifier and PULSE software (Heka Electronik, Laubrecht/pfalz, Germany). The glass electrodes were coated with a silicone elastomer (Dow Corning, Midland, MI, USA) and fire polished as previously described (Pan et al., 2014).

Extracellular solution (Hank's balanced salt solution) for the recording contained (in mM): 138 NaCl, 1 $NaHCO_3$, 0.3 Na2HPO_4, 5 KCl, 0.3 KH_2PO_4, 1.25 $CaCl_2$, 0.5 $MgSO_4$, 0.5 $MgCl_2$, 5 HEPES, 22.2 glucose, pH 7.2. The electrode solution/internal solution (INS) contained (in mM): 130 K-Gluconate, 12 KCl, 1 MgCl2, 10 HEPES, pH 7.2. ATR (1µM) was added to extracellular recording solution. A xenon lamp scanning monochromator (TILL photonics, Munich, Germany) was used to generate light of the wavelengths ranging from 350 nm to 700 nm, to stimulate transfected HEK cells. This light source was connected to the microscope via optical fiber. The different intensity of light stimuli was adjusted with neutral density (ND) filters. The light intensities relative to different ND filters are tabulated below where ND 0 means un-attenuated.

Table 3: Light intensities corresponding to the neutral density filters used.

Filter position	ND	Light intensity (photons/cm^{2}s)	
		at 480 nm	at 530 nm
0	4.5	9.0×10^{13}	8.6×10^{13}
1	4.0	2.3×10^{14}	2.2×10^{14}
2	3.5	7.8×10^{14}	7.4×10^{14}
3	3.0	9.7×10^{14}	9.2×10^{14}
4	2.5	3.7×10^{15}	3.5×10^{15}
5	2.0	1.3×10^{16}	1.2×10^{16}
6	1.0	1.3×10^{17}	1.2×10^{17}
7	0	8.9×10^{17}	8.5×10^{17}

E) Data Analysis:

The electrophysiology data were analyzed by PULSE software (Heka Electronik, Laubrecht/pfalz, Germany). Briefly, peak current (I_{peak}) responses were measured from zero to the maximum level reached upon light stimulation, while the steady state levels ($I_{plateau}$) were measured at the end of the light pulse (Figure 8A). The off-rates were measured by fitting a single exponential function to the decaying phase of the current

evoked by 10 ms light pulse at ND0 (Figure 8B). Using Origin 6.1 software (OriginLab Corporation, Northampton, MA, USA), the independent t-test was performed to find any statistical difference.

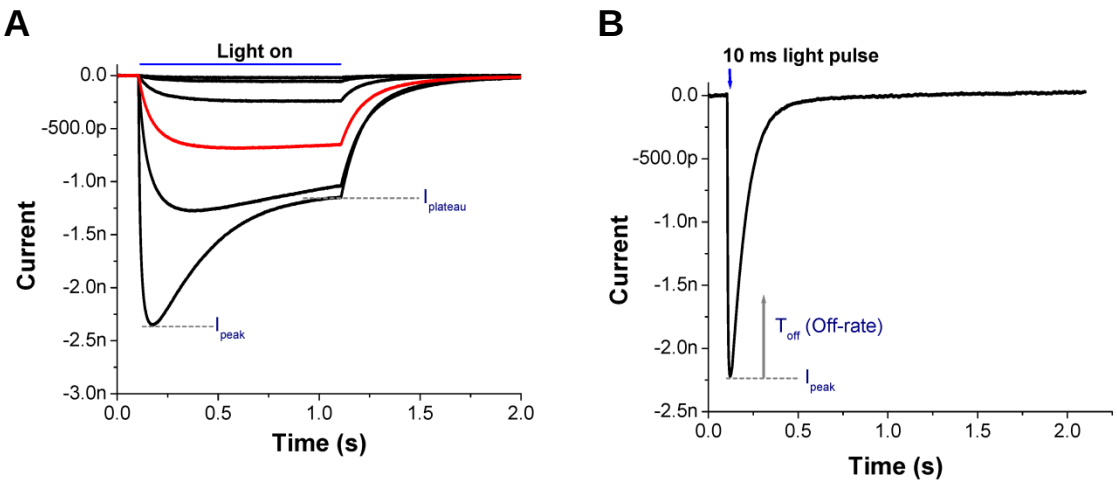

Figure 8: Typical photocurrent responses in ChR expressing HEK cell excited by a 1 s light pulse (**A**; blue bar) and 10 ms short light pulse (**B**; blue down arrow) measured at -60 mV by whole cell patch-clamp. In A, multiple current responses are at different light intensities. During light stimulation, at higher light intensity, current quickly reaches to the peak (I_{peak}) and then decays to the steady state ($I_{plateau}$). The off rate obtained from the decaying phase of the current (generated with 10ms pulse) by applying single exponential function.

Results:

Initially, all the mutant variants of CoChR were evaluated for their expression, off rate and current amplitude to low light intensity at ND 2.5. These results are summarized in Table 4. For the expression assessment, the CoChR-Wt's expression level was considered as standard to grade the expression of mutant variants (Table 4). Relatively, for the CoChR variants L112C (LC), T139C (TC), LC-TC, C108A (CA), H94E (HE), L112C-K264T (LC-KT) and H94E-L112C-K264T (HE-LC-KT or 3Mt), the expression was comparable to the Wt, whereas the expression for the variant L112A (LA), L112S (LS), T139A (TA), T139S (TS) and H94E-L112C (HE-LC) was fairly good. The variant L112D (LD), C108T (CT), D136A (DA), D136C (DC), D136T (DT) and

H94E-K264T (HE-KT) expressed poorly. Exceptionally, the variant K264T expression appeared better than the Wt.

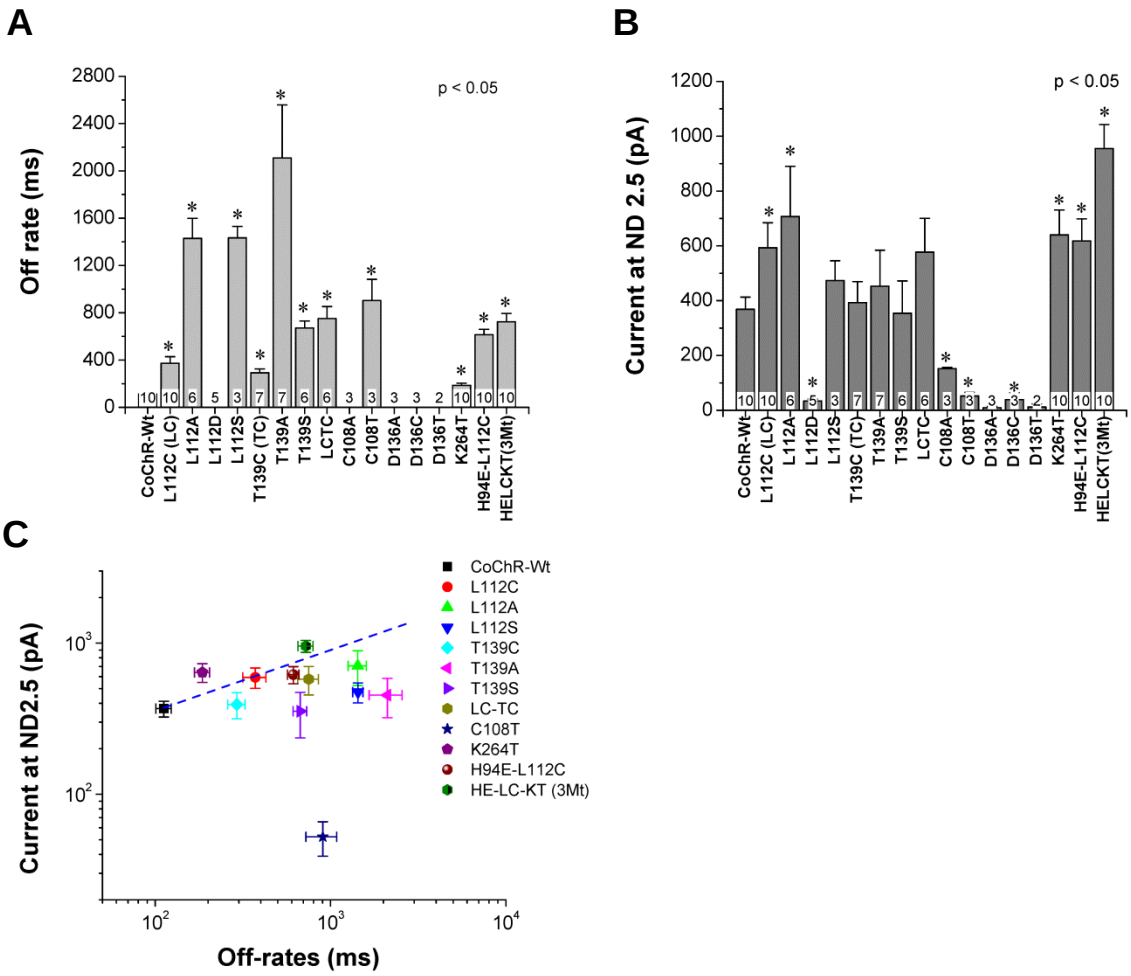

Figure 9: CoChR variants screening for slowed off rate with improved current at ND 2.5. A) Off-rates comparison. **B)** Current responses at lower light intensity (ND 2.5 = 3.7 x 10^{15} photons/cm^2s) comparison. **C)** Current-kinetics relationship plot. Responses measured with 480 nm light pulses of 10ms for the off rate and 1 s for the current amplitudes. The "N" numbers are shown above the X-axis with respective bars in A and B. The mutants with off-rates too slow to be measured are marked with + sign in the section A.

The off-rates and the current are also shown in Table 4. These properties were statistically compared with that of CoChR-Wt. As shown in Figure 9A, the off rate significantly slowed for the mutants LC, LA, LS, TC, TA, TS, LC-TC, CT, HE, KT, HE-LC, LC-KT and HE-LC-KT (3Mt). Consequently, the current increased only for the LC, LA,

KT, HE-LC and HE-LC-KT (3Mt) (Figure 9B). The mutant LA generated large current, but its off rate (~1400 ms) was slower beyond 1 s (Table 4).

Table 4: Light response properties of CoChR variants; characterized in HEK293 cells by whole cell patch clamp recordings at 480 nm. Expression level grading; ▲▲▲▲ = good, ▲▲▲Δ = fairly good, ▲▲▲ = fair, ▲▲Δ and ▲▲ = poor. Data are presented as mean ± SEM. ND0 = 8.9 x 10^{17} photons/cm^2s, ND 2.5 = 3.7 x 10^{15} photons/cm^2s.

CoChR Variants	N	Expression Full =▲, Half =Δ	Off-rate (ms) at ND 0	Peak Current (pA) at ND2.5
Wt	10	▲▲▲▲	112 ± 11	368.5 ± 44
L112C (LC)	10	▲▲▲Δ	372 ± 56	593 ± 91.5
L112A (LA)	6	▲▲▲	1428.5 ± 169.5	707 ± 183
L112D (LD)	5	▲▲Δ	too slow to be measured	34 ± 7
L112S (LS)	3	▲▲▲	1433 ± 97	474 ± 72
T139C (TC)	7	▲▲▲Δ	292 ± 33	393 ± 77
T139A (TA)	7	▲▲▲	2108.6 ± 449	452.5 ± 131.5
T139S (TS)	6	▲▲▲	671.2 ± 59	354 ± 118
LC-TC	6	▲▲▲Δ	750.5 ± 101.5	577 ± 123
C108A (CA)	3	▲▲▲Δ	too slow to be measured	152 ± 4.5
C108T (CT)	3	▲▲Δ	903 ± 180	52 ± 13.4
D136A (DA)	3	▲▲Δ	too slow to be measured	9 ± 5
D136C (DC)	3	▲▲Δ	too slow to be measured	39 ± 25.2
D136T (DT)	2	▲▲	too slow to be measured	12 ± 12
K264T (KT)	10	▲▲▲▲▲Δ	186 ± 18	640 ± 91
H94E (HE)	10	▲▲▲▲	174 ± 13	388 ± 42.2
H94E-L112C (HE-LC)	10	▲▲▲	614 ± 46	618 ± 80
H94E-K264T (HE-KT)	11	▲▲	133 ± 12.5	212 ± 36
L112C-K264T (LC-KT)	13	▲▲▲▲	376 ± 37	516 ± 65.2
HE-LC-KT (3Mt)	10	▲▲▲Δ	723 ± 71	955 ± 87.4

For all these mutants, the off-rates were plotted against their respective currents (Figure 9C). The variants LC, KT, HE-LC and HE-LC-KT (3Mt) appeared to be potentially useful because they exhibited enhanced current with their slowed off rate within 1 s. Among these mutants, H94E-L112C-K264T (3Mt) exhibited the largest current. Therefore, CoChR-3Mt could be a best optimized and the most sensitive variant

of CoChR. This CoChR-3Mt (HE-LC-KT) together with its related mutants, i.e. HE, LC, KT, HE-KT, HE-LC and LC-KT, were chosen for further characterization. The results are described below.

A) Expression level analysis and primary screening of CoChR variants:

The expression of these seven CoChR mutants and of CoChR-Wt was quantified based on the GFP fluorescence intensity in plasma membrane region of HEK cells. A representative fluorescence image of HEK cell expressing different CoChR variants is shown in Figure 10A. Comparison of fluorescence intensities (arbitrary fluorescence intensity per unit area; AFU/pixel^2) are shown in Figure 10B. There was no significant difference in the expression between CoChR-Wt and LC, HE, LC-KT, and 3Mts (Figure 10B). The expression of two mutants, HE-KT and HE-LC, however, was significantly lower (~47% and ~25% respectively) than CoChR-Wt. On the other hand, the expression of K264T (which was targeted to interrupt “KKXX” signal sequence) was significantly higher (~51% better) compared to CoChR-Wt.

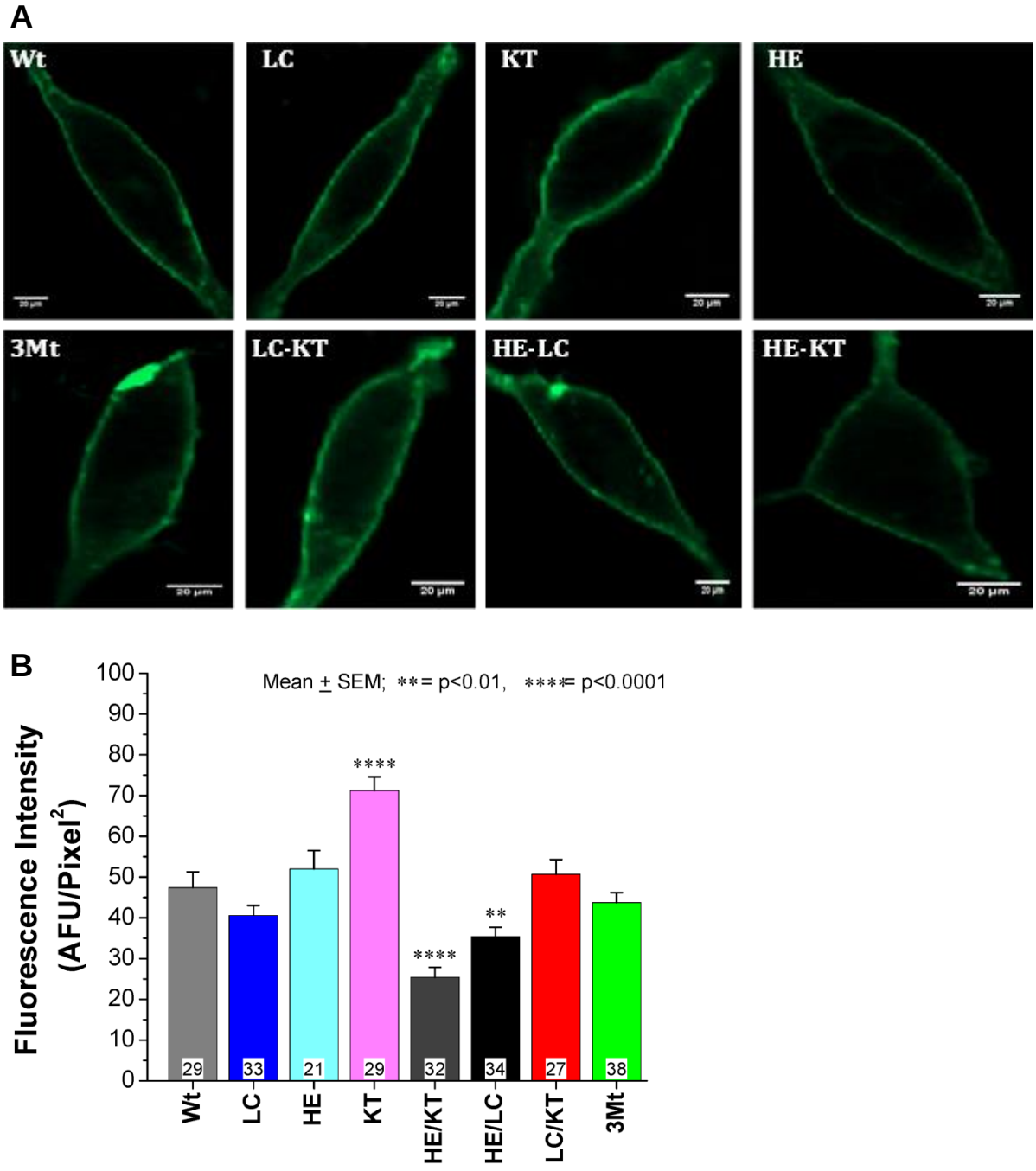

Figure 10: Expression level comparison in HEK293 cells; **A)** Representative image of HEK293 cell expression of CoChR-Wt and its variants L112C (LC), K264T (KT), H94E (HE), HE-KT, HE-LC, LC-KT and 3Mts (HE-LC-KT). Scale bar 20 um. **B)** Mean fluorescence intensities measured in plasma membrane region and represented as arbitrary fluorescence unit per pixel area (AFU/pixel2) ± SEM. The cell numbers (n) are shown in respective bars.

B) Characterization of light response properties of selected CoChR variants in HEK293 cells:

The light response properties of these selected mutants were examined and compared with CoChR-Wt. Their spectral curves were found unchanged, with a λ_{max} of 480 nm (Figure 11). Therefore, all of the further characterizations were conducted with 480 nm light stimulation. Statistical data in comparison of their response properties, including off-rates and current amplitudes are shown in Table 5.

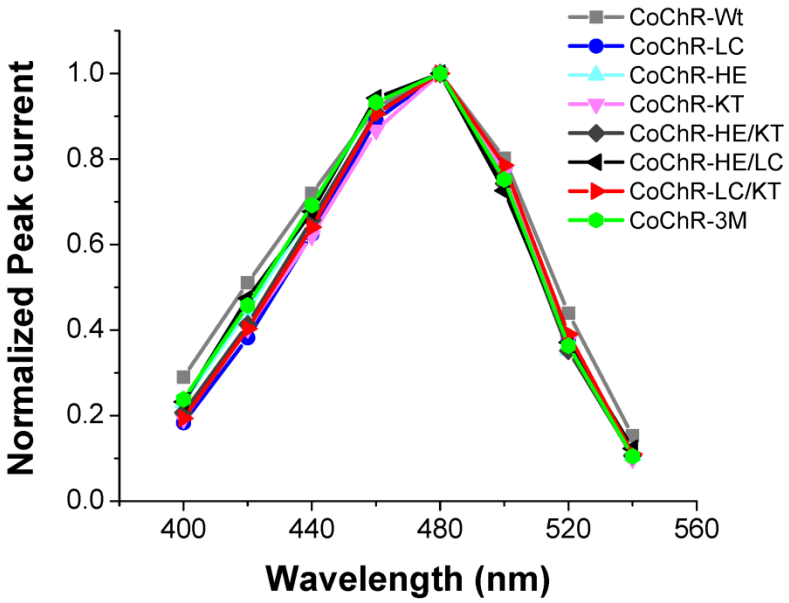

Figure 11: Spectral curve comparison for CoChR variants. Responses to each wavelength (from 400 nm to 560 nm) were recorded under voltage clamp conditions (-60 mV) at ND 2.5. Average of three responses was taken to plot the curve for each variant. ND 2.5 = 3.7 x 10^{15} photons/cm^2s.

The representative current traces in response to 1 s light pulse with incremental light intensities are shown in Figure 12. For all the CoChRs, during 1s light stimulation at the higher light intensities, the current quickly reached to a peak and then decayed to a steady state, which is caused by channel desensitization. The steady state current is referred as plateau current. Overall, the current amplitudes were light intensity dependent (Figure 13A and B). Statistically, the peak currents at ND 0 for all seven

mutants were not significantly different from that of CoChR-Wt (Table 5 and Figure 13C). On the other hand, the peak current for CoChR-HE/KT was significantly lower than that of CoChR-KT and CoChR-3Mt. The level of desensitization for all mutants except HE/KT was reduced in comparison to CoChR-Wt, which resulted in relatively larger plateau currents (Figure 13B). Therefore, although the peak currents were not significantly different for any of the selected variants, the ratios of plateau to peak currents were significantly higher for all mutants except HE/KT (Table 5, Figure 13D). This ratio was especially high for LC, HE-LC, LC-KT and 3Mt.

Table 5: Light response properties of selected CoChR variants; characterized in HEK293 cells by whole cell patch clamp recordings at 480 nm. Data presented as mean ± SEM. ND0 = 8.9 x 10^{17} photons/cm^2s, ND 2.5 = 3.7 x 10^{15} photons/cm^2s.

CoChR Variants	N	Off rate (ms)	Current (pA)		Current ratios	
		ND 0	ND 0	ND 2.5	$I_{Plateau}/I_{peak}$	ND2.5/ND0
Wt	10	112 ± 11	1465 ± 25	368.5 ± 44.25	0.4	0.25
L112C (LC)	10	372 ± 56	1437 ± 22	593 ± 91.47	0.8	0.4
H94E (HE)	10	174 ± 13	1286 ± 11	389 ± 42.17	0.5	0.3
K264T (KT)	10	186 ± 18	2182 ± 30	640 ± 90.70	0.5	0.3
HE/KT	11	133 ± 12.5	917 ± 11	212 ± 35.88	0.4	0.2
HE/LC	10	614 ± 46.2	1229 ± 15	618.2 ± 80.43	0.8	0.5
LC/KT	13	376 ± 37	1238 ± 15	516 ± 65.16	0.8	0.4
HE/LC/KT (3Mt)	10	723 ±71	1614.5 ± 13	955 ± 87.37	0.9	0.6

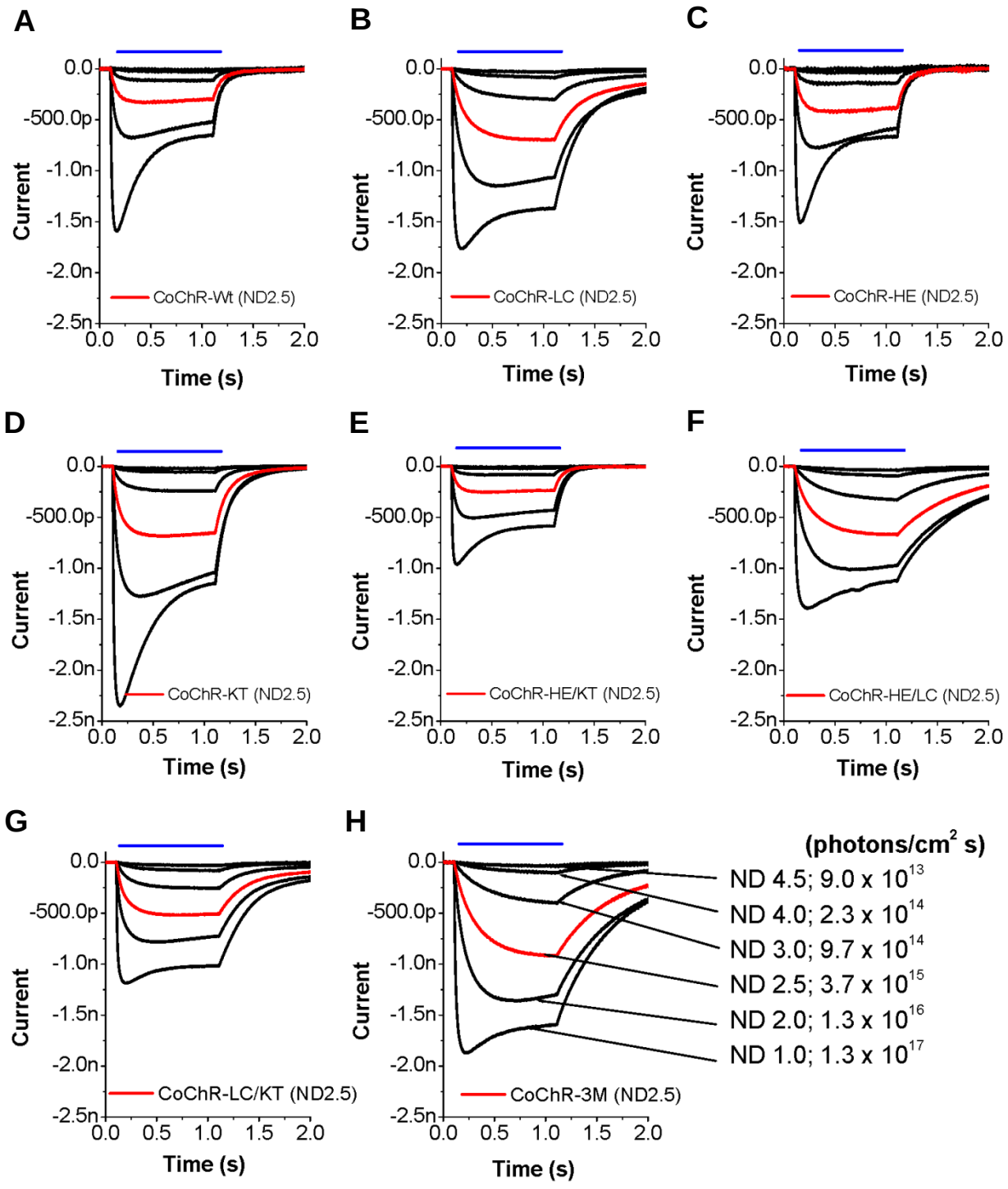

Figure 12: Representative current traces mediated by CoChR and its variants in HEK293 cells. Responses were generated under voltage clamp (-60 mV) conditions with 1 second (480 nm) light stimulation. Light intensities were attenuated by neutral density filters ND 4.5, 4, 3, 2.5, 2 and 1. Blue line/bar on top represents duration of light stimulation.

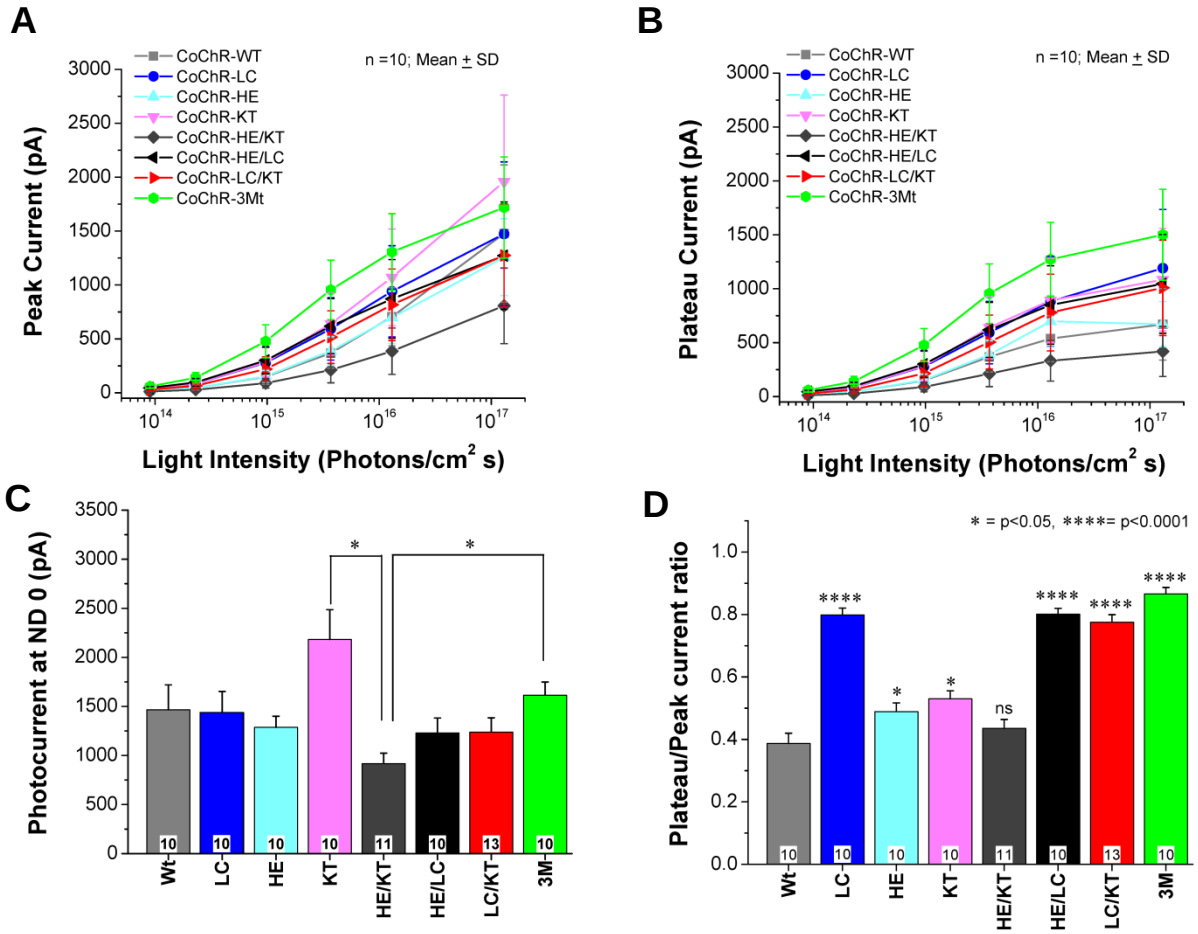

Figure 13: Light intensity response curves of CoChR variants; peak **(A)** and plateau **(B)** currents were obtained in response to different light intensities of 480nm. The data are presented at mean ± SD. Photocurrent response comparison; **C)** Peak current at brightest light, i.e. ND 0, D) Plateau to peak current ratio representing degree of peak current desensitization. ND0 = 8.9 x 10^{17} photons/cm^{2}s, ND 2.5 = 3.7 x 10^{15} photons/cm^{2}s.

Figure 14 summarizes the relationship between current amplitudes and off-rates for all these CoChRs. The off-rates were calculated by fitting a single exponential function to the decaying phase of the currents evoked by a 10 ms light pulse at ND 0 (Figure 14A). The off-rates for the variant LC, HE, KT, HE/LC, LC/KT, and 3Mts were significantly slower than CoChR-Wt (Figure 14A and B). Again, the 3Mts was the slowest. The mean peak currents at ND 2.5 light intensity with the level of significant differences are shown in Figure 14C. For the variant LC, KT, HE-LC, and 3Mt current at ND 2.5 increased significantly compared to CoChR-Wt, which indicated their enhanced

operational light sensitivity. Such increased response to lower light intensity was superior for the 3Mts. These enhancements can also be clearly noticed by comparing responses represented in red lines in the earlier Figure 12. Evidently, the 3Mts generated significantly highest current (at ND 2.5) among all. To determine the relationship between slower off-rates and improved operational light sensitivity, the mean peak currents at lower light intensity (ND 2.5) were plotted against their respective off-rates (Figure 14D). The trend line in the graph indicates a linear relationship for all the variants, which supports the hypothesis of slowing the off rate to improve operational light sensitivity of CoChR.

Higher currents at lower light intensity (ND 2.5) might be due to the overall larger (maximum) current at the brightest light (ND 0). The ratio of current at these two light intensities (ND 2.5/ND 0) indicates the percentage of maximum current generated at lower light intensity. Such ratio distinguishes variant(s) with truly improved operational light sensitivity. For instance, a variant CoChR-K264T generated current comparable to CoChR-L112C at lower light intensity (640 ± 90.7 pA and 593 ± 91.5 pA respectively; refer Table 5), but its ratio to the maximum current, i.e. at ND 0, is not significantly different than the wild type CoChR (Figure 14E). On the contrary, such ratio for a variant CoChR-L112C is significantly higher than wild type CoChR. This implies that the CoChR-L112C have truly improved operational light sensitivity in contrast to the CoChR-K264T. Other variants with significantly higher ND2.5/ND 0 current ratio include HE/LC, LC/KT and HE/LC/KT (3Mts). Evidently, for the 3Mts variant this ratio was the highest (59%) and significantly higher than both the CoChR-Wt (25%) as well as the LC

(41%). Thus, the operational light sensitivity of the 3Mt variant was improved 34%, i.e. from 25% (Wt) to 59% (3Mts).

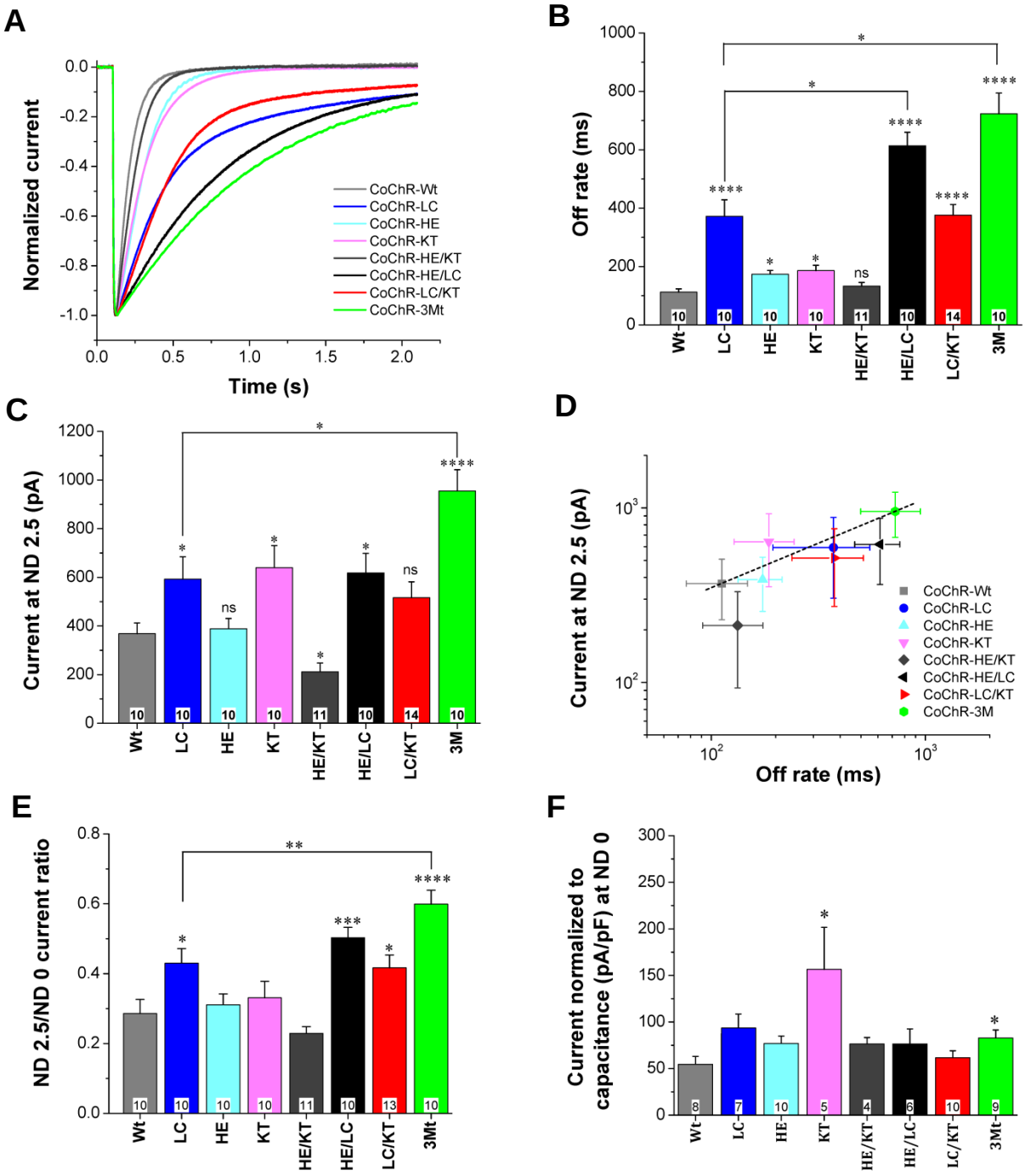

Figure 14: Kinetic properties of CoChR variants characterized in HEK293 cells. A) Representative traces of 10 ms pulse (ND 0) stimulation, for different variants, to compare off kinetics (deactivation). **B)** Mean off-rates (deactivation time constant) comparison. These deactivation time constants were obtained by fitting a single exponential function to the decaying phase of the current evoked by 10 ms pulse at ND 0, as shown in A. C) Comparison of mean peak currents at ND 2.5 (low light intensity), elicited with 1 second light pulse of 480 nm. D) The relationship plot between the off-rates and the peak current at low

light intensity (ND 2.5) , E) ND 2.5 to ND 0 current ratio representing light sensitivity in terms of percentage of maximum current generated, F) Peak current normalized to respective cell capacitance, at ND 0.Data presented as mean + SEM error bars. The “n” numbers are indicated in white box over the top of the X-horizon at their respective bars. ND0 = 8.9 x 10^{17} photons/cm^2s, ND 2.5 = 3.7 x 10^{15} photons/cm^2s.

Figure 14F shows the peak current normalized to the capacitance, which represents the current density. The current density correlates with the number of channels on cell surface (expression level), channel open time, and single channel conductance. Consistent with the observed higher expression level of the variant CoChR-KT, current density (pA/pF) was found to be significantly higher compared to CoChR-Wt (Figure 14F). Such current density was also significantly higher for the CoChR-3Mt, which is consistent with its longer channel open time since its expression level was not different from CoChR-Wt (see Figure 10B).

Since the magnitude of the current generated was light intensity dependent, a dosage response curve was generated to obtain the threshold light intensity required to generate half-maximum current (Ip50). It is referred to as effective power density for 50% activation (EPD50), which is similar to the EC50 (Mattis et al., 2012). Such dose response curve shifted leftward for all variants compared to that of the CoChR-Wt (Figure 15A). Especially for the 3Mt variant, it was the most leftward shifted, and its EPD50 was lowest among all (Figure 15B), which is consistent with its higher operational light sensitivity. Moreover, the EPD50 and the off rate were highly correlated (Figure 15C), suggesting that the off rate contributed to higher operational light sensitivity which is again consistent with proposed hypothesis.

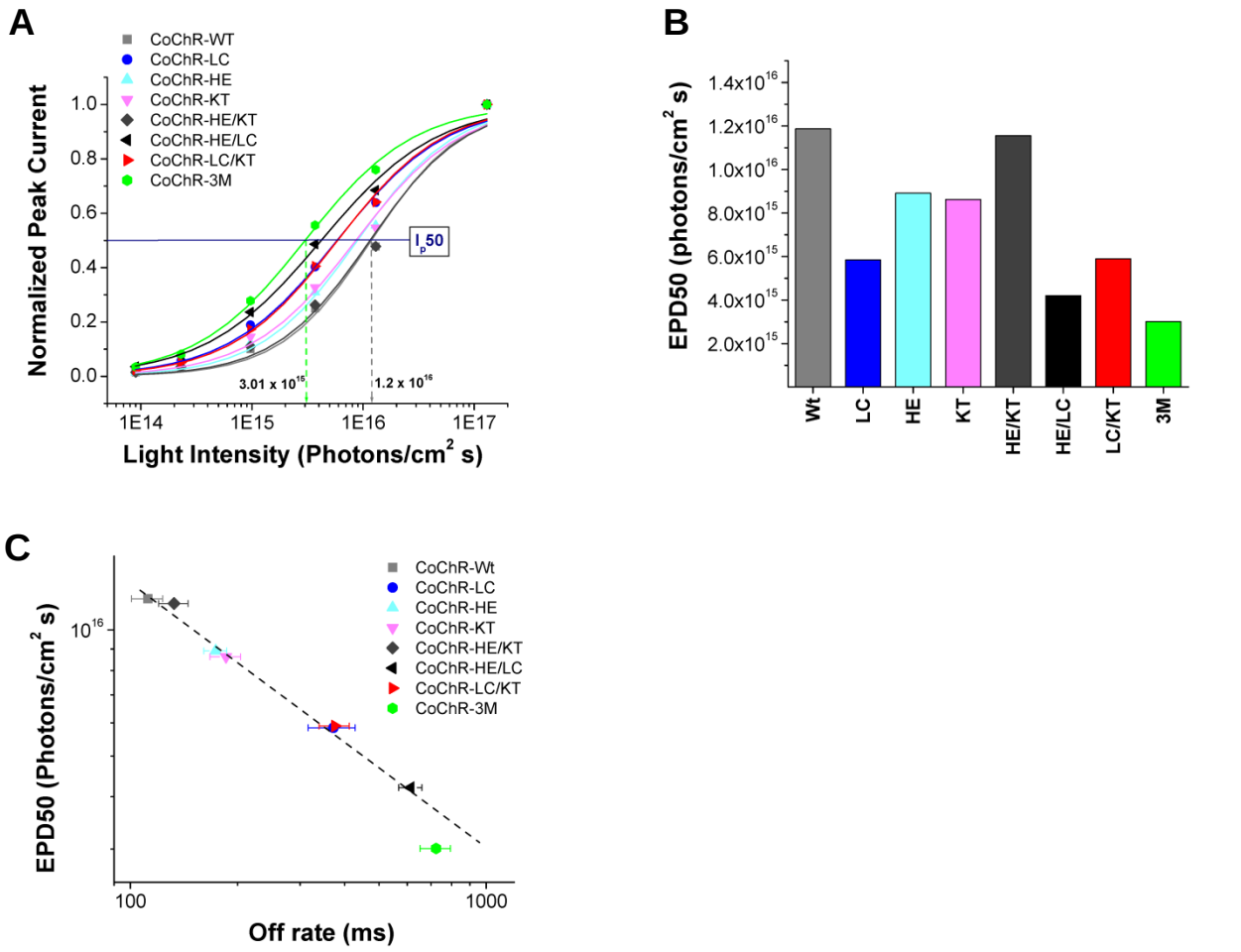

Figure 15: Light sensitivity comparisons between CoChR variants. A) Dosage response curve generated using nonlinear least square fitter function; $y(x) = \{A_1\text{-}A_2/1+(x/x_0)^p\} + A_2$, where A_1 = initial y value, A_2 = final y value, x_0 = center value, p = power. **B)** EPD50, i.e. effective power density to generate half-max current. **C)** EPD50 vs off rate (± SEM) relationship plot.

Conclusion:

For the first time to the best of my knowledge, I have identified two additional sites and specific mutations, i.e. H94E and K264T, which together in combination with L112C mutation (i.e. CoChR-HE-LC-KT), further enhanced the operational light sensitivity of CoChR (beyond the CoChR-L112C). This newly engineered variant CoChR-3Mts (CoChR-HE-LC-KT) has promise to be a better optogenetic tool for the ChR based optogenetic approach to restore vision.

Discussion:

For improving light sensitivity of CoChR, mutations were introduced at amino acid sites L112, T139, C108, and D136, corresponding to the L132, T159, C128 and D156 of ChR2. Except for the mutants L112C and L112A, all of these either showed poor expression in HEK cells or no significant improvement in current at ND 2.5 light intensity as a consequence of slower off-rate. However, the off rate of the variant L112A was above the anticipated 1s limit.

Additionally, a point mutation variant K264T (KT), interrupting a likely ER-retrieval signal sequence of CoChR, was tested. Evidently, the KT variant had higher current density (pA/pF) owing to its superior expression level in the plasma membrane. It showed significantly enhanced expression level with little slower off-rate, which together contributed to its higher photocurrent at lower light intensity (ND 2.5). However, this was not considered as increased operational light sensitivity since the current ratio of ND2.5/ND0 was not significantly higher than that of the CoChR-Wt. Such a ratio helps to segregate the mutants with improved operational light sensitivity from those with improved protein expression.

Another mutant variant H94E was created to test whether or not a negatively charged amino acid E (at the site H94) can inhibit cation influx of CoChR. In addition to the CoChR-Wt, two of its variants L112C and K264T were also tested for H94E mutation effect. No cation inhibition was found since all the variants carrying the H94E mutation, i.e. HE alone, HE-LC, HE-KT and HE-LC-KT (3Mts), were fully functional. Moreover, the triple mutant variant HE-LC-KT (3Mts) was found to be the most light-sensitive CoChR variant reported to date. This 3Mts variant exhibited slower off rate as

well as the least of current desensitization. These properties together contributed to its highest current, especially at low light intensity, implying its higher operational light sensitivity.

Differences in intrinsic light sensitivity of the channel, off kinetics or both can cause differences in EPD50, also referred to as population light sensitivity (Mattis et al., 2012). The intrinsic light sensitivity of the channel is simply the efficiency with which an individual channel gets activated by light (Sugimaya et al., 2009). For the selected CoChR variants, their operational light sensitivity was found to be correlated with slowed off-rates, and this is consistent with proposed hypothesis.

Overall, the CoChR-3Mt was identified as an optimized and most light sensitive ChR variant for several reasons based on data obtained. First, its expression and membrane trafficking was as good as CoChR-Wt. Second, it generated largest current at lower light intensity, implying its highest operational light sensitivity. Third, its slower off rate was still within the anticipated limit of 1 second, and hence, it can be expected to render suitable temporal coding ability to CoChR-3Mts expressing RGCs *in-vivo*. Fourth, it showed lowest EPD50 indicating its higher operational light sensitivity.

CHAPTER 3: IMPROVING LIGHT SENSITIVITY OF ReaChR

Introduction:

Since current ChR based optogenetic vision restoration requires supremely high intensity light stimulation (>10^{16} photons/cm^2 s), the longer wavelength light (red light) is considered safer (at such high intensity) than the shorter wavelength light (blue light). ReaChR is a chimera of two different ChRs, VChR1 and VChR2, from the algal species Volvox carteri, developed by Lin et al. in 2013. Its peak spectral sensitivity was observed at 530 nm which is 60 nm red shifted than that of ChR2 (470 nm), and this is an advantage over using blue light sensitive ChRs in general. It has been shown to restore visual response in mouse model of retinal degeneration (rd1), macaque retina and post mortem retinas of RP patients (Sengupta et al., 2016). However, the responses were evoked only at the higher light intensity (>10^{15} photons/cm^2s; 590 nm) and no further efforts were made to improve operational light sensitivity of the ReaChR. Such a high intensity was described to be safer (for the retina tissue) only because of the red spectral sensitivity (at 590 nm) of the ReaChR compared to that of the ChR2. Therefore, the development of the ReaChR variant with enhanced operational light sensitivity was desired.

Based on its light response properties in HEK cells, the ReaChR appears to be equally efficient as ChR2 (Table 6, Figure 16). For instance, the ReaChR generated lager current at low light intensity (ND2.5) than that of the ChR2-Wt and ChR2-L132C/T159C owing to its slower off rate. The current-kinetics relationship curve further clarifies it as the data point of ReaChR followed the relationship line of ChR2 (Figure 16). Hence, the operational light sensitivity of ReaChR could be improved by slowing its

kinetics via molecular engineering approach. Such optimized variant(s) will have an additional advantage of red-shifted peak spectral sensitivity.

Table 6: Comparison of light response properties of wild type ReaChR (ReaChR-Wt), ChR2 and its optimized variants. Data for ChR2 and its variants (tested at 460nm) are taken from Pan et al. 2014. Data are presented at mean ± SEM. ReaChR tested at 530nm. For 530nm ND0 = 8.5 x 10^{17} photons/cm^2s, ND 2.5 = 3.5 x 10^{15} photons/cm^2s.

ChR variants	N	Off-rate (ms)	Peak current (pA)	
		ND 0	ND0	ND2.5
ReaChR-Wt	10	414 ± 28	782 ± 69	291 ± 23
ChR2-Wt	7	18 ± 1	782 ± 84	26 ± 2.5
ChR2-L132C/T159C	6	199 ± 17	1062 ± 11	212 ± 19
ChR2-L132C/T159S	9	1090 ± 64	1037 ± 69	470 ± 34

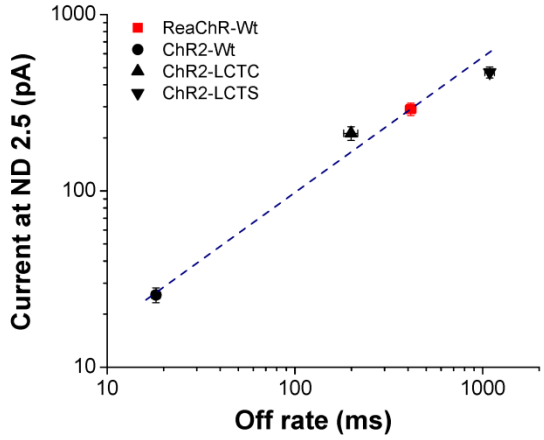

Figure 16: Comparison of current-kinetics relationship of ReaChR and ChR2 variants.

Aim2: Improving light sensitivity of ReaChR via molecular engineering.

Rationale:

Slowing channel's off-kinetics has been reported to increase operational light sensitivity of the ChR2 (Pan et al., 2014). A possible reason is that the longer the time a channel remains open more the cations move into the cell which is estimated as larger current amplitude. An example includes ChR2 mutants C128T, D156A, L132C, L132A, T159C, T159S, and double mutants L132C/T159C and L132C/T159 (Berndt et al., 2009;

Pan et al., 2014). In addition to the slower off rate, the ChR2-L132C mutant also showed reduced desensitization and increased Ca^{++} ion permeability contributing to its larger plateau photocurrent (Prigge et al., 2012). It was hypothesized that corresponding mutations in the ReaChR may result in similar gain. For the ReaChR, the amino acids L172, C199, C168, and D196 were corresponding to the ChR2-L132, T159, C128, and D156, respectively (see Figure 5), and they were mutated accordingly. Briefly, the L172 was mutated to “A”, “S”, “C” and “D”; the C199 was mutated to ‘A’, ‘S’ and ‘G’; the C168 was mutated to ‘A’ and ‘T’; the D196 was mutated to ‘C’ and ‘T’. These specific mutations at respective sites were chosen because similar mutations, at corresponding sites, have been shown to slower ChR2’s off rate (Berndt et al., 2009; Pan et al., 2014). Similarly, it was hypothesized that corresponding mutants of ReaChR might slow down its off rate and consequently some of them also improve current response at lower light intensity. Hence, primarily all these mutant variants were screened for their off rate kinetics and current level in response to low light intensity (ND 2.5) via whole cell patch clamp recordings.

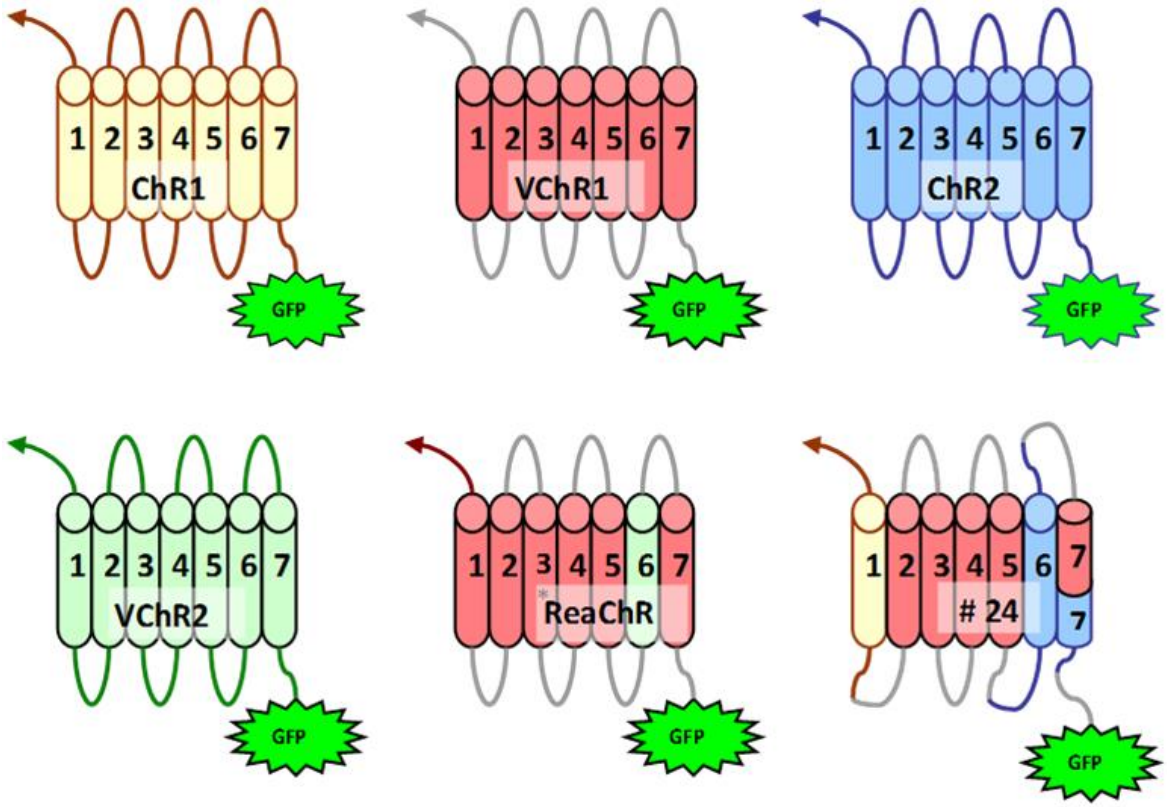

Figure 17: Schematics of chimeras ReaChR and #24 (and their constituent ChRs) showing difference in their respective trans-membrane domains TM1, TM6 and TM7.

Next, ReaChR was compared with one of the designed chimera #24 (unpublished preliminary data), which has spectral property similar to the ReaChR. As shown in the Figure 17, the ReaChR and the chimera #24 have differences in the TM1, TM6 and TM7. In these regions, 16 sites differences (as shown in black boxes individually for ReaChR in Figure 5) were selected for performing mutation. These sites were chosen because most of them have identical amino acids between ChR2 and CoChR. The goal was to find mutations among these sites to enhance the operational light sensitivity of ReaChR. Therefore, logically first ReaChR residues V98, V99, V104, A105, G108, W109, A114, A117, L247, L251, R253, V268, M299, V302, N305 and K310 were mutated according to matching CoChR residues to generate V98I/V99T, V98F/V99G, V104I/A104L, G108M, G108I/W109Y, A114T, A117S, L247R,

L251V/R253T, V268I, M299C, V302L, N305H, V302L/N305H and K310E variants of the ReaChR. Upon preliminary screening of these ReaChR mutants, two new sites V302 and N305 were identified as potential new targets in addition to sites corresponding to the L132, T159, C128 and D156 of the ChR2. Hence, additional mutations were created at these two sites, which included V302A, V302M, V302C, V302I, V302S, N305A, N305R, N305C, N305D, N305W, V302L-N305C and V302M-N305C.

Next, the site I171 was chosen to mutate since it was originally mutated from L171 to I to increase photocurrent amplitude of a precursor variant of the ReaChR (Lin et al., 2013). Briefly, the residue I171 was mutated to M, A, C, S, N and T. Additionally, the mutation I171M was combined with a double mutant V302L/N305H to optimize the slower off rate within the anticipated limit of 1 s, and thus the triple mutant variant ReaChR-I171M/V302L/N305H (3Mt) was generated.

Additionally, the site N154 corresponding to CoChR-H94 was mutated to E, similar to CoChR-H94E. It was also mutated to C and in combination with its neighboring site G155 to create N154C and N154H/G155R (respectively based on ChR2-H114/R115, see Figure 5). As described earlier for the CoChR, for all of ReaChR mutants, their expression level, off rate and peak current at low light intensity (ND2.5) were checked via whole cell patch clamp recording. Since, these mutations were aimed to slow the off rate and consequently improve the current at low light intensity, any variant which did not fulfill this expectation were excluded from further detailed characterization.

Methods and Materials

Same as described for CoChR in the aim-1 section (see pages 26-29), except that the wavelength of the light used was 530 nm.

Results:

A) Targeted mutations at the sites corresponding to the ChR2

The results of the expression quality, off-rate, and the current amplitude to a low light intensity (ND 2.5) are tabulated in Table 7. Although the off rate of the mutants L172C, L172A, L172S, and C199A slowed significantly, it did not improve their current responses at low light (Figure 18). In fact, none of the mutants targeted to the amino acids L172, C199, C168, and D196 sites showed the increase in current (Figure 18B). On the contrary, the off rate for the mutants C199G, C168A, and C168T was accelerated which in turn reduced their current, except for C168A, which remained unaffected.

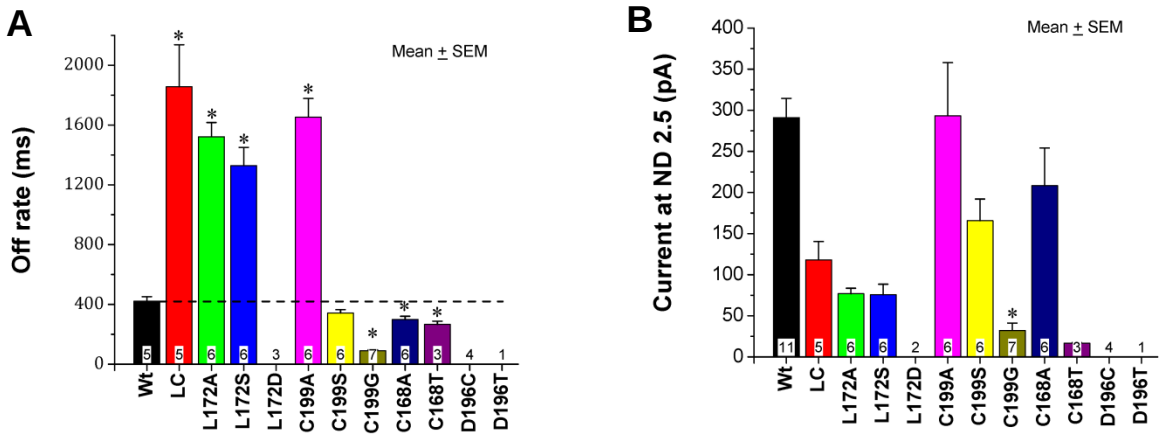

Figure 18: Primary screening of ReaChR variants for slowed off rate with improved current at ND 2.5. A) Mean off-rates (deactivation time constant) comparison. These deactivation time constants were obtained by fitting a single exponential function to the decaying phase of the current evoked by 10 ms pulse at ND 0. **B)** Comparison of mean peak currents at ND 2.5, elicited with 1 second light pulse of 530 nm. ND 2.5 = 3.5 x 10^{15} photons/cm^2s.

Table 7: Light response properties of ReaChR variants (part-1); characterized in HEK293 cells by whole cell patch clamp recordings at 530 nm. Expression level grading; ▲▲▲▲ = good, ▲▲▲Δ = fairly good, ▲▲▲ = fair, ▲▲Δ and ▲▲ = poor. Data are presented as mean ± SEM. ND0 = 8.5 x 10^{17} photons/cm^2s, ND 2.5 = 3.5 x 10^{15} photons/cm^2s.

ReaChR	N	Expression	Off-rate (ms)	Peak Current (pA)
Variants		**Full =▲, Half =Δ**	**ND 0**	**ND2.5**
		Aggregations = *		
ReaChR-Wt	11	▲▲▲▲	414 ± 28	291 ± 23
L172C	5	▲▲▲▲	1856 ± 281	118 ± 22.3
L172A	6	▲▲▲	1522 ± 95	77 ± 7
L172S	6	▲▲▲	1328 ± 122	76 ± 13
L172D	2	▲	No current	No current
C199A	6	▲▲▲▲	1653 ±124.22	293.4 ± 64.5
C199S	6	▲▲▲▲	342.5 ± 22	166 ± 26.3
C199G	7	▲▲▲	90 ± 6.5	32 ± 9
C168A	6	▲▲▲▲	299 ± 21.5	208 ± 46
C168T	3	▲▲▲▲	266 ± 22	17 ± 1
D196C	4	▲▲▲	No current	No current
D196T	1	▲▲Δ	No current	No current

In summary, mutations at the sites corresponding to the ChR2 mutants failed to improve the operational light sensitivity of ReaChR. This suggested that the amino acid residues involved in ReaChR's ion conduction pathway differer from those of ChR2. Therefore, finding different target sites that can slow its kinetics was desired.

B) Targeted mutations based on the chimera #24:

Firstly, mutant variants at 16 different sites were screened for differences in off rate and peak current. The ReaChR mutants G108I/Y109W, V302L, N305H, and V302L/N305H were found to slow the off rate significantly (Figure 19A). Among them, the double mutant V302L/N305H (VL/NH) exhibited an increase in the current significantly (Figure 19B). Although the current increased for the variant VL/NH, its off rate (~1.67 s; Table 8) appeared to be too slow for optogenetic vision restoration.

Nevertheless, the results identified the mutations V302L and N305H that were able to slow the kinetics and improve the current. Additional mutations were created at these two sites to find better ReaChR variant.

An alternative approach was to combine the VL/NH mutant with additional mutations to accelerate its off rate to within one second. One such mutation was I171M. Therefore, the triple mutant of I171M/V302L/N305H (IM/VL/NH or 3Mt) was created. Furthermore, these three sites (I171, V302 and N305) were explored with different amino acid replacements, and their combinations (Figure 19). Among these, the mutation I171M upon combining with VL/NH accelerated its off rate from ~1.7 s to ~900 ms (Table 8), i.e. within the limit of 1 s. Also as expected, the acceleration of the off rate of the 3Mt reduced its current amplitude in compared to VL/NH; however, the current was still significantly larger than that of wild type ReaChR (Figure 19B).

The 3Mts (IM/VL/NH) generated the best performance among all of the mutations tested (Figure 19, Table 8). Moreover, none of the additional mutations of 3Mts improved its light response property. Thus, in summary, two sites V302 and N305 were identified, which improved the light sensitivity of ReaChR. In particular, two mutant variants, ReaChR-VL/NH and ReaChR-3Mts, with improved operational light sensitivity were found. ReaChR-3Mts was characterized further because of its optimized kinetics and improved light sensitivity.

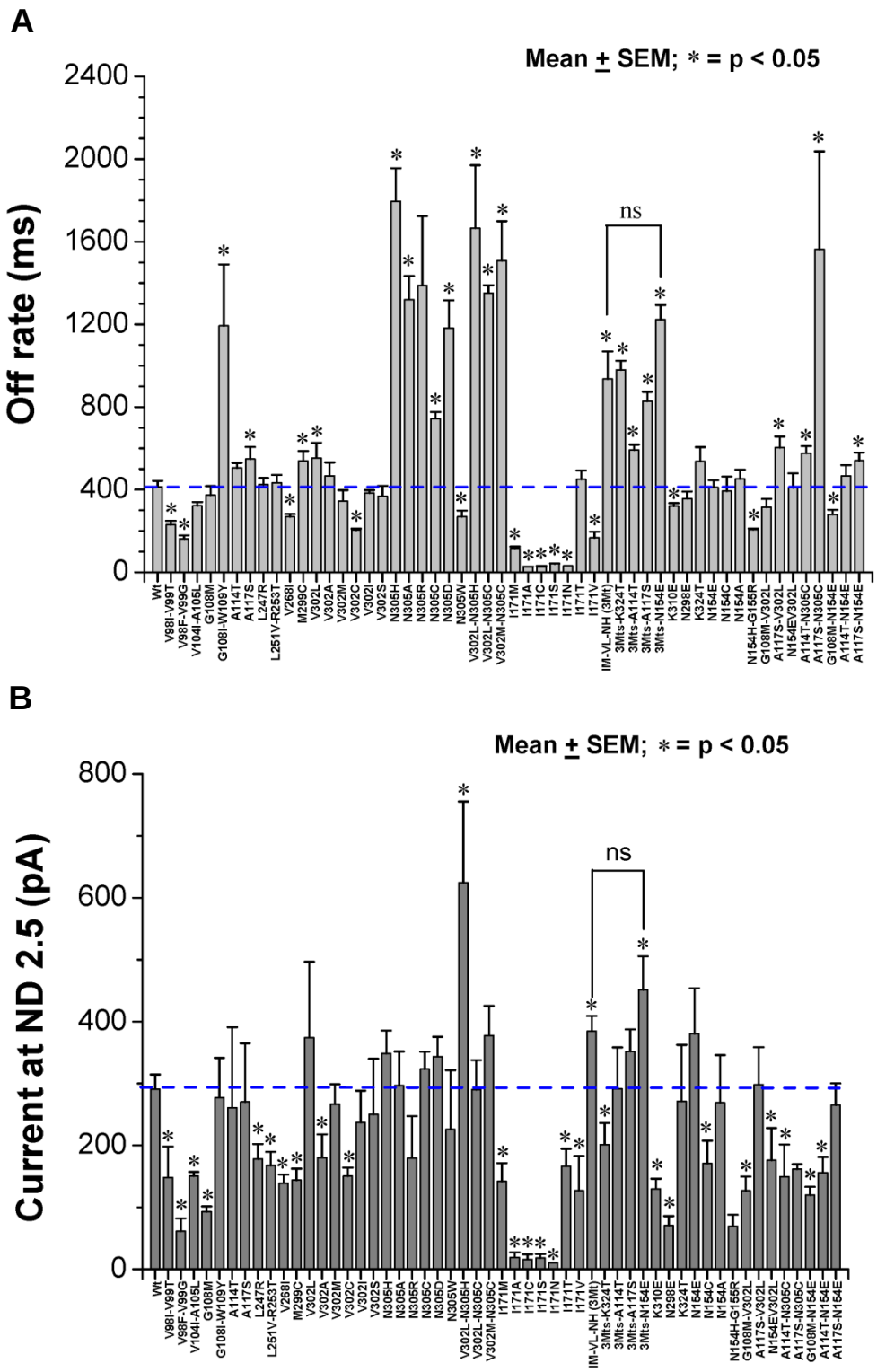

Figure 19: Primary screening of additional ReaChR variants for slowed off rate with improved current at ND 2.5. A) Mean off-rates (deactivation time constant) comparison. These deactivation time constants were obtained by fitting a single exponential function to the decaying phase of the current evoked by 10 ms pulse at ND 0. **B)** Comparison of mean peak currents at ND 2.5, elicited with 1 s light pulse of 530 nm. ND 2.5 = 3.5 x 10^{15} photons/cm^2s.

Table 8: Light response properties of additional ReaChR variants (part-2); characterized in HEK293 cells by whole cell patch clamp recordings at 530 nm. Expression level grading; ▲▲▲▲ = good, ▲▲▲Δ = fairly good, ▲▲▲ = fair, ▲▲Δ, ▲▲ = poor, and * = aggregations. ND0 = 8.5 x 10^{17} photons/cm^2s, ND 2.5 = 3.5 x 10^{15} photons/cm^2s.

ReaChR	N	Expression	Off-rate (ms)	Peak current (pA)
Variants		**Full =▲, Half =Δ**	**ND 0**	**ND2.5**
ReaChR-Wt	11	▲▲▲▲	414 ± 28	291 ± 23
V98I-V99T	4	▲▲▲Δ	230 ± 19	148 ± 50
V98F-V99G	3	▲▲▲Δ	162 ±16.5	61.5 ± 21
V104I-A105L	3	▲▲▲	322 ± 18	151 ± 6.5
G108M	3	▲▲▲Δ	374 ± 43	93 ± 8.6
G108I-W109Y	4	▲▲▲▲	1193 ± 297	277.4 ± 64
A114T	2	▲▲▲Δ	505 ± 24	261 ± 130
A117S	3	▲▲▲▲	548 ± 58	270 ± 95
L247R	8	▲▲Δ	425 ± 32	178 ± 24
L251V-R253T	8	▲▲▲	434 ± 38	167.4 ± 22.3
V268I	5	▲▲▲ + *	269 ± 13	139 ± 14
M299C	4	▲▲▲Δ + *	540 ± 47	144 ± 18.4
V302L	4	▲▲Δ + *	554 ± 73	374.4 ± 122
V302A	4	▲▲▲▲	467 ± 64	180.4 ± 37.5
V302M	7	▲▲▲Δ	345 ± 53	266.5 ± 32
V302C	3	▲▲▲Δ	204 ± 6	150.5 ± 13.6
V302I	4	▲▲▲▲	384 ± 14	237 ± 51
V302S	3	▲▲▲+ *	369 ± 49	250 ± 90
N305H	7	▲▲▲Δ	1796 ± 160.4	348.5 ± 37.2
N305A	3	▲▲▲Δ	1320 ± 114	297 ± 55
N305R	4	▲▲Δ	1389 ± 334	180 ± 67.5
N305C	8	▲▲▲Δ	744 ± 32	323 ± 28
N305D	7	▲▲▲	1182 ± 134	343.6 ± 32
N305W	3	▲▲▲Δ	269 ± 29	226 ± 95.6
V302L-N305H	7	▲▲▲Δ	1665.71 ± 304.55	624.36 ± 131.11
V302L-N305C	8	▲▲▲Δ	1351.67 ± 38.25	290.13 ± 47.82
V302M-N305C	7	▲▲▲Δ	1508.00 ± 191.19	377.60 ± 47.71
I171M	7	▲▲▲	116.23 ± 7.94	142.01 ± 29.38
I171A	4	▲▲▲Δ	26.53 ± 1.01	19.19 ± 7.91
I171C	3	▲▲▲	26.90 ± 4.02	15.85 ± 8.29
I171S	4	▲▲▲Δ	40.95 ± 1.36	18.15 ± 6.40
I171N	1	Toxic	31 ± 0.0	10.4 ± 0.0
I171T	4	▲▲▲▲Δ	450 ± 42.5	166 ± 28

Table 8 continued…!				
I171V	3	▲▲Δ	167 ± 29	127 ± 56
IM-VL-NH (3Mt)	11	▲▲▲▲	935 ± 133.5	385 ± 24
3Mts-K324T	4	▲▲▲	979.5 ± 44	201 ± 35
3Mts-A114T	6	▲▲▲	592 ± 26	292 ± 66.5
3Mts-A117S	6	▲▲▲	828 ± 45.5	352 ± 35.4
3Mts-N154E	6	▲▲▲▲	1223 ± 70	451 ± 54
K310E	10	▲▲Δ	320 ± 14.5	130 ± 16
N298E	6	▲▲▲Δ	356.5 ± 34.5	70.5 ± 15.4
K324T	5	▲▲▲▲	537 ± 69	271.3 ± 91
N154E	6	▲▲▲+ *	411 ± 34.5	380.4 ± 73.5
N154C	3	▲▲▲Δ	393 ± 70	171 ± 37
N154A	4	▲▲▲	452 ± 45	269 ± 77
N154H-G155R	3	▲▲▲+ *	207 ± 5	70 ± 18
G108M-V302L	2	▲▲▲	315 ± 40	127 ± 23
A117S-V302L	3	▲▲▲Δ	603 ± 54	299 ± 60.4
N154E-V302L	3	▲▲▲	410 ± 70	176 ± 52
A114T-N305C	3	▲▲▲▲	576 ± 34	149.6 ± 52
A117S-N305C	3	▲▲Δ	1563 ± 474	162 ± 8
G108M-N154E	3	▲▲▲Δ	280 ± 23	120 ± 13
A114T-N154E	4	▲▲▲Δ	467 ± 52	156 ± 25
A117S-N154E	3	▲▲▲	540 ± 39	265 ± 35

C) Characterizing the optimized variant ReaChR-3Mts (IM-VL-NH) in HEK cells.

First, ReaChR-3Mts's expression in HEK cells was compared with that of ReaChR-Wt. The representative images of HEK cell expressing wild type and 3Mts are shown in Figure 20A. There was no statistical difference found in quantified level of mean fluorescence intensity (AFU/Pixel^2) of these two (Figure 20B).

The light response properties were characterized in HEK cells with whole cell patch clamp recordings. The peak spectral sensitivity and the overall spectral curve for the ReaChR-3Mt variant shifted towards blue with the peak at around 500 nm compared to 530 nm of the wild type ReaChR (Figure 21A). However, for the comparison purpose

all the characterization was done with 530 nm light. The representative current traces in response to light with incremental intensity stimulation are shown in Figure 21B and C.

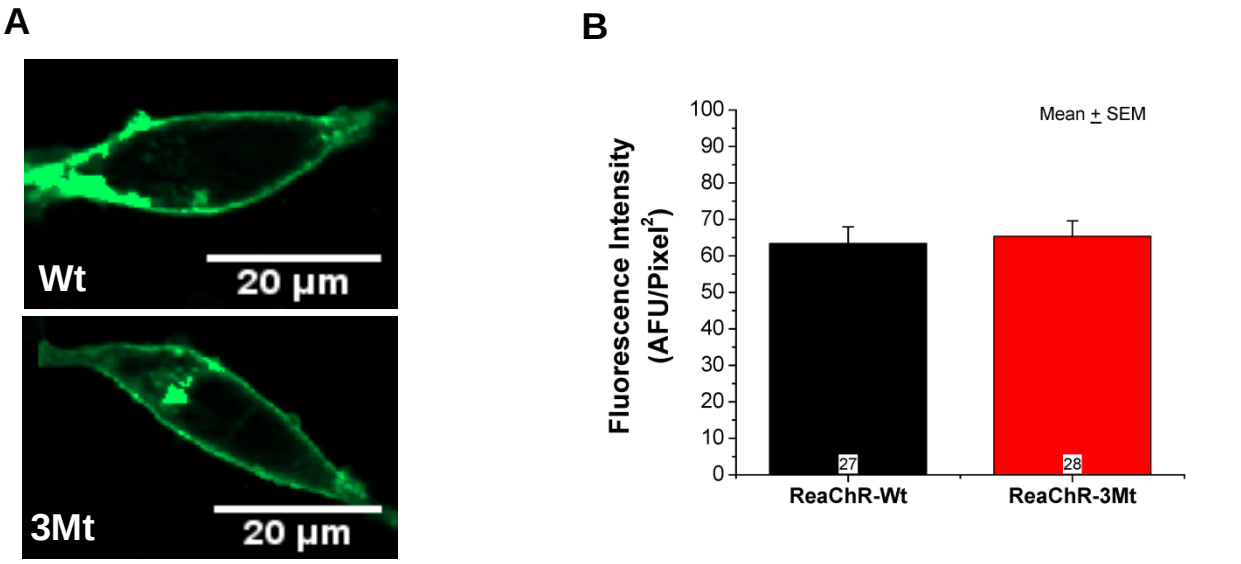

Figure 20: **Expression level comparison in HEK293 cells. A)** Representative image of HEK293 cell expression of ReaChR-Wt and its variant 3Mt (I171M-V302L-N305H). Scale bar 20 um. **B)** Mean fluorescence intensities measured in plasma membrane region, and it is represented as arbitrary fluorescence unit per pixel area (AFU/pixel^2) ± SEM. The numbers (n) are shown in respective bars.

The values of the current responses and the kinetics are summarized in Table 9. For the ReachR-3Mt, the peak current at the highest light intensity (ND 0) observed was 842 ± 57, which is higher but not significantly different than that of the wild type ReaChR (782 ± 69) (Figure 22A). The level of peak current desensitization was reduced to 33% for the 3Mt compared to 45% of the wild type. This is represented in Table 9 as a ratio of plateau current (I_{Pla}) and peak current (I_P), and this ratio for 3Mt variant is significantly higher than that of the wild type ReaChR (Figure 22B). Overall, the current responses were light intensity dependent and the reduced desensitization contributed to higher currents (both peak and plateau) at different lower light intensities (Figure 22C and D).

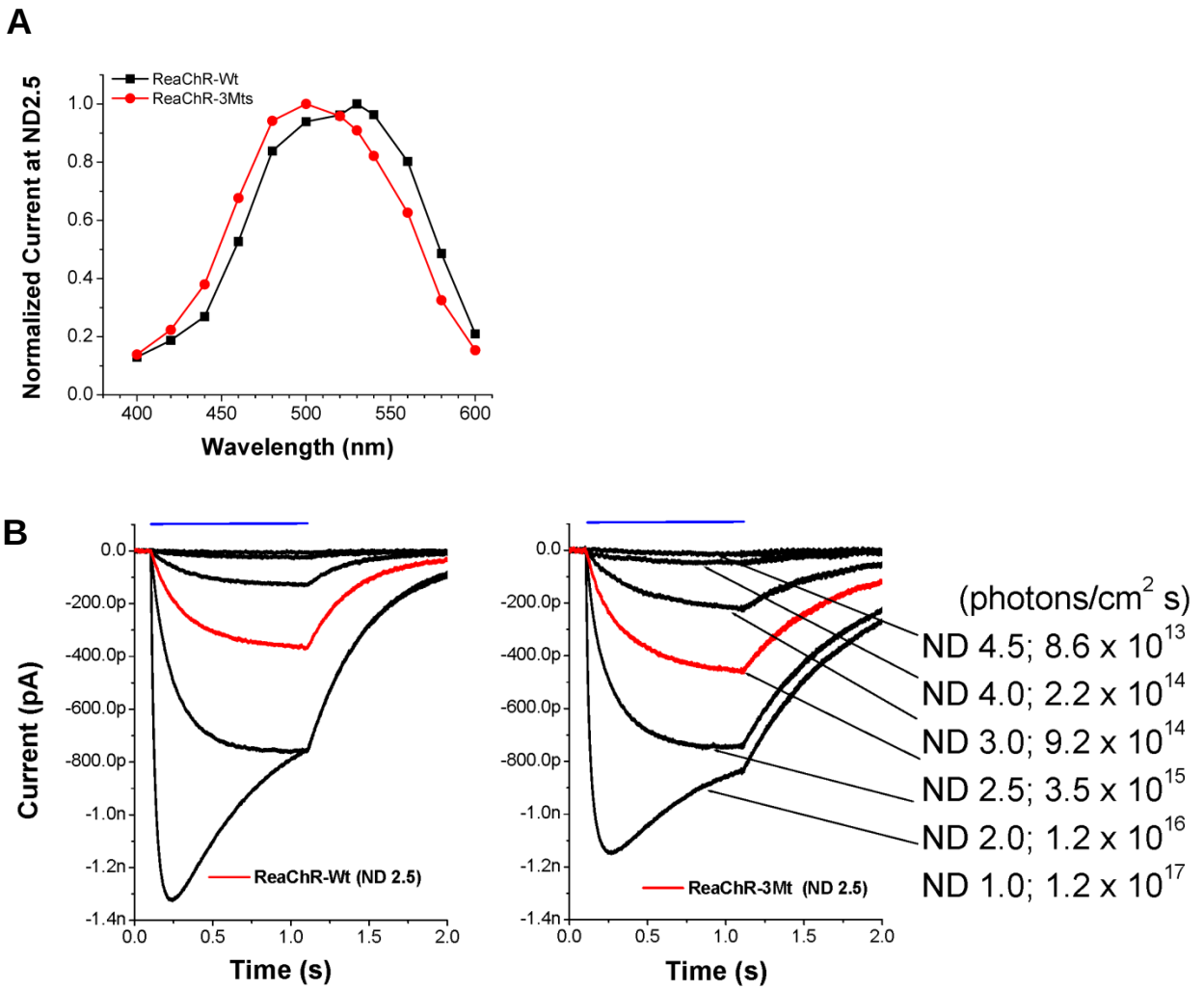

Figure 21: **Spectral and Current properties of ReaChR variants. A)** Spectral curve comparison. **B)** Representative current traces mediated by CoChR and its variants in HEK293 cells. Responses were generated under voltage clamp (-60 mV) conditions with 1 second (530 nm) light stimulation. Light intensities were attenuated by neutral density filters ND 4.5, 4, 3, 2.5, 2 and 1.

Table 9: Light response properties of ReaChR-Wt and ReaChR-I171M-V302L-N305H (3Mt) variant; characterized in HEK293 cells by whole cell patch clamp recordings at 480 nm. Data presented as mean ± SEM. ND0 = 8.5 x 10^{17} photons/cm^2s, ND 2.5 = 3.5 x 10^{15} photons/cm^2s.

ReaChR Variants	N	Off rate (ms)	Peak Current (pA)		Ratios	
		ND 0	ND 0	ND 2.5	I_{Pla}/I_P	ND2.5/ND0
Wt	11	414 ± 28	782 ± 69	291 ± 23.34	0.55	0.37
3Mt	11	935 ± 133.5	841.5 ± 57	385 ± 24.28	0.67	0.46

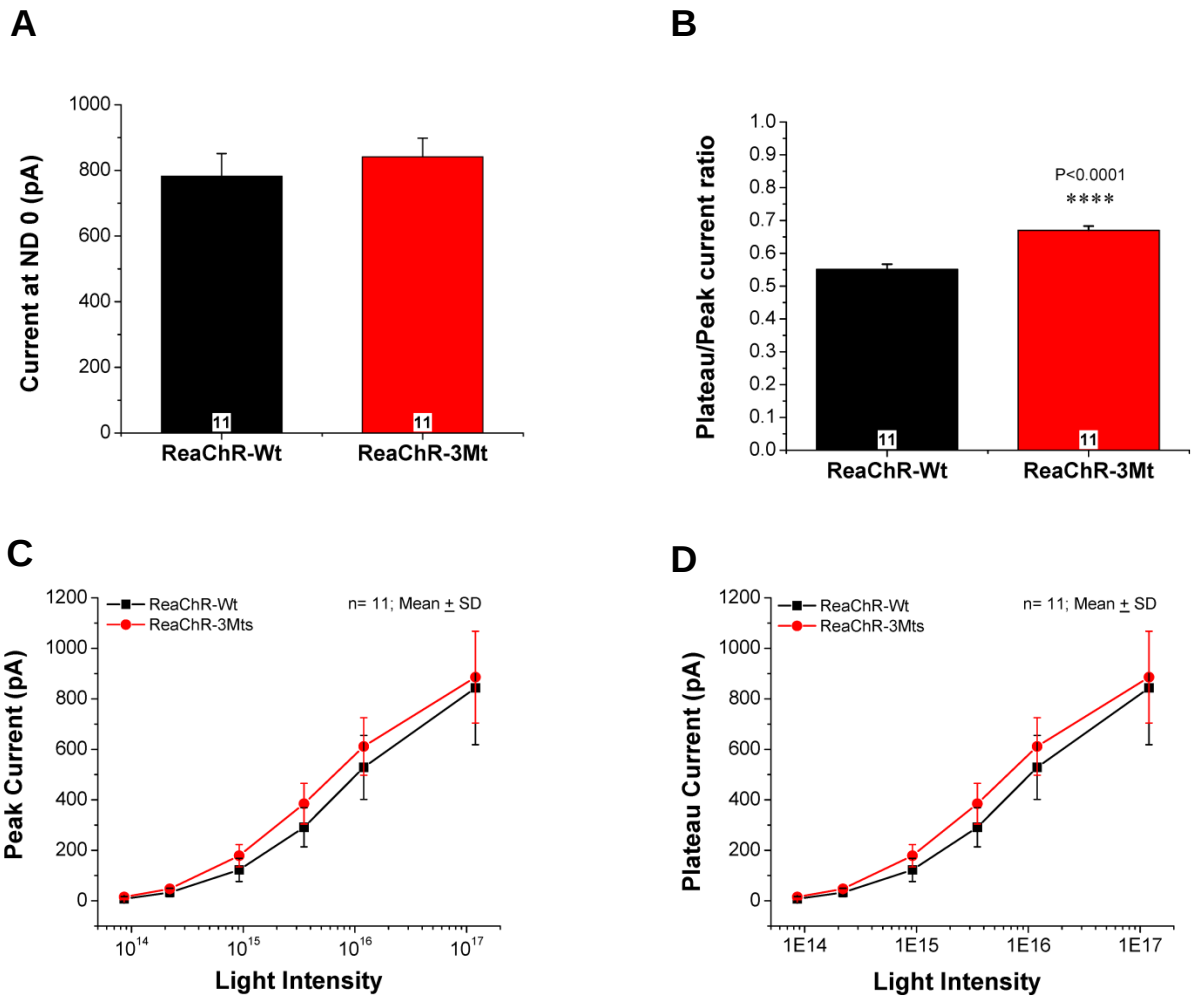

Figure 22: Comparison of current amplitudes at different light intensities of ReaChR variants. A) Mean peak currents at ND 0. **B)** Mean ratio of plateau to peak current at ND 0. **C** and **D)** Light intensity response curve. Peak and plateau currents were obtained in response to different light intensities of 530nm. ND0 = 8.5 x 10^{17} photons/cm^2s, ND 2.5 = 3.5 x 10^{15} photons/cm^2s.

As shown in Table 9, the channel off rate for the 3Mts variant observed was 935 ± 134 ms, which is significantly slower than that of the ReaChR-Wt, i.e. 414 ± 28 ms (Figure 23A and B). As anticipated, this led to increased current response at lower light intensity. In response to low light intensity the ReaChR-3Mts generated 385 ± 24 pA current which is significantly larger than that of the ReaChR-Wt (291 ± 23 pA) (Figure 23C). Upon plotting the off rate against the current, a trend line shows that the current amplitude of the ReaChRs is inversely related to its off rate, i.e. slower the off rate

larger is the current amplitude to the low light intensity (Figure 23D), which is consistent with proposed hypothesis.

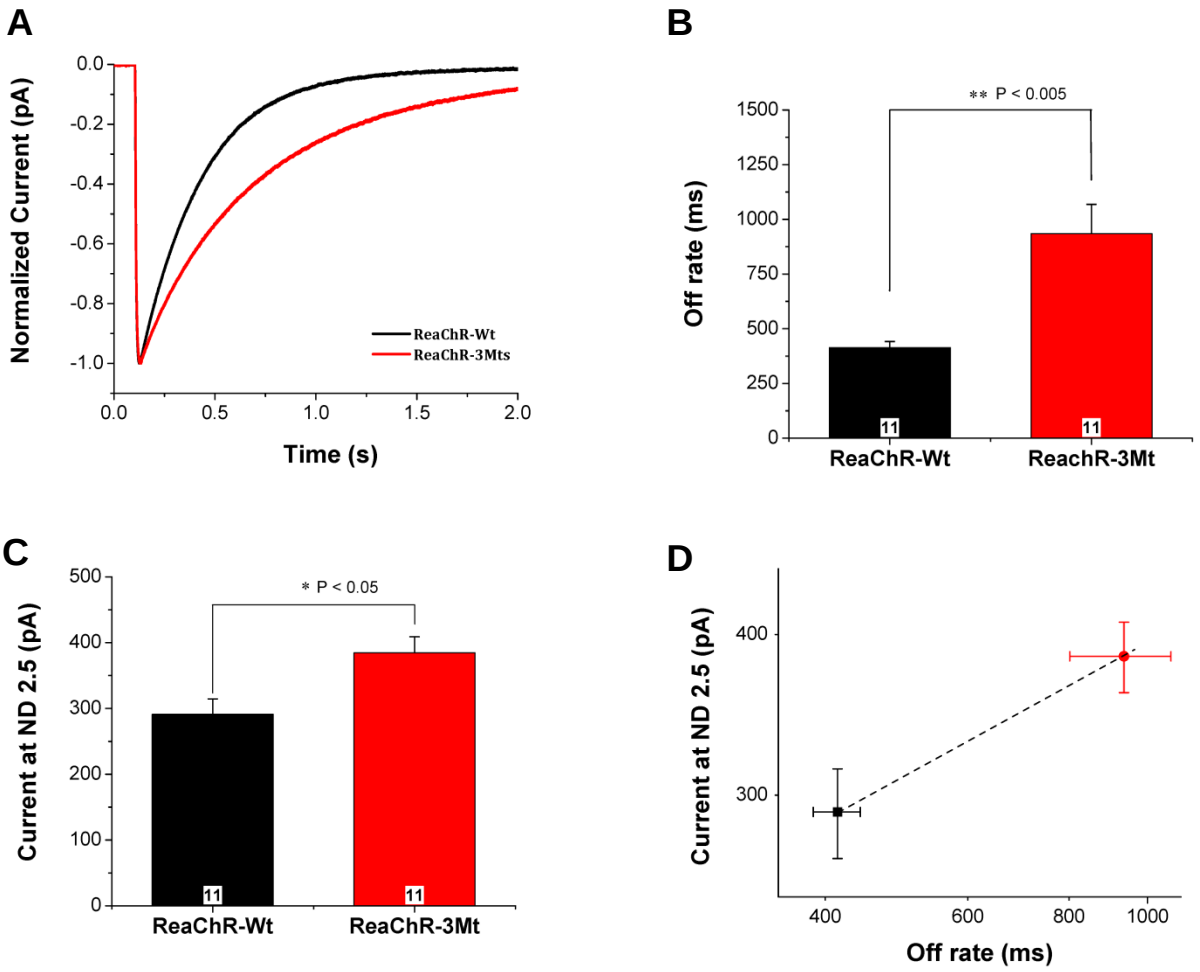

Figure 23: Kinetic properties of ReaChR variants characterized in HEK293 cells. A) Representative traces of 10 ms pulse (ND 0) stimulation, for different variants, to compare off kinetics (deactivation). **B)** Mean off-rates (deactivation time constant) comparison. These deactivation time constants were obtained by fitting a single exponential function to the decaying phase of the current evoked by 10 ms pulse at ND 0, as shown in A. **C)** Comparison of mean peak currents at ND 2.5 (low light intensity), elicited with 1 second light pulse of 530 nm. **D)** The relationship plot between the off-rates and the peak current at low light intensity (ND 2.5). Data presented as mean ± SEM error bars. The "n" numbers are indicated in white box over the top of the X-horizon at their respective bars. ND0 = 8.5×10^{17} photons/cm^{2}s, ND 2.5 = 3.5×10^{15} photons/cm^{2}s.

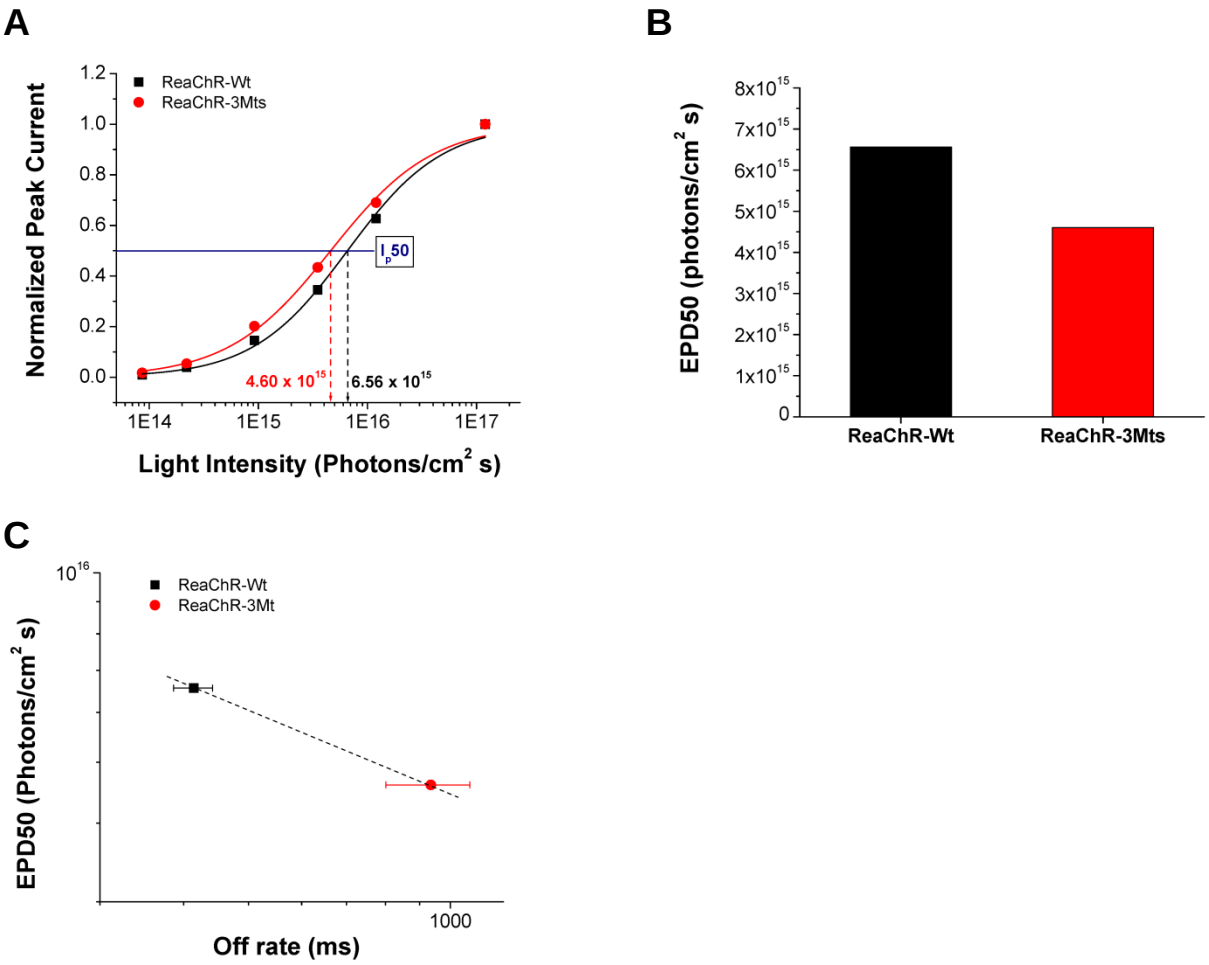

Figure 24: Light sensitivity comparisons. A) Dosage response curve generated using nonlinear least square fitter function; $y(x) = \{A_1\text{-}A_2/1+(x/x_0)^p\} + A_2$, where A_1 = initial y value, A_2 = final y value, x_0 = center value, p = power. **B)** EPD50, i.e. effective power density to generate half-max current. **C)** EPD50 vs off rate (± SEM) relationship plot.

Discussion:

The ReaChR is a chimeric ChR, which was originally optimized for its red spectral sensitivity. Its use as an optogenetic tool to restore light responses (via optogenetics) in rd1 mice, macaque as well as human retina has recently been reported (Sengupta et al., 2016). However, its light sensitivity is low. Here, several point mutations were explored to improve ReaChR's light sensitivity by slowing its kinetics (off rate). ReaChR mutations created at the sites corresponding to those improving light

sensitivity of ChR2 failed to enhance its light sensitivity. One possible reason can be the difference in their respective molecular determinants of channel function. Importantly, since ReaChR is a chimera of three different ChRs (ChR1, vChR1 and vChR2) it is difficult to relate the molecular determinants of just any one type of ChR, e.g. ChR2, with ReaChR. For instance, ReaChR has its majority of TM domains form VChR1 (see Figure 17 on page 47), which is more related to ChR1 (Zhang et al., 2008); and hence, ReaChR mutations at the sites corresponding to those enhancing current properties of ChR1 may improve its light sensitivity. However, such variants of ChR1 are not discovered yet

Alternatively, mutations screening based on our chimera #24 successfully identified variant V302H-N305H, which improved the light sensitivity of ReaChR as a consequence of slower off rate. However, its off rate exceeded the projected limit of 1 s. Therefore, the mutation I171M combined with V302H-N305H to optimize its off rate. The variant ReaChR-3Mts (I171M/V302H/N305H) found to be optimized and more light-sensitive variant of the ReaChR.

CHAPTER 4: SHIFTING SPECTRAL SENSITIVITY OF CoChR TOWARDS RED

Aim 3: To shift CoChR's spectral sensitivity towards red

By targeted mutations at the sites predicted to be nearby to β-ionone ring of the chromophore ATR.

Rationale:

Preliminary data from our laboratory indicated that the Chrimson is less efficient than ChR2, ReaChR and CoChR. Thus, red shift in peak spectrum of more efficient ChR variant CoChR was desirable. Recently, a polar to nonpolar amino acid difference around the β-ionone ring of the chromophore (retinal) has been proposed to be responsible for the diverse spectral sensitivity of primate red and green cone photoreceptors (Katayama et al., 2015). Interestingly, both Chrimson and ReaChR have polar amino acid residues around the β-ionone ring position, e.g. S223 of Chrimson and analogous ReaChR-S221 (Figure 5). Moreover, these residues are corresponding to one of the four amino acid residues predicted (by Zhang et al., 2008) for VChR1's red-shifted spectral sensitivity (see pages 18-19). Additionally, such polarity differences among blue light sensitive ChRs (CoChR and ChR2) and green-red light sensitive ChRs (ReaChR and Chrimson) revealed at two neighboring residues CoChR-S86-M87 (Figure 5). Thus, replacing polar and nonpolar residues according to the Chrimson at analogous positions in CoChR might shift the spectral sensitivity towards red. To test this hypothesis, four of the CoChR's non-polar residues M87, G161, I163, and M205 were mutated to polar residues, T, S, S and S, respectively. On the other hand, two polar residues S86 and S236 were mutated to a non-polar residue A. Thus, CoChR variant S86A/M87T, G161S, I163S, M205S, and S236A were generated.

Results:

For each mutant variant, current response to the short light pulses of 200 ms at ND2.5 with different wavelengths ranging from 400 nm to 600 nm was tested. Additionally, their off rate and current amplitude (at their respective λ_{max}) were also checked. The current amplitudes to each wavelength were normalized to respective maximum values (Table 10) then plotted to generate spectral curves. The peak spectral sensitivity remained unchanged for all mutant variants tested (Figure 25). However, the overall spectral curve for the mutant CoChR-S236A (SA) shifted ~9 nm towards the red (Figure 25A and B), and this remained effective with other combination of mutation too, i.e. S236A-K264T, SA-LC/TC and SA-3Mts (Figure 25C). On the other hand, the spectral curves for the mutations S86A/M87T, G161S, I163S and M205S appeared to be narrowed compared to CoChR-Wt.

The current and kinetic properties of these spectral shift mutants are summarized in Table 11. Compared to the CoChR-Wt, the off-rates significantly slowed for the spectral-shift mutants S86A-M87T, S236A, S236A-L112C-T139C, SA-K264T and SA-3Mt (Figure 26 A). Consequently, current at ND 2.5 was also improved for the variants S236A, SA/LC/TC and SA-3Mt, compared to the CoChR-Wt (Figure 26 B). However, the off-rates of SA/LA/TC and SA-3Mt were too slow (>3 s and 1.5 s respectively, see Table 12) to be useful. For any of these variants, no significant difference was found in currents at ND 0 (Figure 26C). For the mutant S236A, the ratio of current at ND 2.5 to current at ND 0 was not any different from that of the CoChR-Wt (Figure 25D). Hence, the improvement in current at low light intensity for CoChR-SA is not a true enhancement in its light sensitivity.

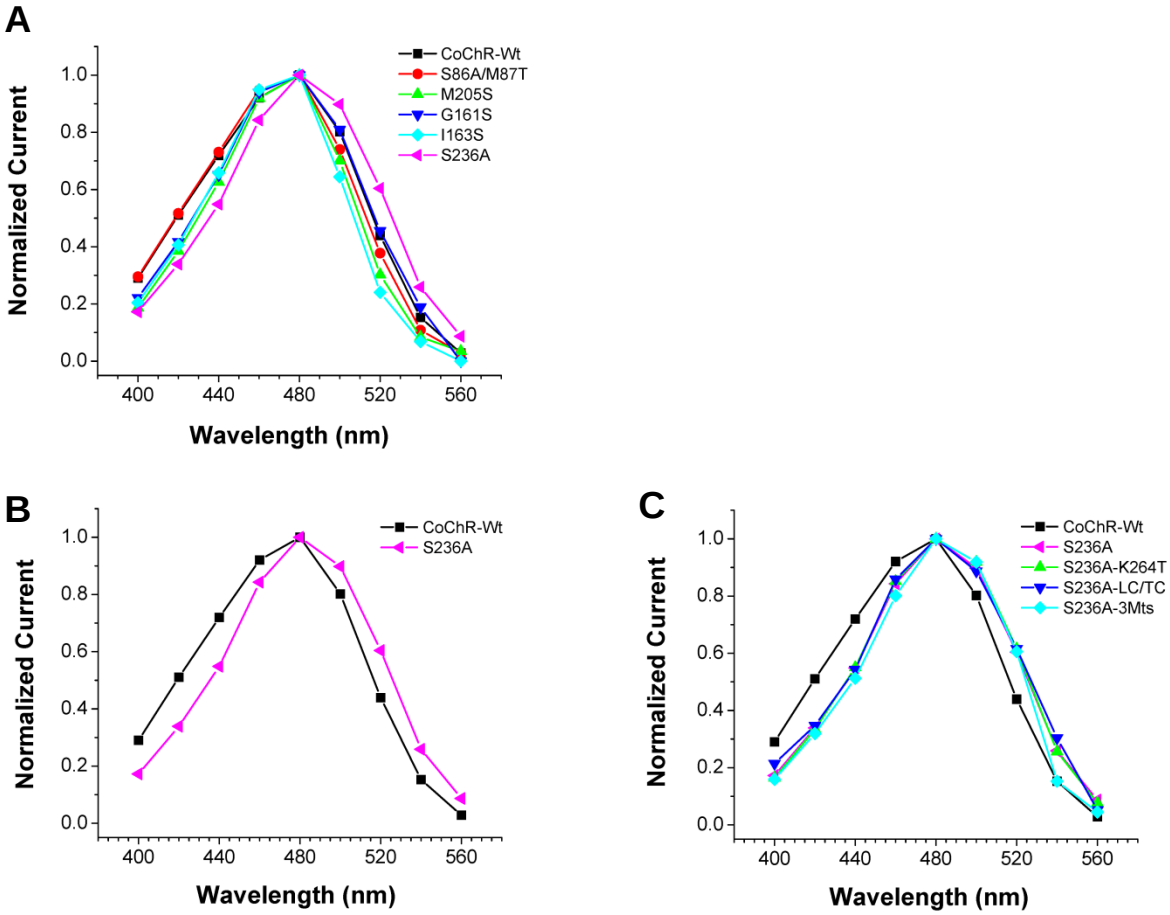

Figure 25: Spectral curve comparison for CoChR chimera variants. Responses to each wavelength (from 400 nm to 560 nm) were recorded under voltage clamp conditions (-60mV) at ND 2.5. **A)** Spectral curves of all variants together, **B)** Spectral curves of CoChR-Wt and S236A variant, **C)** Spectral curves of S236A/K264T, S36A/LC-TC and S236A/3Mt compared with CoChR-Wt.

Table 10: Normalized peak current, at different wavelength of light, of CoChR spectral mutant variants.

	Normalized currents at ND 2.5								
CoChR variants	**Wt**	**S86A-M87T**	**M205S**	**G161S**	**I163S**	**S236A (SA)**	**SA-K264T**	**SA-LC/TC**	**SA-3Mts**
λ (nm)									
400	0.29	0.29	0.18	0.22	0.19	0.15	0.15	0.17	0.15
420	0.51	0.51	0.37	0.40	0.40	0.31	0.31	0.31	0.30
440	0.72	0.73	0.62	0.64	0.64	0.52	0.52	0.52	0.50
460	0.92	0.95	0.91	0.92	0.93	0.83	0.83	0.85	0.79
480	**1.00**	**1.00**	**1.00**	**1.00**	**1.00**	**1.00**	**1.00**	**1.00**	**1.00**
500	0.80	0.72	0.70	0.81	0.66	0.90	0.92	0.91	0.92
520	0.44	0.35	0.30	0.46	0.26	0.59	0.60	0.63	0.61
540	0.15	0.10	0.08	0.18	0.07	0.24	0.25	0.29	0.18
560	0.03	0.03	0.03	0.00	0.00	0.07	0.11	0.04	0.06

Table 11: Light response properties of CoChR spectral mutant variants.

CoChR Variants	**N**	**Off rate (ms)**	**Current (pA)**		**Ratios**
		ND 0	**ND 0**	**ND 2.5**	**ND2.5/ND0**
Wt	10	112 ± 11	1465 ± 254	368.52 ± 44	0.29
S86A/M87T	5	263 ± 33	1415 ± 271	565.96 ± 166.3	0.37
G161S	5	79 ± 18	787 ± 152	114.89 ± 38	0.13
I163S	5	110 ± 18	1462 ± 160	234.94 ± 32.6	0.17
M205S	5	80.4 ± 21.5	1107 ± 335	154.37 ± 75	0.13
S236A (SA)	5	288 ± 43	1953 ± 405	619.12 ± 126	0.32
SA/LC-TC	5	3438 ± 664	1228.5 ± 227	872.10 ± 183	0.70
SA/KT	5	205 ± 27	2321 ± 240	512.20 ± 53.2	0.23
SA/3Mt	5	1574 ± 115.5	1598 ± 142	818.48 ± 73.6	0.52

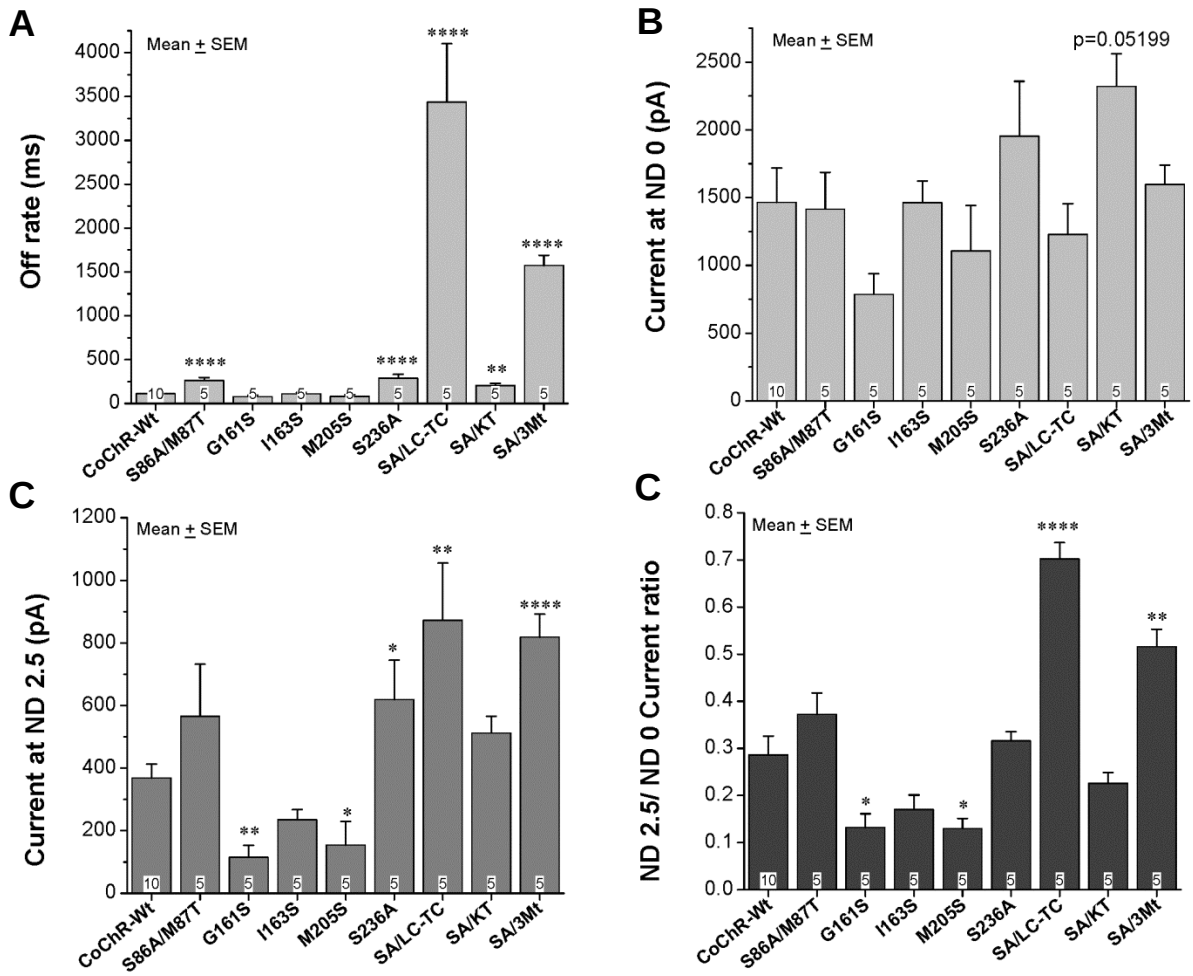

Figure 26: Light response properties of CoChR spectral mutant variants.

Discussion:

From the results obtained, it can be concluded that the residues targeted are not capable of shifting peak spectral sensitivity of the CoChR, at least not independently. However, the mutation at S236 shifted the overall spectral curve towards red, which suggests that it has some role in shifting the spectrum but not the peak sensitivity. Further analysis is required for identification of amino acid residues that influence spectral sensitivity of the CoChR. One possible approach attempted is discussed in next section.

By chimera approach to identify important regions for spectral sensitivity of the CoChR and Chrimson.

Rationale:

Alternatively, earlier studies have demonstrated that determinants of wavelength sensitivity reside on TM5 (E) and/or TM6 (F) for ChR2 and ChR1 (Wang et al., 2009; Wen et al, 2010). Moreover, preliminary data also suggest involvement of TM4, TM5 and TM7 in spectral red-shift (unpublished data.). Additionally, polar residues of red sensitive ChR variants described above are also located on ECL1, TM2, TM5, TM6 and TM7 (Figure 5). Thus, if not these proposed polar residue mutants alone, some other residues of TM4, TM5, TM6 and/or TM7 in combination could be the determinant of spectral sensitivity. To test this several chimeras of CoChR and Chrimson were generated. A schematic of chimeras designed by replacing different domains of the CoChR with that of Chrimson, in different combinations, are shown in Figures 27 and 28. All of the chimera gene sequences were synthesized and obtained from the GeneScript (Piscataway, NJ, USA).

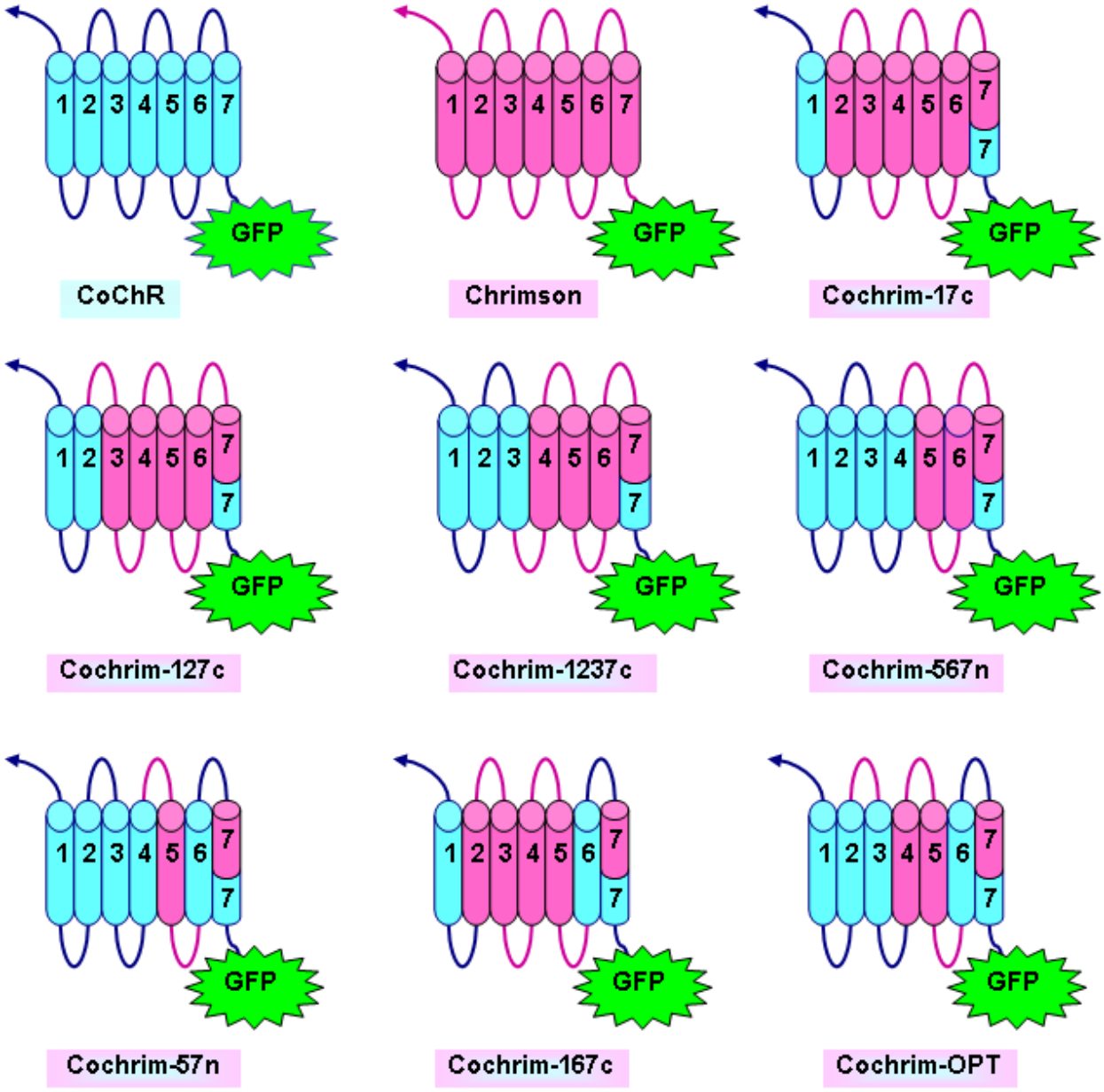

Figure 27: Schematic of proposed chimeras (Part-1). On the top left, first two represents CoChR (cyan) and Chrimson (pink) domains schematic as a reference for the different chimeras.

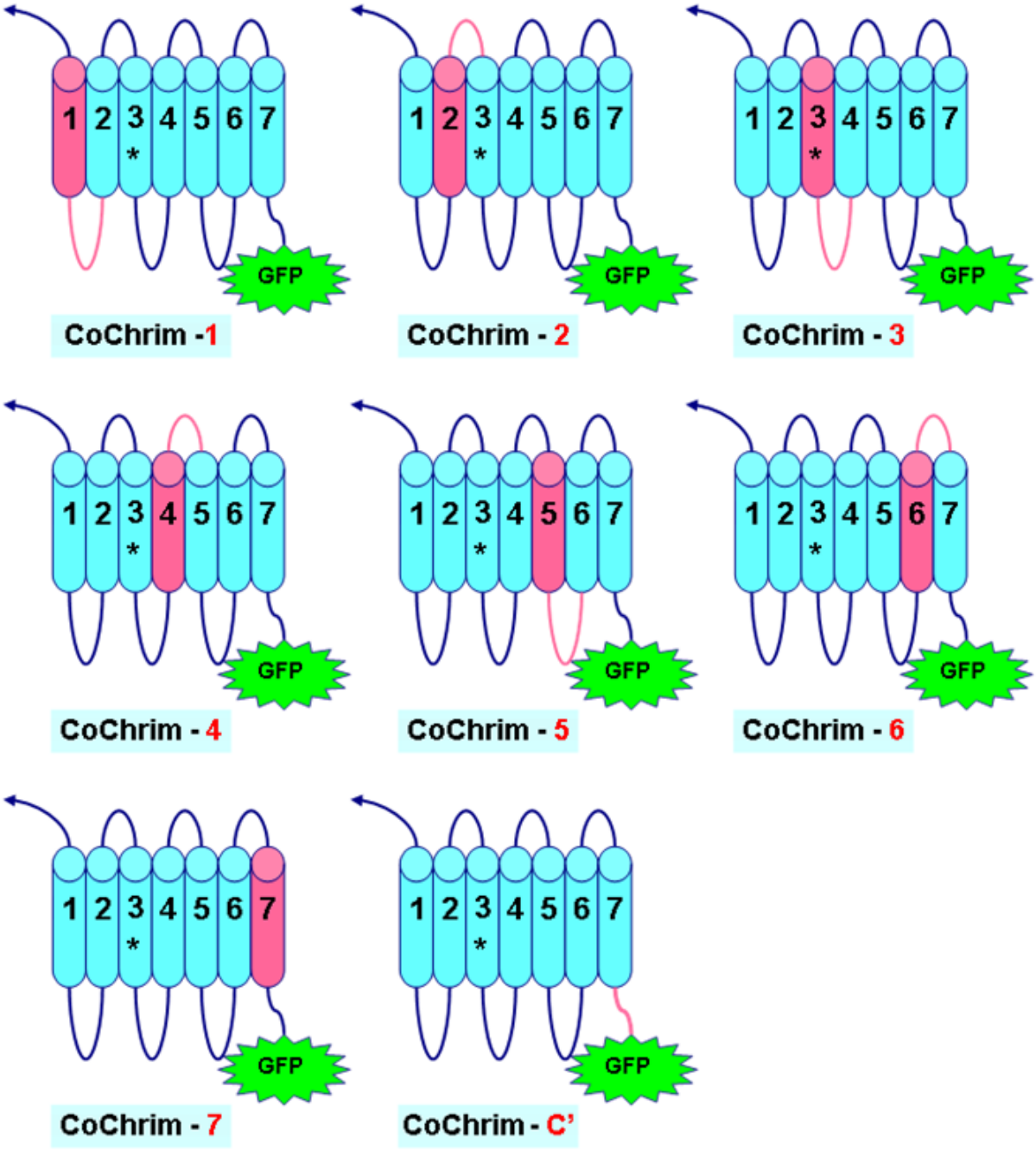

Figure 28: Schematic of proposed chimeras (Part-2).

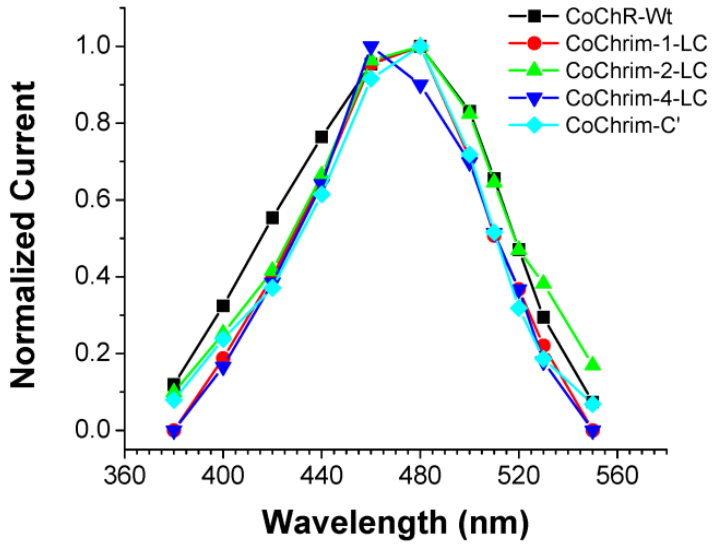

Figure 29: Spectral curve comparison for CoChrim chimera variants. Responses to each wavelength (from 400 nm to 560 nm) were recorded under voltage clamp conditions (-60mV) at ND 2.5.

Results:

Most of the chimeras did not express well and/or were toxic to the cells. Hence, out of the total 15 chimeras, only the chimeras CoChrim-1-LC, CoChrim-2-LC, CoChrim-4-LC and CoChrim-C' could be tested for their spectral sensitivity. The peak spectral sensitivity of the chimera CoChrim-4-LC found to shift from 480 nm to 460 nm (Figure 29). For all other tested chimeras, peak spectral sensitivity remained unchanged. None of the chimeras showed red shift in their spectral curve compared to the CoChR-Wt. Moreover, all four chimeric variants generated very small currents compared to the CoChR-Wt (Table 13).

Table 12: Normalized peak current, at different wavelength of light, of CoChR and Chrimson chimeras.

	Normalized currents at ND 2.5				
CoChR Chimeras	**CoChR-Wt**	**CoChrim-1-LC**	**CoChrim-2-LC**	**CoChrim-4-LC**	**CoChrim-C'**
λ (nm)					
380	0.12	0.00	0.10	0.00	0.08
400	0.32	0.19	0.25	0.17	0.24
420	0.55	0.40	0.42	0.38	0.37
440	0.76	0.65	0.66	0.64	0.61
460	0.95	0.95	0.96	**1.00**	0.92
480	**1.00**	**1.00**	**1.00**	0.90	**1.00**
500	0.83	0.71	0.82	0.70	0.72
510	0.66	0.51	0.65	0.51	0.52
520	0.47	0.37	0.47	0.37	0.32
530	0.29	0.22	0.38	0.18	0.19
550	0.07	0.00	0.17	0.00	0.07

Table 13: Peak current responses of the chimeras at different wavelength of light.

	Mean currents ± SEM (pA) at ND 2.5				
CoChR Chimeras	**CoChR-Wt**	**CoChrim-1-LC**	**CoChrim-2-LC**	**CoChrim-4-LC**	**CoChrim-C'**
λ(nm)	**n = 3**	**n = 2**	**n = 2**	**n = 2**	**n = 2**
380	63.7 ± 21	0.0 ± 0.0	8.6 ± 0.5	0.0 ± 0.0	13 ± 3
400	173 ± 46	7.5 ± 7.5	22 ± 4	7 ± 7	38.4 ± 0.0
420	295 ± 60	16 ± 2.7	36.2 ± 3.4	16.1 ± 5.1	60 ± 10
440	408 ± 63	26 ± 6.2	58 ± 5.8	27 ± 11.4	99.3 ± 15.5
460	509 ± 60	38.3 ± 8.4	84 ± 6.2	**42 ± 15.5**	148 ± 21
480	**534 ± 60.3**	**40 ± 8.5**	**87.2 ± 6.9**	38 ± 14.4	**162 ± 23**
500	443 ± 77.2	28.5 ± 5.6	72 ± 10.4	29.3 ± 11	116 ± 13.3
510	350± 79	20.3 ± 4	56.3 ± 10.6	21.5 ± 8	83.4 ± 12.2
520	251 ± 69.5	15 ± 2	41 ± 8	15.4 ± 5.5	51.5 ± 5.6
530	157 ± 53	9 ± 1	33 ± 7	7.5 ± 7.5	30.2 ± 5
550	39.3 ± 14	0.0 ± 0.0	15 ± 3.7	0.0 ± 0.0	11 ± 3

Discussion:

Poor or toxic expression in HEK cells significantly limited the spectral sensitivity evaluation of majority of the designed chimeras. However, from the tested chimera results, it appears that the residues of the TM1, TM2, TM4 and the C' terminal do not play a major role in red-spectral selectivity, at least not by themselves alone. In addition, some residues of the TM3, TM5, TM6 and TM7 seem to be very important for the ChR expression. Careful screenings of amino acid differences on these TMs, by replacing one residue at a time, to exclude residues affecting the expression so severely might be a way to test their (TM3, 5, 6 and 7) effect on spectral sensitivity. Alternatively, one can also screen for the residues affecting spectral sensitivity. Nevertheless, it is important to keep in mind that spectral properties can be the cumulative effect of different residues on all or some TMs, and hence, more thorough investigation is required to develop/shift the spectral sensitivity towards red.

APPENDIX

Table 14: The amino acid codes and categories.

Amino acid codes and types			
Amino acid	**Three letters code**	**Single letter code**	**Amino acid type**
Arginine	Arg	R	Positively charged
Histidine	His	H	Positively charged, Sulfur containing
Lysine	Lys	K	Positively charged
Aspartic aicd	Asp	D	Negatively charged
Glutamic acid	Glu	E	Negatively charged
Serine	Ser	S	Polar
Threonine	Thr	T	Polar
Aspargine	Asn	N	Polar
Glutamine	Gln	Q	Polar
Cysteine	Cys	C	Special class, Sulfur containing
Glycine	Gly	G	Special class
Proline	Pro	P	Special class
Alanine	Ala	A	Hydrophobic
Iso-leucine	Ile	I	Hydrophobic
Leucine	Leu	L	Hydrophobic
Metheonine	Met	M	Hydrophobic
Phenylalanine	Phe	F	Hydrophobic
Tryptophan	Trp	W	Hydrophobic
Tyrosine	Tyr	Y	Hydrophobic
Valine	Val	V	Hydrophobic

REFERENCES

FDA approves novel gene therapy to treat patients with a rare form of inherited vision loss. (2017). [Press release]. Retrieved from https://www.fda.gov/newsevents/newsroom/pressannouncements/ucm589467.htm

Awasthi, M., Ranjan, P., Sharma, K., Veetil, S. K., and Kateriya, S. (2016). The trafficking of bacterial type rhodopsins into the Chlamydomonas eyespot and flagella is IFT mediated. *Sci Rep, 6*, 34646. doi:10.1038/srep34646

Babitzki, G., Denschlag, R., and Tavan, P. (2009). Polarization effects stabilize bacteriorhodopsin's chromophore binding pocket: a molecular dynamics study. *J Phys Chem B, 113*(30), 10483-10495. doi:10.1021/jp902428x

Barrett, J. M., Berlinguer-Palmini, R., and Degenaar, P. (2014). Optogenetic approaches to retinal prosthesis. *Vis Neurosci, 31*(4-5), 345-354. doi:10.1017/s0952523814000212

Berndt, A., Lee, S. Y., Wietek, J., Ramakrishnan, C., Steinberg, E. E., Rashid, A. J., . . . Deisseroth, K. (2016). Structural foundations of optogenetics: Determinants of channelrhodopsin ion selectivity. *Proc Natl Acad Sci U S A, 113*(4), 822-829. doi:10.1073/pnas.1523341113

Berndt, A., Schoenenberger, P., Mattis, J., Tye, K. M., Deisseroth, K., Hegemann, P., and Oertner, T. G. (2011). High-efficiency channelrhodopsins for fast neuronal stimulation at low light levels. *Proc Natl Acad Sci U S A, 108*(18), 7595-7600. doi:10.1073/pnas.1017210108

Berndt, A., Yizhar, O., Gunaydin, L. A., Hegemann, P., and Deisseroth, K. (2009). Bi-stable neural state switches. *Nat Neurosci, 12*(2), 229-234. doi:10.1038/nn.2247

Berson, D. M., Dunn, F. A., and Takao, M. (2002). Phototransduction by retinal ganglion cells that set the circadian clock. *Science, 295*(5557), 1070-1073. doi:10.1126/science.1067262

Berson, E. L., Rosner, B., Sandberg, M. A., Weigel-DiFranco, C., and Willett, W. C. (2012). omega-3 intake and visual acuity in patients with retinitis pigmentosa receiving vitamin A. *Arch Ophthalmol, 130*(6), 707-711. doi:10.1001/archophthalmol.2011.2580

Bi, A., Cui, J., Ma, Y. P., Olshevskaya, E., Pu, M., Dizhoor, A. M., and Pan, Z. H. (2006). Ectopic expression of a microbial-type rhodopsin restores visual responses in mice with photoreceptor degeneration. *Neuron, 50*(1), 23-33. doi:10.1016/j.neuron.2006.02.026

Busskamp, V., Duebel, J., Balya, D., Fradot, M., Viney, T. J., Siegert, S., . . . Roska, B. (2010). Genetic reactivation of cone photoreceptors restores visual responses in retinitis pigmentosa. *Science, 329*(5990), 413-417. doi:10.1126/science.1190897

Cai, J., Nelson, K. C., Wu, M., Sternberg, P., Jr., and Jones, D. P. (2000). Oxidative damage and protection of the RPE. *Prog Retin Eye Res, 19*(2), 205-221.

Cehajic-Kapetanovic, J., Eleftheriou, C., Allen, A. E., Milosavljevic, N., Pienaar, A., Bedford, R., . . . Lucas, R. J. (2015). Restoration of Vision with Ectopic Expression of Human Rod Opsin. *Curr Biol, 25*(16), 2111-2122. doi:10.1016/j.cub.2015.07.029

Chang, B., Hawes, N. L., Hurd, R. E., Davisson, M. T., Nusinowitz, S., and Heckenlively, J. R. (2002). Retinal degeneration mutants in the mouse. *Vision Res, 42*(4), 517-525.

Cideciyan, A. V. (2010). Leber congenital amaurosis due to RPE65 mutations and its treatment with gene therapy. *Prog Retin Eye Res, 29*(5), 398-427. doi:10.1016/j.preteyeres.2010.04.002

Cideciyan, A. V., Sudharsan, R., Dufour, V. L., Massengill, M. T., Iwabe, S., Swider, M., . . . Beltran, W. A. (2018). Mutation-independent rhodopsin gene therapy by knockdown and replacement with a single AAV vector. *Proc Natl Acad Sci U S A, 115*(36), E8547-e8556. doi:10.1073/pnas.1805055115

Cronin, T., Vandenberghe, L. H., Hantz, P., Juttner, J., Reimann, A., Kacso, A. E., . . . Bennett, J. (2014). Efficient transduction and optogenetic stimulation of retinal bipolar cells by a synthetic adeno-associated virus capsid and promoter. *EMBO Mol Med, 6*(9), 1175-1190. doi:10.15252/emmm.201404077

Cuenca, N., Fernandez-Sanchez, L., Campello, L., Maneu, V., De la Villa, P., Lax, P., and Pinilla, I. (2014). Cellular responses following retinal injuries and therapeutic approaches for neurodegenerative diseases. *Prog Retin Eye Res, 43*, 17-75. doi:10.1016/j.preteyeres.2014.07.001

Daiger, S. P., Sullivan, L. S., and Bowne, S. J. (2013). Genes and mutations causing retinitis pigmentosa. *Clin Genet, 84*(2), 132-141. doi:10.1111/cge.12203

de Jong, P. T. (2006). Age-related macular degeneration. *N Engl J Med, 355*(14), 1474-1485. doi:10.1056/NEJMra062326

Deisseroth, K. (2011). Optogenetics. *Nat Meth, 8*(1), 26-29. doi:10.1038/nmeth.f.324

Deisseroth, K., Feng, G., Majewska, A. K., Miesenbock, G., Ting, A., and Schnitzer, M. J. (2006). Next-generation optical technologies for illuminating genetically targeted brain circuits. *J Neurosci, 26*(41), 10380-10386. doi:10.1523/jneurosci.3863-06.2006

Doroudchi, M. M., Greenberg, K. P., Liu, J., Silka, K. A., Boyden, E. S., Lockridge, J. A., . . . Horsager, A. (2011). Virally delivered channelrhodopsin-2 safely and effectively restores visual function in multiple mouse models of blindness. *Mol Ther, 19*(7), 1220-1229. doi:10.1038/mt.2011.69

Eisenhauer, K., Kuhne, J., Ritter, E., Berndt, A., Wolf, S., Freier, E., . . . Gerwert, K. (2012). In channelrhodopsin-2 Glu-90 is crucial for ion selectivity and is deprotonated during the photocycle. *J Biol Chem, 287*(9), 6904-6911. doi:10.1074/jbc.M111.327700

Ernst, O. P., Lodowski, D. T., Elstner, M., Hegemann, P., Brown, L. S., and Kandori, H. (2014). Microbial and Animal Rhodopsins: Structures, Functions, and Molecular Mechanisms. *Chem Rev, 114*(1), 126-163. doi:10.1021/cr4003769

Fariss, R. N., Li, Z. Y., and Milam, A. H. (2000). Abnormalities in rod photoreceptors, amacrine cells, and horizontal cells in human retinas with retinitis pigmentosa. *Am J Ophthalmol, 129*(2), 215-223.

Govorunova, E. G., Sineshchekov, O. A., Janz, R., Liu, X., and Spudich, J. L. (2015). NEUROSCIENCE. Natural light-gated anion channels: A family of microbial rhodopsins for advanced optogenetics. *Science, 349*(6248), 647-650. doi:10.1126/science.aaa7484

Gradinaru, V., Zhang, F., Ramakrishnan, C., Mattis, J., Prakash, R., Diester, I., . . . Deisseroth, K. (2010). Molecular and cellular approaches for diversifying and extending optogenetics. *Cell, 141*(1), 154-165. doi:10.1016/j.cell.2010.02.037

Greenberg, K. P., Pham, A., and Werblin, F. S. (2011). Differential targeting of optical neuromodulators to ganglion cell soma and dendrites allows dynamic control of center-surround antagonism. *Neuron, 69*(4), 713-720. doi:10.1016/j.neuron.2011.01.024

Gunaydin, L. A., Yizhar, O., Berndt, A., Sohal, V. S., Deisseroth, K., and Hegemann, P. (2010). Ultrafast optogenetic control. *Nat Neurosci, 13*(3), 387-392. doi:10.1038/nn.2495

Hartong, D. T., Berson, E. L., and Dryja, T. P. (2006). Retinitis pigmentosa. *Lancet, 368*(9549), 1795-1809. doi:10.1016/s0140-6736(06)69740-7

Hatori, M., and Panda, S. (2010). The emerging roles of melanopsin in behavioral adaptation to light. *Trends Mol Med, 16*(10), 435-446. doi:10.1016/j.molmed.2010.07.005

Hattar, S., Liao, H. W., Takao, M., Berson, D. M., and Yau, K. W. (2002). Melanopsin-containing retinal ganglion cells: architecture, projections, and intrinsic photosensitivity. *Science, 295*(5557), 1065-1070. doi:10.1126/science.1069609

Hegemann, P., Ehlenbeck, S., and Gradmann, D. (2005). Multiple photocycles of channelrhodopsin. *Biophys J, 89*(6), 3911-3918. doi:10.1529/biophysj.105.069716

Ivanova, E., Hwang, G. S., Pan, Z. H., and Troilo, D. (2010). Evaluation of AAV-mediated expression of Chop2-GFP in the marmoset retina. *Invest Ophthalmol Vis Sci, 51*(10), 5288-5296. doi:10.1167/iovs.10-5389

Ivanova, E., and Pan, Z.-H. (2009). Evaluation of the adeno-associated virus mediated long-term expression of channelrhodopsin-2 in the mouse retina. *Molecular Vision, 15*, 1680-1689.

Katayama, K., Okitsu, T., Imai, H., Wada, A., and Kandori, H. (2015). Identical Hydrogen-Bonding Strength of the Retinal Schiff Base between Primate Green- and Red-Sensitive Pigments: New Insight into Color Tuning Mechanism. *J Phys Chem Lett, 6*(7), 1130-1133. doi:10.1021/acs.jpclett.5b00291

Kato, H. E., Zhang, F., Yizhar, O., Ramakrishnan, C., Nishizawa, T., Hirata, K., . . . Nureki, O. (2012). Crystal structure of the channelrhodopsin light-gated cation channel. *Nature, 482*(7385), 369-374. doi:10.1038/nature10870

Klapoetke, N. C., Murata, Y., Kim, S. S., Pulver, S. R., Birdsey-Benson, A., Cho, Y. K., . . . Boyden, E. S. (2014). Independent optical excitation of distinct neural populations. *Nat Methods, 11*(3), 338-346. doi:10.1038/nmeth.2836

Kleinlogel, S., Feldbauer, K., Dempski, R. E., Fotis, H., Wood, P. G., Bamann, C., and Bamberg, E. (2011). Ultra light-sensitive and fast neuronal activation with the Ca(2)+-permeable channelrhodopsin CatCh. *Nat Neurosci, 14*(4), 513-518. doi:10.1038/nn.2776

Kuhne, J., Eisenhauer, K., Ritter, E., Hegemann, P., Gerwert, K., and Bartl, F. (2015). Early formation of the ion-conducting pore in channelrhodopsin-2. *Angew Chem Int Ed Engl, 54*(16), 4953-4957. doi:10.1002/anie.201410180

Lagali, P. S., Balya, D., Awatramani, G. B., Munch, T. A., Kim, D. S., Busskamp, V., . . . Roska, B. (2008). Light-activated channels targeted to ON bipolar cells restore visual function in retinal degeneration. *Nat Neurosci, 11*(6), 667-675. doi:10.1038/nn.2117

Lamba, D. A., Karl, M. O., and Reh, T. A. (2009). Strategies for retinal repair: cell replacement and regeneration. *Prog Brain Res, 175*, 23-31. doi:10.1016/s0079-6123(09)17502-7

Lechner, H. A., Lein, E. S., and Callaway, E. M. (2002). A genetic method for selective and quickly reversible silencing of Mammalian neurons. *J Neurosci, 22*(13), 5287-5290. doi:20026527

Li, X., Gutierrez, D. V., Hanson, M. G., Han, J., Mark, M. D., Chiel, H., . . . Herlitze, S. (2005). Fast noninvasive activation and inhibition of neural and network activity by vertebrate rhodopsin and green algae channelrhodopsin. *Proc Natl Acad Sci U S A, 102*(49), 17816-17821. doi:10.1073/pnas.0509030102

Lin, B., Koizumi, A., Tanaka, N., Panda, S., and Masland, R. H. (2008). Restoration of visual function in retinal degeneration mice by ectopic expression of melanopsin. *Proc Natl Acad Sci U S A, 105*(41), 16009-16014. doi:10.1073/pnas.0806114105

Lin, B., and Peng, E. B. (2013). Retinal ganglion cells are resistant to photoreceptor loss in retinal degeneration. *PLoS One, 8*(6), e68084. doi:10.1371/journal.pone.0068084

Lin, J. Y., Knutsen, P. M., Muller, A., Kleinfeld, D., and Tsien, R. Y. (2013). ReaChR: a red-shifted variant of channelrhodopsin enables deep transcranial optogenetic excitation. *Nat Neurosci, 16*(10), 1499-1508. doi:10.1038/nn.3502

Lin, J. Y., Lin, M. Z., Steinbach, P., and Tsien, R. Y. (2009). Characterization of engineered channelrhodopsin variants with improved properties and kinetics. *Biophys J, 96*(5), 1803-1814. doi:10.1016/j.bpj.2008.11.034

Lorenz-Fonfria, V. A., and Heberle, J. (2014). Channelrhodopsin unchained: structure and mechanism of a light-gated cation channel. *Biochim Biophys Acta, 1837*(5), 626-642. doi:10.1016/j.bbabio.2013.10.014

Lorenz-Fonfria, V. A., Resler, T., Krause, N., Nack, M., Gossing, M., Fischer von Mollard, G., . . . Heberle, J. (2013). Transient protonation changes in channelrhodopsin-2 and their relevance to channel gating. *Proc Natl Acad Sci U S A, 110*(14), E1273-1281. doi:10.1073/pnas.1219502110

Lu, Q., Ganjawala, T. H., Ivanova, E., Cheng, J. G., Troilo, D., and Pan, Z. H. (2016). AAV-mediated transduction and targeting of retinal bipolar cells with improved mGluR6 promoters in rodents and primates. *Gene Ther, 23*(8-9), 680-689. doi:10.1038/gt.2016.42

Lucas, R. J., Douglas, R. H., and Foster, R. G. (2001). Characterization of an ocular photopigment capable of driving pupillary constriction in mice. *Nat Neurosci, 4*(6), 621-626. doi:10.1038/88443

Lund, R. D., Kwan, A. S., Keegan, D. J., Sauve, Y., Coffey, P. J., and Lawrence, J. M. (2001). Cell transplantation as a treatment for retinal disease. *Prog Retin Eye Res, 20*(4), 415-449.

Mace, E., Caplette, R., Marre, O., Sengupta, A., Chaffiol, A., Barbe, P., . . . Dalkara, D. (2015). Targeting channelrhodopsin-2 to ON-bipolar cells with vitreally

administered AAV Restores ON and OFF visual responses in blind mice. *Mol Ther, 23*(1), 7-16. doi:10.1038/mt.2014.154

Marc, R. E., Jones, B. W., Watt, C. B., and Strettoi, E. (2003). Neural remodeling in retinal degeneration. *Prog Retin Eye Res, 22*(5), 607-655.

Miesenbock, G. (2011). Optogenetic control of cells and circuits. *Annu Rev Cell Dev Biol, 27*, 731-758. doi:10.1146/annurev-cellbio-100109-104051

Milam, A. H., Li, Z. Y., and Fariss, R. N. (1998). Histopathology of the human retina in retinitis pigmentosa. *Prog Retin Eye Res, 17*(2), 175-205.

Nack, M., Radu, I., Gossing, M., Bamann, C., Bamberg, E., von Mollard, G. F., and Heberle, J. (2010). The DC gate in Channelrhodopsin-2: crucial hydrogen bonding interaction between C128 and D156. *Photochem Photobiol Sci, 9*(2), 194-198. doi:10.1039/b9pp00157c

Nagel, G., Ollig, D., Fuhrmann, M., Kateriya, S., Musti, A. M., Bamberg, E., and Hegemann, P. (2002). Channelrhodopsin-1: a light-gated proton channel in green algae. *Science, 296*(5577), 2395-2398. doi:10.1126/science.1072068

Nagel, G., Szellas, T., Huhn, W., Kateriya, S., Adeishvili, N., Berthold, P., . . . Bamberg, E. (2003). Channelrhodopsin-2, a directly light-gated cation-selective membrane channel. *Proc Natl Acad Sci U S A, 100*(24), 13940-13945. doi:10.1073/pnas.1936192100

Nagel, G., Szellas, T., Kateriya, S., Adeishvili, N., Hegemann, P., and Bamberg, E. (2005). Channelrhodopsins: directly light-gated cation channels. *Biochem Soc Trans, 33*(Pt 4), 863-866. doi:10.1042/bst0330863

Nathans, J., Thomas, D., and Hogness, D. S. (1986). Molecular genetics of human color vision: the genes encoding blue, green, and red pigments. *Science, 232*(4747), 193-202.

Nikolic, K., Grossman, N., Grubb, M. S., Burrone, J., Toumazou, C., and Degenaar, P. (2009). Photocycles of channelrhodopsin-2. *Photochem Photobiol, 85*(1), 400-411. doi:10.1111/j.1751-1097.2008.00460.x

Olshevskaya, E. V., Calvert, P. D., Woodruff, M. L., Peshenko, I. V., Savchenko, A. B., Makino, C. L., . . . Dizhoor, A. M. (2004). The Y99C mutation in guanylyl cyclase-activating protein 1 increases intracellular Ca2+ and causes photoreceptor degeneration in transgenic mice. *J Neurosci, 24*(27), 6078-6085. doi:10.1523/jneurosci.0963-04.2004

Oprian, D. D., Asenjo, A. B., Lee, N., and Pelletier, S. L. (1991). Design, chemical synthesis, and expression of genes for the three human color vision pigments. *Biochemistry, 30*(48), 11367-11372.

Palczewski, K. (2006). G protein-coupled receptor rhodopsin. *Annu Rev Biochem, 75*, 743-767. doi:10.1146/annurev.biochem.75.103004.142743

Pan, Z. H., Ganjawala, T. H., Lu, Q., Ivanova, E., and Zhang, Z. (2014). ChR2 mutants at L132 and T159 with improved operational light sensitivity for vision restoration. *PLoS One, 9*(6), e98924. doi:10.1371/journal.pone.0098924

Pan, Z.-H., Lu, Q., Bi, A., Dizhoor, A. M., and Abrams, G. W. (2015). Optogenetic Approaches to Restoring Vision. *Annual Review of Vision Science, 1*(1), 185-210. doi:doi:10.1146/annurev-vision-082114-035532

Parmeggiani, F. (2011). Clinics, epidemiology and genetics of retinitis pigmentosa. *Curr Genomics, 12*(4), 236-237. doi:10.2174/138920211795860080

Plazzo, A. P., De Franceschi, N., Da Broi, F., Zonta, F., Sanasi, M. F., Filippini, F., and Mongillo, M. (2012). Bioinformatic and mutational analysis of channelrhodopsin-2 protein cation-conducting pathway. *J Biol Chem, 287*(7), 4818-4825. doi:10.1074/jbc.M111.326207

Prigge, M., Schneider, F., Tsunoda, S. P., Shilyansky, C., Wietek, J., Deisseroth, K., and Hegemann, P. (2012). Color-tuned channelrhodopsins for multiwavelength optogenetics. *J Biol Chem, 287*(38), 31804-31812. doi:10.1074/jbc.M112.391185

Roska, B., and Sahel, J.-A. (2018). Restoring vision. *Nature, 557*, 359-367.

Santos, A., Humayun, M. S., de Juan, E., Jr., Greenburg, R. J., Marsh, M. J., Klock, I. B., and Milam, A. H. (1997). Preservation of the inner retina in retinitis pigmentosa. A morphometric analysis. *Arch Ophthalmol, 115*(4), 511-515.

Schiller, P. H., Sandell, J. H., and Maunsell, J. H. (1986). Functions of the ON and OFF channels of the visual system. *Nature, 322*(6082), 824-825. doi:10.1038/322824a0

Schneider, F., Grimm, C., and Hegemann, P. (2015). Biophysics of Channelrhodopsin. *Annu Rev Biophys, 44*, 167-186. doi:10.1146/annurev-biophys-060414-034014

Scholl, H. P., Strauss, R. W., Singh, M. S., Dalkara, D., Roska, B., Picaud, S., and Sahel, J. A. (2016). Emerging therapies for inherited retinal degeneration. *Sci Transl Med, 8*(368), 368rv366. doi:10.1126/scitranslmed.aaf2838

SP Daiger, B. R., J Greenberg, A Christoffels, W Hide. Data services and software for identifying genes and mutations causing retinal degeneration. RetNet Retrieved

1-4-2019, from Invest. Ophthalmol.Vis. Sci. 39:S295,1998 RetNet, http://www.sph.uth.tmc.edu/RetNet/

Spudich, J. L. (2006). The multitalented microbial sensory rhodopsins. *Trends Microbiol, 14*(11), 480-487. doi:10.1016/j.tim.2006.09.005

Spudich, J. L., Yang, C. S., Jung, K. H., and Spudich, E. N. (2000). Retinylidene proteins: structures and functions from archaea to humans. *Annu Rev Cell Dev Biol, 16*, 365-392. doi:10.1146/annurev.cellbio.16.1.365

Stingl, K., Bartz-Schmidt, K. U., Besch, D., Braun, A., Bruckmann, A., Gekeler, F., . . . Zrenner, E. (2013). Artificial vision with wirelessly powered subretinal electronic implant alpha-IMS. *Proc Biol Sci, 280*(1757), 20130077. doi:10.1098/rspb.2013.0077

Stone, J. L., Barlow, W. E., Humayun, M. S., de Juan, E., Jr., and Milam, A. H. (1992). Morphometric analysis of macular photoreceptors and ganglion cells in retinas with retinitis pigmentosa. *Arch Ophthalmol, 110*(11), 1634-1639.

Sugiyama, Y., Wang, H., Hikima, T., Sato, M., Kuroda, J., Takahashi, T., . . . Yawo, H. (2009). Photocurrent attenuation by a single polar-to-nonpolar point mutation of channelrhodopsin-2. Photochem Photobiol Sci, 8(3), 328-336. doi:10.1039/b815762f

Tan, E. M., Yamaguchi, Y., Horwitz, G. D., Gosgnach, S., Lein, E. S., Goulding, M., . . . Callaway, E. M. (2006). Selective and quickly reversible inactivation of mammalian neurons in vivo using the Drosophila allatostatin receptor. *Neuron, 51*(2), 157-170. doi:10.1016/j.neuron.2006.06.018

Tochitsky, I., Polosukhina, A., Degtyar, V. E., Gallerani, N., Smith, C. M., Friedman, A., . . . Kramer, R. H. (2014). Restoring visual function to blind mice with a photoswitch that exploits electrophysiological remodeling of retinal ganglion cells. *Neuron, 81*(4), 800-813. doi:10.1016/j.neuron.2014.01.003

Tomita, H., Sugano, E., Isago, H., Hiroi, T., Wang, Z., Ohta, E., and Tamai, M. (2010). Channelrhodopsin-2 gene transduced into retinal ganglion cells restores functional vision in genetically blind rats. *Exp Eye Res, 90*(3), 429-436. doi:10.1016/j.exer.2009.12.006

Tomita, H., Sugano, E., Murayama, N., Ozaki, T., Nishiyama, F., Tabata, K., . . . Tamai, M. (2014). Restoration of the majority of the visual spectrum by using modified Volvox channelrhodopsin-1. *Mol Ther, 22*(8), 1434-1440. doi:10.1038/mt.2014.81

Tomita, H., Sugano, E., Yawo, H., Ishizuka, T., Isago, H., Narikawa, S., . . . Tamai, M. (2007). Restoration of visual response in aged dystrophic RCS rats using AAV-mediated channelopsin-2 gene transfer. *Invest Ophthalmol Vis Sci, 48*(8), 3821-3826. doi:10.1167/iovs.06-1501

Verhoefen, M. K., Bamann, C., Blocher, R., Forster, U., Bamberg, E., and Wachtveitl, J. (2010). The photocycle of channelrhodopsin-2: ultrafast reaction dynamics and subsequent reaction steps. *Chemphyschem, 11*(14), 3113-3122. doi:10.1002/cphc.201000181

Vincent, M. J., Martin, A. S., and Compans, R. W. (1998). Function of the KKXX motif in endoplasmic reticulum retrieval of a transmembrane protein depends on the length and structure of the cytoplasmic domain. *J Biol Chem, 273*(2), 950-956.

Wang, H., Sugiyama, Y., Hikima, T., Sugano, E., Tomita, H., Takahashi, T., . . . Yawo, H. (2009). Molecular determinants differentiating photocurrent properties of two channelrhodopsins from chlamydomonas. *J Biol Chem, 284*(9), 5685-5696. doi:10.1074/jbc.M807632200

Wassle, H. (2004). Parallel processing in the mammalian retina. *Nat Rev Neurosci, 5*(10), 747-757. doi:10.1038/nrn1497

Watanabe, H. C., Welke, K., Schneider, F., Tsunoda, S., Zhang, F., Deisseroth, K., . . . Elstner, M. (2012). Structural model of channelrhodopsin. *J Biol Chem, 287*(10), 7456-7466. doi:10.1074/jbc.M111.320309

Watanabe, H. C., Welke, K., Sindhikara, D. J., Hegemann, P., and Elstner, M. (2013). Towards an understanding of channelrhodopsin function: simulations lead to novel insights of the channel mechanism. *J Mol Biol, 425*(10), 1795-1814. doi:10.1016/j.jmb.2013.01.033

Wen, L., Wang, H., Tanimoto, S., Egawa, R., Matsuzaka, Y., Mushiake, H., . . . Yawo, H. (2010). Opto-current-clamp actuation of cortical neurons using a strategically designed channelrhodopsin. *PLoS One, 5*(9), e12893. doi:10.1371/journal.pone.0012893

Wen, R., Tao, W., Li, Y., and Sieving, P. A. (2012). CNTF and retina. *Prog Retin Eye Res, 31*(2), 136-151. doi:10.1016/j.preteyeres.2011.11.005

Werblin, F. S., and Dowling, J. E. (1969). Organization of the retina of the mudpuppy, Necturus maculosus. II. Intracellular recording. *J Neurophysiol, 32*(3), 339-355.

West, E. L., Pearson, R. A., MacLaren, R. E., Sowden, J. C., and Ali, R. R. (2009). Cell transplantation strategies for retinal repair. *Prog Brain Res, 175*, 3-21. doi:10.1016/s0079-6123(09)17501-5

Wietek, J., Beltramo, R., Scanziani, M., Hegemann, P., Oertner, T. G., and Simon Wiegert, J. (2015). An improved chloride-conducting channelrhodopsin for light-induced inhibition of neuronal activity in vivo. *Sci Rep, 5*, 14807. doi:10.1038/srep14807

Wietek, J., Wiegert, J. S., Adeishvili, N., Schneider, F., Watanabe, H., Tsunoda, S. P., . . . Hegemann, P. (2014). Conversion of channelrhodopsin into a light-gated chloride channel. *Science, 344*(6182), 409-412. doi:10.1126/science.1249375

Williams, S. (2017, 01-07-2019). Optogenetic Therapies Move Closer to Clinical Use. Retrieved from https://www.the-scientist.com/news-opinion/optogenetic-therapies-move-closer-to-clinical-use-30611

Wong, W. L., Su, X., Li, X., Cheung, C. M., Klein, R., Cheng, C. Y., and Wong, T. Y. (2014). Global prevalence of age-related macular degeneration and disease burden projection for 2020 and 2040: a systematic review and meta-analysis. *Lancet Glob Health, 2*(2), e106-116. doi:10.1016/s2214-109x(13)70145-1

Wu, C., Ivanova, E., Zhang, Y., and Pan, Z. H. (2013). rAAV-mediated subcellular targeting of optogenetic tools in retinal ganglion cells in vivo. *PLoS One, 8*(6), e66332. doi:10.1371/journal.pone.0066332

Yao, K., Qiu, S., Wang, Y. V., Park, S. J. H., Mohns, E. J., Mehta, B., . . . Chen, B. (2018). Restoration of vision after de novo genesis of rod photoreceptors in mammalian retinas. *Nature, 560*(7719), 484-+. doi:10.1038/s41586-018-0425-3

Yizhar, O., Fenno, L. E., Prigge, M., Schneider, F., Davidson, T. J., O'Shea, D. J., . . . Deisseroth, K. (2011). Neocortical excitation/inhibition balance in information processing and social dysfunction. *Nature, 477*(7363), 171-178. doi:10.1038/nature10360

Yue, L., Pawlowski, M., Dellal, S. S., Xie, A., Feng, F., Otis, T. S., . . . Pepperberg, D. R. (2012). Robust photoregulation of GABA(A) receptors by allosteric modulation with a propofol analogue. *Nat Commun, 3*, 1095. doi:10.1038/ncomms2094

Yue, L., Weiland, J. D., Roska, B., and Humayun, M. S. (2016). Retinal stimulation strategies to restore vision: Fundamentals and systems. *Prog Retin Eye Res, 53*, 21-47. doi:10.1016/j.preteyeres.2016.05.002

Zemelman, B. V., Lee, G. A., Ng, M., and Miesenbock, G. (2002). Selective photostimulation of genetically chARGed neurons. *Neuron, 33*(1), 15-22.

Zhang, F., Prigge, M., Beyriere, F., Tsunoda, S. P., Mattis, J., Yizhar, O., . . . Deisseroth, K. (2008). Red-shifted optogenetic excitation: a tool for fast neural control derived from Volvox carteri. *Nat Neurosci, 11*(6), 631-633. doi:10.1038/nn.2120

Zhang, F., Vierock, J., Yizhar, O., Fenno, L. E., Tsunoda, S., Kianianmomeni, A., . . . Deisseroth, K. (2011). The microbial opsin family of optogenetic tools. *Cell, 147*(7), 1446-1457. doi:10.1016/j.cell.2011.12.004

Zhang, Y., Ivanova, E., Bi, A., and Pan, Z. H. (2009). Ectopic expression of multiple microbial rhodopsins restores ON and OFF light responses in retinas with photoreceptor degeneration. *J Neurosci, 29*(29), 9186-9196. doi:10.1523/jneurosci.0184-09.2009.

ABSTRACT

DEVELOPMENT OF MORE LIGHT SENSITIVE AND RED-SHIFTED CHANNELRHODOPSIN VARIANTS FOR OPTOGENETIC VISION RESTORATION

by

TUSHAR H. GANJAWALA

May 2019

Advisor: Dr. Zhuo-Hua Pan

Major: Anatomy and Cell Biology

Degree: Doctor of Philosophy

Discovery of channelrhodopsin (ChR), a light sensitive protein from green algae, has revolutionized the field of neuroscience research by empowering scientist to control neuron through the light, the technology popularly known as optogenetics. The ChR based optogenetics is one of the promising approaches for treating blindness caused by photoreceptor degenerative diseases such as retinitis pigmentosa (RP) and age-related macular degeneration (AMD). Fundamentally, the approach is about imparting light sensitivity to surviving inner retinal cells by ectopic expression of genetically encoded light sensitive proteins, such as ChR2. Although the concept of optogenetic approach has been proved by using ChR2, a major obstacle of using the wild type ChR2 or in general ChRs for vision restoration is their low light-sensitivity. With the molecular engineering approach more light sensitive variants of ChR2 have been created recently, however, their light sensitivity remained 2-3 log units below the threshold of cone photoreceptors. Additionally, most of the ChR variants with improved light sensitivity are blue light sensitive. Since the longer wavelength light can have better tissue penetration

and less photo-toxicity, the development of ChR with higher light-sensitivity and red-shifted peak spectra (λ_{max}) was desired. In this study, two newly reported ChRs, the CoChR (*Chloromoas oogama* ChR) and the ReaChR (Red activable ChR, a chimera variant) were chosen to improve their light sensitivity by molecular engineering. The CoChR was chosen because of its larger photocurrent compared to that of ChR2, while ReaChR was selected because of its red-shifted peak spectral sensitivity (λ_{max}). Additionally, attempts were made to shift the λ_{max} of the CoChR towards the red. For CoChR, three different sites with specific mutations, specifically H94E (HE), L112C (LC) and K264T (KT) were identified, which together created the most light-sensitive CoChR-3Mt (CoChR-HE/LC/KT). The CoChR-3Mt markedly enhances photocurrent to low light intensity and, thus, increases operational light sensitivity in compared to the wild type CoChR (CoChR-Wt). The enhanced light sensitivity was found to be correlated with the slower off-kinetics. However, the λ_{max} of CoChR could not shift towards longer wavelengths (red) either by site-direct mutagenesis or by chimera approaches. This suggested that the spectral sensitivity of the ChR, in general, is tightly regulated by a complex mechanism that is yet to be revealed. For ReaChR, a combination of three mutations, specifically I171M-V302L-N305H (IM-VL-NH), was identified which moderately enhanced its light sensitivity. Again, the enhanced light sensitivity was correlated with slower off-kinetics.

In conclusion, the CoChR-3Mt was found to be the most light-sensitive ChR variant that can be a better optogenetic tool for vision restoration.

AUTOBIOGRAPHICAL STATEMENT

Education:

2014-2019	PhD	Anatomy and Cell Biology	Wayne State University School of Medicine, Detroit, MI, USA.
2008-2010	M.S.	Biology	University of Michigan, Flint, MI, USA.
2004-2006	M.Sc.	Microbiology	Bangalore University, India.
2002-2003	DMLT		South Gujarat University, India.
2000-2002	B.Sc.	Microbiology	South Gujarat University, India.

Publications:

1) Q. Lu, **T.H. Ganjawala**, S. Hattar, G.W. Abrams, Z.H. Pan, A Robust Optomotor Assay for Assessing the Efficacy of Optogenetic Tools for Vision Restoration, Investigative ophthalmology and visual science, 59 (2018) 1288-1294.
2) Q. Lu, **T.H. Ganjawala**, E. Ivanova, J.G. Cheng, D. Troilo, Z.H. Pan, AAV-mediated transduction and targeting of retinal bipolar cells with improved mGluR6 promoters in rodents and primates, Gene therapy, 23 (2016) 680-689.
3) Z.H. Pan, **T.H. Ganjawala**, Q. Lu, E. Ivanova, Z. Zhang, ChR2 mutants at L132 and T159 with improved operational light sensitivity for vision restoration, PloS one, 9 (2014).
4) Q. Lu, E. Ivanova, **T.H. Ganjawala**, Z.H. Pan, Cre-mediated recombination efficiency and transgene expression patterns of three retinal bipolar cell-expressing Cre transgenic mouse lines, Molecular vision, 19 (2013) 1310-1320.

Research Presentations:

1) **Tushar Ganjawala**, Diane Fiander, Anding Bi, Qi Lu, Zhuo-Hua Pan; Channelrhodopsin Engineering for Better Optogenetic Tools for Vision Restoration. Abstract presented at KEI Vision Research Workshop 2014, Detroit, MI.
2) **T. H. Ganjawala**, Q. Lu, A. Bi, E.S. Boyden, Z.-H. Pan; Evaluation and Optimization of An Ultra-Light-Sensitive Channelrhodopsin Variant of CoChR for Vision Restoration. Abstract presented at ARVO 2015, Denver, CO; GSRD 2015 and KEI Vision Research Workshop 2015, Detroit, MI.
3) **Tushar H. Ganjawala**; Qi Lu; Gary Abrams; Zhuo-Hua Pan; Development of Highly Light-Sensitive and Red-shifted ChR Variants for Vision Restoration.Abstract presented at GSRD 2016 and KEI Vision Research Workshop 2016, Detroit, MI.
4) **Tushar H. Ganjawala;** Qi Lu; Mitchell D. Fenner; Gary Abrams; Zhuo-Hua Pan; Development of Highly Light-Sensitive CoChR Mutants for Optogenetic Vision Restoration. Abstract presented at GSRD 2017 and KEI Vision Research Workshop 2017, Detroit, MI.
5) **Tushar H. Ganjawala**; Qi Lu; Mitchell D. Fenner; Gary Abrams; Zhuo-Hua Pan; An ultra-light-sensitive CoChR mutant restores functional vision in a blind mouse model under ambient light conditions. Abstract presented at ARVO 2018, Honolulu, HI and at FASEB 2018, Buffalo, NY.